Department of Exploration Geophysics,
School of Physical Sciences

Advancements in the technique of low fold three dimensional seismic reflection surveying

Brian J.Evans,
Dip Elec. Eng (L'pool), Grad. Dip. App Phys (WAIT),
M.App. Sc. (WAIT)

This thesis is presented as part of the
requirements for the award of the
Degree of Doctor of Philosophy
of
Curtin University of Technology

December, 1996.

Abstract

Three dimensional (3-D) seismic reflection surveying is accepted as the preferred method for imaging complex geology for proving and developing commercial oil and gas fields. However, the cost of 3-D seismic recording and processing is substantial and often can be as expensive as the cost of production drilling. This is particularly the case for land oil field development, where the cost of 3-D surveying is often unacceptably high. Such high costs also restrict its application in coal exploration, where 2-D seismic methods have long been accepted.

During the early 1980's, a low fold technique for recording land 3-D data was devised which offered significant cost savings. The technique was adapted by the author for land 3-D surveying over coal fields. Inherent in the technique was a requirement that the data must have a high signal-to-noise ratio, which is not generally the case in land surveying due to the presence of strong source generated surface wave noise. A further major impediment to the technique was its inability to perform an acceptable stacking velocity analysis because of the a low number of seismic traces generated. This thesis defines three data collection and processing advancements in low fold 3-D technology which go some way towards resolving these impediments.

The first advancement is a method to enhance the signal-to-noise ratio of the stacked seismic data, and consists of a Radon-based transform which stacks shot domain data along a curved trajectory, thereby attenuating surface waves on swath recorded data. This transform is termed the 'Radial Transform' of 3-D data.

The second advancement is a statics method to improve the stacked image from a low number of input traces. The method uses the concept that if both the reflected and refracted waves pass through a weathering layer with very similar travel paths, then static corrections to remove the effects of weathering variations on the refraction travel times would be very similar to those required for the reflections. This method, which was patented, is used equally for both 2-D and 3-D field data, and is regularly used in high resolution seismic processing for coal at Curtin University.

The third advancement resolves the problem of azimuthal variation of stacking velocities. By predicting the true reflector dip and its azimuth, apparent dip can be included in the normal moveout equation, which is named the Generalized Moveout equation. The requirement for an azimuthally dependent stacking velocity is then no longer an impediment in low fold 3-D processing of coal data.

After developing these transforms and applying them to synthetic data, they were tested with success on modelled field data. All field data used within this thesis were either recorded in the field by the author, or were produced with a physical modelling system, which was built by the author at the University of Houston and later at Curtin University.

Results indicate that the procedures described in this thesis enable the low fold 3-D technique to be used as a viable method for recording seismic data when survey economics are a major issue. Furthermore, all three advancements are suitable for application in conventional two dimensional (2-D) and swath seismic surveying.

ACKNOWLEDGEMENTS

I would like to acknowledge the personal contributions by Dr. Norm Uren (Curtin University), Dr. Brian Kennett (Australian National University) and Dr. John McDonald, as Supervisor and Associate Supervisors of this research. Mr. Brian White and Dr. Jamie Simpson of Curtin University provided perceptions of three dimensional geometry which were invaluable in this work, for which I am most grateful.

The research was performed on a part-time basis and consequently took some seven years to complete. I would like to thank Dr. Roger Young, now of the University of Oklahoma, for his early supervision and support during the development of a new transformation technique.

I acknowledge the strong encouragement of Dr. John McDonald while at the University of Houston's Allied Geophysical Laboratories (U.H.-A.G.L. and laterly at Curtin University), who continually encouraged completion of the research.

Theory could not have been tested without the use of a physical modelling facility. As a result, I spent the majority of 1991 building such a facility at the U.H.-A.G.L., and later rebuilding it at Curtin University. I wish to express my gratitude to Dr. K.K.Sekharan and Barbara Murray at AGL, for their technical assistance in providing input and administration whilst building the modelling laboratory. I would also like to thank the sponsors of AGL who underwrote the cost of the original equipment.

This research would not have been possible without the use of the Curtin University Department of Exploration Geophysics laboratory facilities. This also includes the use of the Cogniseis 'Disco' software and Sierra Geophysics modelling software. For these facilities, I am grateful.

Finally, I wish to acknowledge my wife's help in allowing valuable family time to be spent on the research and thesis write-up. She retired from a close interest in this work years ago, and the only reward she has is that the bane of her life (this thesis) has been completed.

CONTENTS

LIST OF FIGURES

FIGURES **PAGE**

CHAPTER 1
Introduction

The three-dimensional seismic surveying method is the major tool for imaging oil and gas reservoir geology. The method is equally suited to other geology such as that found in coal fields. However, the cost of 3-D seismic makes the method unacceptably high for adoption by the coal mining industry. One cost effective approach is to record less data, but this must be compensated for by alternative processing methods. The objective of this thesis is to define a method for reducing the cost of 3-D seismic over coal field geology, then resolve subsequent problems presented by acquiring and processing a reduced data set.

Since the early days of petroleum exploration, the seismic method has been the major tool for imaging sediments beneath the Earth's surface. The explosion of an energy source within the regolith, radiates energy which is refracted and reflected from geological boundaries returning to the surface yielding sub-surface geological detail.

By placing detectors in a line along the surface, seismic waves appear to change velocity at different offsets from the source and thus it is possible to understand how waves may travel downwards, be reflected at a geological boundary, and return to the surface. Until the early 1960s, geological horizons were interpreted from either lineations or curved events observed on shot records, which were merely a record of seismic waves arriving at the detectors. Interpretations were crude because the reflected signal strength was often low compared to the high level of ambient background and surface wave noise.

The invention of the common depth point (CDP) method of stacking (Mayne, 1962) involved the summing of data recorded with the same common mid-point. The CDP method is often referred to today as the common mid-point (CMP) method. The enhanced signal-to-noise ratio from stacked gathers of different offset shot/receiver pairs provided better images of reflected events.

However, rocks are three-dimensional (3-D) and reflections may arrive at detector or geophone stations from a point directly beneath or off the line of the seismic profile. Geological discontinuities, such as faults, fractures or

bed terminations, produce diffracted energy both from within and outside the plane of the profile being recorded.

Maginness (1972) was the first to publish results from the simulation of elastic waves using ultrasonic transducers on a plate, and gave a numerical solution to integral equations describing the wave motion. Walton (1972) first demonstrated the possibilities of 3-D data acquisition of seismic data. French (1974) applied the modelling approach to seismic exploration over 3-D physical models representing simple structures. He showed that the diffractions or reflections that emanated from points beneath the line of profile could be collapsed or imaged reasonably well by two-dimensional (2-D) migration, but reflections originating from outside the line of profile could not be properly imaged. It was recognised that data have to be recorded three-dimensionally and three-dimensionally migrated to ensure that the targets are imaged properly.

Today, 2-D seismic surveys are commonly recorded by the petroleum exploration industry as a reconaissance tool prior to drilling. However, when a potential hydrocarbon trap has been discovered, a 3-D survey is frequently carried out to determine the areal extent of the trap. Such data are preferable for structural mapping and the reflection imaging quality is improved dramatically by the use of 3-D processing techniques. In addition to the superior quality of 3-D data its use also makes good economic sense (Nestfold, 1992).

In practice the nature of 3-D surveying is dependent upon whether the survey is land based or marine based, since different equipment is required. For example, a land survey uses geophones as detectors, a surface seismic source, and has the particular problem of low signal-to-noise ratio because most of the source energy generates noise such as strong surface waves. An advantage in land surveys is that a line of source points can be orthogonal to the receiver line and is not limited to remaining collinear or near them (as in the marine case).

In contrast, the basic seismic recording of marine surveys requires a single ship which can tow one or more seismic cables containing hydrophones, with the source/receiver arrays configured along the line of the seismic profiles (Evans, 1984). Multiple ships are occasionally used in the North Sea and Gulf of Mexico, but this is not a routine situation.

A great deal of effort has been directed at obtaining the correct subsurface image, with much of the research being concentrated on correcting the effects of dip on 2-D seismic data. This is adequate for a limited source/receiver configuration, such as that used by the two-dimensional seismic methods. The two-dimensional processing technique is based on the assumption that the reflection points are in the vertical plane of the seismic profile, when in fact they may be from outside of this plane.

Land 3-D surveying techniques in petroleum and coal exploration, allow the source to be at any location with respect to the receiver line, so that CMP data gathered over an area can be added or "binned". In land 3-D surveying, it is usual to obtain from 24 to 30 common mid-point traces which are stacked in each bin (Denham, 1989, pers. com.). To collect data typically 30 source shots are fired into 30 receivers at different offsets and different azimuthal directions with respect to a reference survey direction (Lansley and Gonzalez, 1992). Land 3-D surveying therefore requires the seismic crew to lay out manually many geophone receiver lines in different directions in an areal manner rather than the simpler single receiver line required for 2-D surveying.

Consequently, 3-D land surveying is more labour intensive than 2-D surveying. Recording costs are therefore far greater and the requirement for a large number of areal source and receiver locations not only increases the cost of data collection, but also demands a greater effort in processing. In addition, the strong source generated noise in land data causes a reduction in the reflected signal-to-noise ratio, resulting in a need to maintain a high level of fold. This demands a large number of CMP bin traces. Consequently, the 3-D method of land surveying is sometimes prohibitively expensive to perform over marginal hydrocarbon discoveries and many operators accept that such surveying is not financially viable.

In an effort to lower the cost of 3-D surveying, a method was established for recording less binned traces, thereby reducing the fold of 3-D data. This method originated at the Allied Geophysical Laboratories (University of Houston), and was named 'LOFOLD3-D' (McDonald, 1985, pers. com.). A LOFOLD3-D minimum number of traces has been defined as any number from four (Evans, 1988) to eight (Allen and Howell, 1987). Allen and Howell did not require special treatment because their signal-to-noise

ratios were high, there were no effective dips present (resulting in consistent stacking velocities) and there were no surface statics problems. However, that was a rare case history and in reality there is invariably a geophysical problem with at least one of these.

A reduced fold technique will reduce costs but to be effective it must maintain an acceptable level of signal-to-noise ratio. Thus the challenge in this research was to determine methods to maintain a high signal-to-noise ratio while reducing the level of fold, in order to minimise survey and processing costs.

The quality of 3-D data, in which individual traces are binned with different shot-receiver azimuths, can be affected by:

(i) low signal-to-noise ratio resulting from the arrival of azimuthally variable surface waves,
(ii) poor stack imaging due to the application of incorrect surface statics corrections, and
(iii) reflector dip, which causes an azimuthal variation in stacking velocity making normal moveout (NMO) corrections difficult (Levin, 1971).

Reducing the number of binned traces for LOFOLD3-D demands a solution to these problems, if a good quality 3-D image is to be obtained.

In (i), variable source to receiver azimuths preclude the use of geophone arrays commonly deployed in 2-D surveys. Arriving surface waves cannot be effectively attenuated and as a consequence, the reflection signal-to-noise ratios cannot be reduced. Furthermore, surface waves travel at such a slow velocity that they can arrive at the receivers at the same time as the deeper higher velocity reflections. In addition, surface wave amplitude values are frequently much larger than the desirable reflection amplitudes, so they very often mask the reflections.

In 2-D data acquisition, surface waves appear as a linear event on a shot record recorded by in-line receivers, and various data transformations may be used to recover reflected data curved events which do not have a similar arrival moveout. However, in variable azimuth 3-D recording, surface wave arrivals appear as a curved event also, due to the unequal incremental distances from the shot location to successive receiver locations. Such an

arrival can have similar moveout to that associated with reflections though different frequency content. Hence, 3-D surface wave attenuation is quite difficult. This problem is studied, and a method of solving it is developed in Chapter 4.

In (ii), poor statics can result in a defocussing of the reflector image causing a reduction in the signal-to-noise ratio. The use of a reduced number of traces for statics computations compounds the problem. If arriving reflections can be considered as having similar travel paths through the weathering layer as refracted arrivals, then it may be reasonable to apply conventional reflection correlation methods on the refracted arrivals, to assist reflection event line-up. Such a method will be tested in this thesis, and evaluated using seismic data recorded over coal mines.

Finally in point (iii), if a reflector dips in any particular direction with respect to the source and receiver line, then the apparent dip will change for each 3-D source/receiver pair. Since the presence of dip causes the stacking velocity to change, this demands a different stacking velocity for each source receiver pair in any 3-D bin. The lack of gathered traces with the same azimuth precludes the accurate determination of stacking velocities at any azimuth.

The problem of dip is therefore generally ignored, and stacking velocities are used which produce the best image while acknowledging that the images are smeared. An approach has been to establish a 3-D velocity model based on stacking velocities along orthogonal 2-D lines, and apply the NMO correction to each binned trace using the in-line and cross-line corrections (Meinardus and McMahon, 1981).

3-D dip moveout (DMO) processing may then be applied assuming a single velocity function for all traces (Hale, 1991). The DMO process moves data to the correct zero-offset location for a dipping reflection. To quote Sheriff (1991) "DMO effectively corrects for the reflection point smear that results when dipping reflections are stacked". The application of DMO processing is generally accepted as a pre-conditioning step prior NMO analysis and then to zero offset migration. The problem of data from dipping reflections requiring different stacking velocities for each trace in a bin is then conveniently ignored.

The large number of traces required for 3-D DMO processing makes 3-D DMO inapplicable when the number of traces in a 'LOFOLD3-D' volume is of the order of four traces per bin. As a result, 'LOFOLD3-D' does not benefit from processing techniques such as 3-D DMO and the image smearing is not corrected.

If it were possible to separate the apparent dip term from the velocity term in the 3-D NMO equation, then it would be possible to apply the same velocity value during NMO correction of traces in each bin. This approach would also ameliorate the need to perform extensive velocity analyses on low fold binned traces, and would have further application in 2-D processing if the apparent dip were known.

In this thesis, I present a 3-D normal moveout equation which separates velocity and dip terms in the NMO equation, allowing the velocity term to be kept constant for all the CMP traces. I name this the 'Generalised Moveout' (GMO) equation.

With this equation, the stacking velocity is constant for all traces in bins along a line, and the requirement to perform a velocity analysis on individual chosen gathers is no longer so important. A method for the determination of the dip between each source/receiver pair is presented as a pre-requisite to the use of this 3-D GMO equation. I evaluate the application of the method using a physical model of known dip and velocity.

The LOFOLD3-D method is most applicable to seismic surveying over coal mine geology where low fold levels are commonly recorded. The physical model used in this thesis therefore simulates a single layer block of geology above a coal seam (such as the Hawkesbury sandstone above the Bulli seam of Appin Colliery, NSW, Australia).

This thesis therefore commences with a discussion on the method of 3-D land surveying detailing the major problems affecting LOFOLD3-D, i.e. low signal-to-noise ratio reflections (resulting from surface wave interference). The problem of surface statics, and that of changing apparent velocity due to the presence of dip, are discussed next. The relative success of these solutions is data dependent, and no single data set available to the author contained all of the problems discussed. Hence, the application of the solutions to these problems is shown with different field data sets. Finally,

as a result of the need to separate the velocity term in the dip dependent NMO expression, I present a method for the determination of the three-dimensional dip and azimuth of a dipping reflection plane.

Data are used which were recorded during LOFOLD3-D deep reflection surveys at Moora, W.A.; and during shallow reflection surveys at German Creek and Appin Collieries, NSW. The Appin Colliery data are used to illustrate the effectiveness of the LOFOLD3-D reflection method, where the method has been used productively to generate three-dimensional interpretations of the Bulli seam, before underground mining takes place at a cost saving to the mining company (Poole, 1994, pers. comm.).

Conclusions are drawn about the three advancements in the technique of low fold three-dimensional surveying, and recommendations are made about the adoption of both the noise attenuation method and the dip detection method to marine surveying. The Appendices to the thesis provide the mathematical derivation of a three-dimensional GMO equation, the true dip determination, and sample computer programs.

CHAPTER 2
Seismic exploration in 2-D and 3-D.

This chapter introduces the basic approach used by the seismic method to image the sub-surface. The problem of the generation of waves which interfere with useful reflected waves is then considered, with an emphasis on that caused by surface waves. Field records are used to discuss the relative merits of 2-D and 3-D seismic data using different data acquisition approaches.

An alternative low fold 3-D approach is then reviewed, along with the major problems of that method's implementation. Once again, surface wave noise is a major obstacle, as well as the difficulty in performing an accurate velocity analysis due to the presence of weathering statics and reflection surface dip. The chapter concludes with proposed approaches to resolving these problems.

2.1 The seismic method

In an isotropic medium, the seismic energy initially propagates spherically outwards from the energy source point (Figure 2.1). This energy is considered to travel in the form of a wavefront which can be reflected and refracted, so that in the field, the land based geophones often observe at least four different wave types, namely refracted waves, direct waves, surface waves and reflected waves. Only surface and reflected waves will be discussed in this thesis, because they are the two major waves of interest in land surveying and the others are often filtered in the data processing stage. Reflections are considered to be the useful signal, while surface waves are the noise.

As a wave arrives at the surface, any additional travel path length at increasing offsets due to propagation to and from a reflecting horizon, causes an increase in traveltime or a delay in arrival time. For an isotropic,

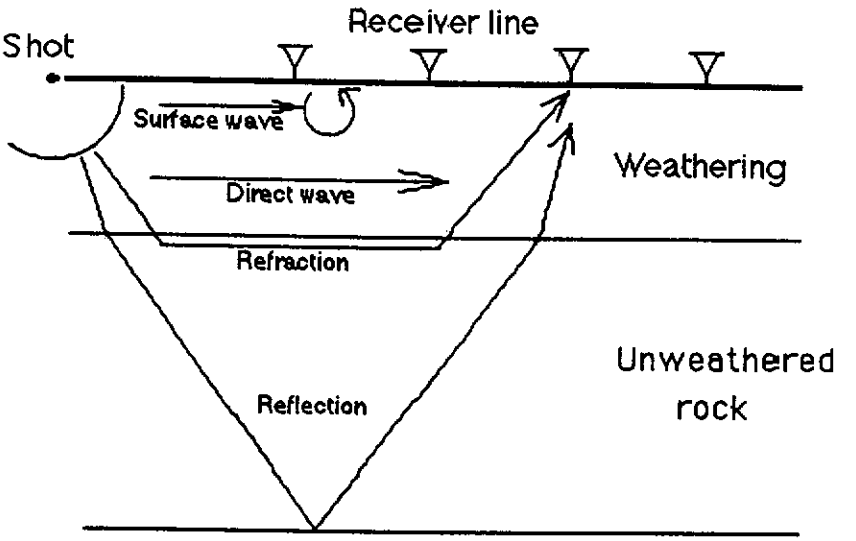

Figure 2.1. Principal waves investigated which are generated by a seismic shot. The energy source located at the shot point location generates four principal waves which travel to the receiver line. In this simplistic model, the 'refracted' wave which travels down through the weathering layer and is refracted at a horizon of higher velocity than the weathering. It travels along the lower layer refracting once more and returning to the surface. The second wave often observed to arrive first is called the 'direct' wave, travels along the weathering layer with the particle motion of a compressional wavefront at the velocity of the medium. The third wave may be the 'surface' wave which also travels along the surface but with an elliptical motion. A fourth wave may be a 'reflection' from a subsurface interface, which arrives at a surface geophone with either a compressional or a transverse particle motion.

single medium, this variation as a function of the offset is known as the move-out (or NMO), and the time delay (δt) for a horizontally layered Earth is given by:

$$\delta t = \frac{(4h^2 + x^2)^{1/2}}{V} - \frac{h}{V} , \qquad (2.1)$$

where h is the depth to the reflector, x is the offset from the source to a particular receiver and V is the velocity of the medium.

Mayne (1962) introduced the method of common depth point stacking, in which source and receivers are positioned along a straight line and the common depth point traces (CDPs) are NMO corrected and summed to improve the reflection signal-to-noise ratio. However, Mayne's NMO correction and stack assumes a reflection arriving from a horizontal layer and not a dipping layer, which is a relatively good assumption for sedimentary geology.

Where the reflecting layer has dip, the reflection point moves in the up-dip direction (Slotnick, 1959). Cressman (1968) noted that because of the way the NMO correction was applied, CMP stacking works as well for dipping beds as it does for horizontal beds, although the reflections from dipping beds do not have common reflection points. Brown (1969) examined the NMO correction and velocity relations for dipping beds which had their true dip direction in the direction of the seismic line. He showed that errors in the NMO correction value must be no more than a quarter of the dominant period of the reflection wavelet, for an acceptable stack.

Levin (1971), provided the first insight into the effect of three-dimensional dip on the apparent velocity. He discussed how 3-D dip can affect 2-D in-line data, and concluded that for dips at less than 10 degrees, the NMO (stacking) velocity was approximately the same as the zero-dip stacking velocity. However, Levin (1971) only analysed a 2-D in-line recording configuration in terms of apparent dip angle.

Reflection points must lie somewhere on an ellipsoidal surface with the source and receiver locations as foci. It is possible to create apparent common reflection point gathers by a convolution applied to adjacent CMP gathers. This correction is known as dip move-out or 'DMO' (Deregowski,

1986). When the line of seismic recording does not lie in the true dip direction, the reflection image is still constructed in the vertical plane of the receiver line. This image will not only have an incorrect amplitude but will be misplaced since the reflection would have occurred from out of the plane of the receiver line. Such dip is said to be three-dimensional, and as Levin (1971) showed, the NMO velocity for a CMP gather over such a dipping plane depends on both the strike and dip angles, as well as the velocity of the medium.

2.2 Surface waves and their effect on reflection data.

Where a weathering layer exists, it often has a lower velocity than deeper horizons. As a result surface waves, which propagate with a retrograde elliptical particle motion within the weathering, appear as an apparent linear arrival on a time-distance plot (Figure 2.2) when the shot is collinear with the line of receivers.

Surface waves are frequently observed as a series of wave-trains in the form of a cone with the longer wavelengths travelling faster, as shown in Figure 2.3. Such a record shows that the surface waves 'B' mask the useful reflections 'A'.

In 3-D surveys where the source is often not collinear with the receivers, surface waves will be recorded as a curved event. This is due to the nearest receivers having an almost equal offset distance from the source, whereas the far receivers have an offset distance increment which is similar to the receiver station interval. Consequently, the surface wave has a flat appearance on a shot record at the near traces, curving to become more linear at the far traces. As the azimuth and therefore the offset distance of the source to each receiver changes, so the arrival time of the surface wave changes causing a change in the appearance of the surface wave arrival curvature on the shot record.

Such a surface wave arrival's appearance on a shot record is shown schematically in Figure 2.4, in which the source is located off the receiver line, and a typical field record using an off-line or 'swath' shot is shown in Figure 2.5.

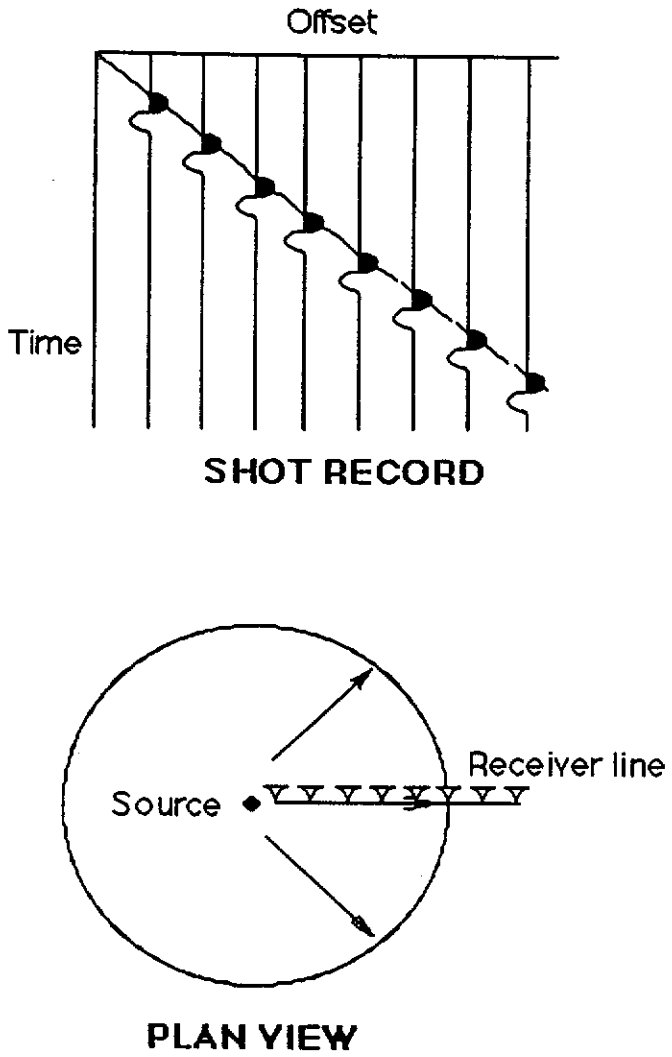

Figure 2.2. Plan view of the surface wave travelling along the in-line receiver line. The result is that the surface wave move-out has a linear appearance on a shot record as shown schematically above.

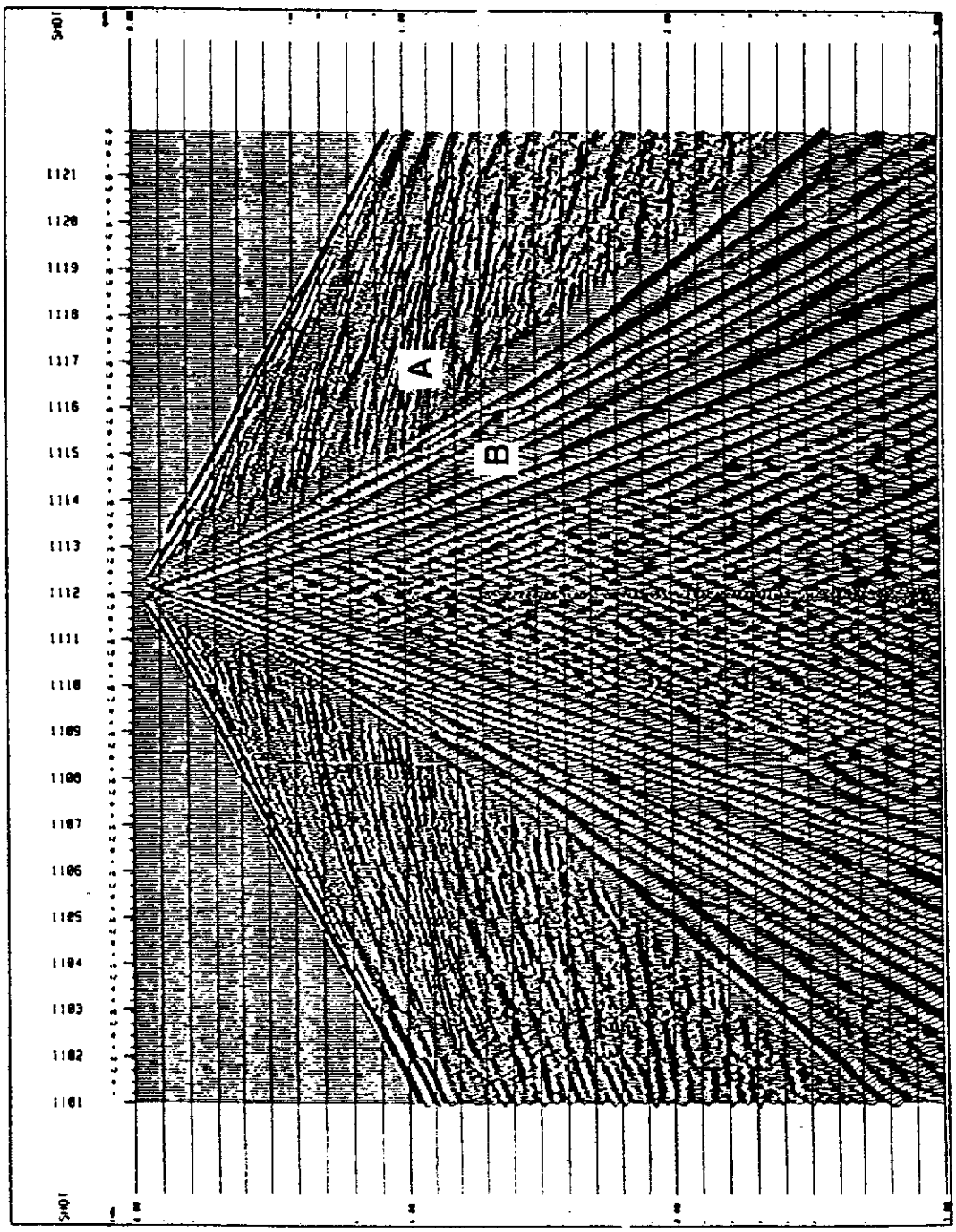

Figure 2.3. Field record using in-line split-spread recording at Moora, showing the useful reflections 'A' being masked by the surface wave noise cone 'B'. The right half of the display is equivalent to the configuration shown in Figure 2.2. (from Stewart and Evans, 1989).

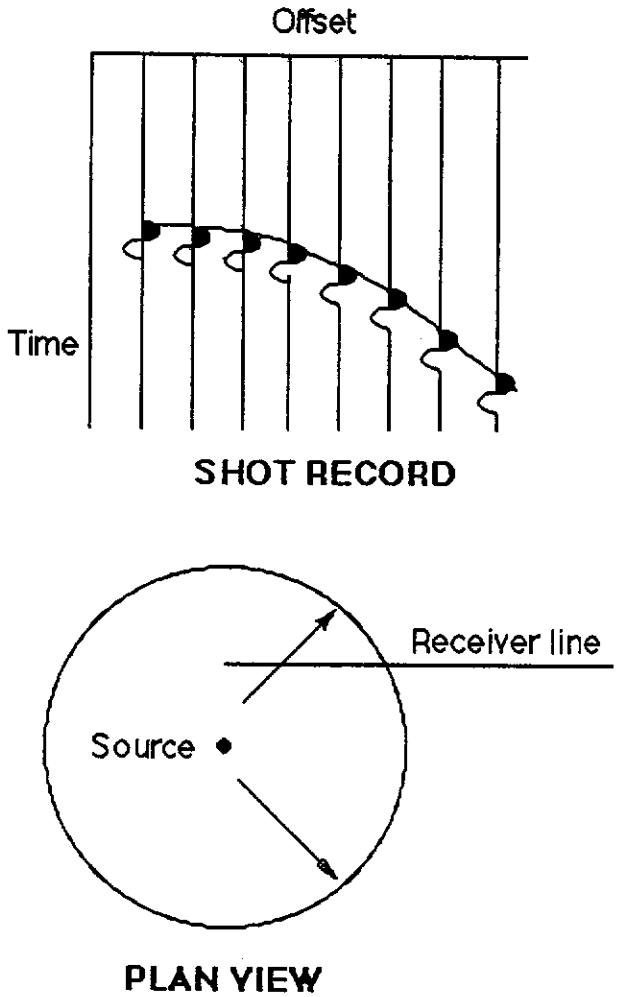

Figure 2.4. Plan view of surface waves travelling towards a receiver line, which is not collinear with the source line. The offset is the distance from the source to each individual receiver. The surface wave move-out has a curved appearance, similar to that of a reflection, due to the unequal azimuthal distances travelled from the source to each receiver, causing a change in arrival times at the receivers. The flattening effect of the arriving surface wave on the record for the near offset receivers is caused by almost equal offset distances to each receiver.

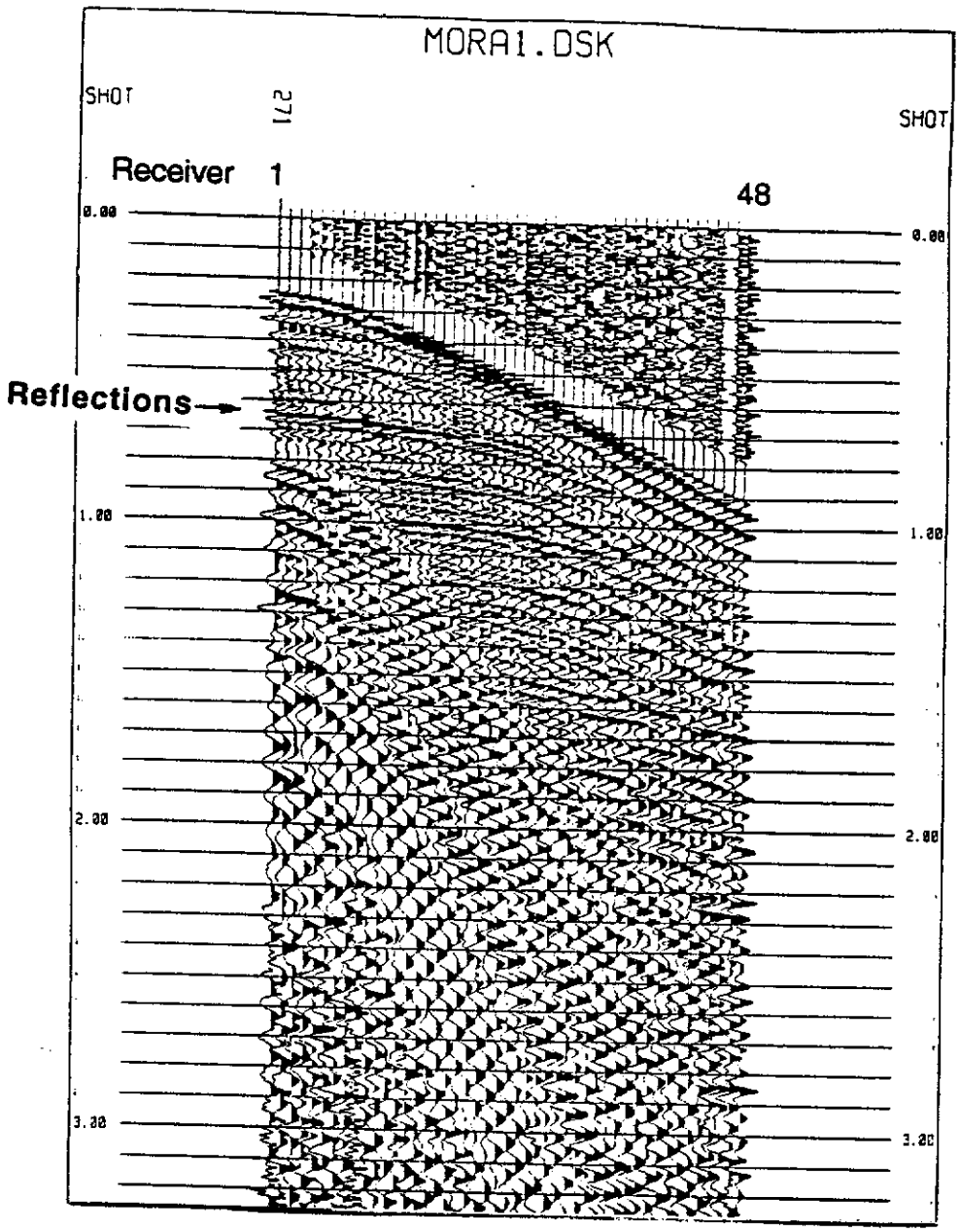

Figure 2.5. Moora 3-D field record with the shot lateral to the receiver line. There is a 411 m offset distance from the source to the nearest receiver station 1, increasing to a far offset distance of 1652 m at receiver 48. The in-line station interval was 34 m. Because the source location is offset from the receiver line, the source/receiver offset distance changes by 4 m for the nearest two receiver stations, and by 33 m for the farthest two receiver stations. This change in 'radial offset' increment results in the surface wave appearing to flatten at the near offsets, becoming linearly dipping with radial offset increase. (from Stewart and Evans, 1989).

The Moora shot records of Figures 2.3 and 2.5 show how the surface waves mask useful reflections. The curved surface wave arrival on Figure 2.5 indicates that surface waves can have near offset move-out which is similar in appearance to reflections. The situation is exacerbated in 3-D high resolution seismic recording for coal seam imaging, where lateral offsets can be large relative to the receiver line length. This causes surface wave curvature on a shot record to show a "flat" appearance similar to that of reflections.

For example, a 3-D survey was recorded using a MiniSosie source at German Creek, Queensland during 1989 where surface and reflected waves had similar frequency content (Lambourne et al., 1991). At the far offsets, the reflections had a similar apparent velocity, move-out and frequency to the surface wave. However the reflections had a lower amplitude and therefore were totally masked by the surface waves.

A 3-D shot record from that survey is shown as Figure 2.6 which shows a plan view of the shot and receiver geometry as well as the resulting record. The surface wave indicated at 'B' and a weak reflection at 'A' are similarly positioned on the record. The separation of such reflections from surface waves requires an approach which can be applied from shot record to shot record, with a minimum of field or processor interaction.

The application of transform methods for shot record events followed by filtering in a transform domain (such as the F/K transform) often work best on linear events. However in 3-D shot records, surface wave events are not linear at the near offsets, so the transform methods are not ideal. Filtering in transform domains is often based upon surface wave trains having a linear appearance on the shot records, and this is not the case where the swath source constantly moves with respect to a static receiver line. The greater the lateral source offset from the receiver line, the flatter and more reflection-like the surface wave event curvature becomes.

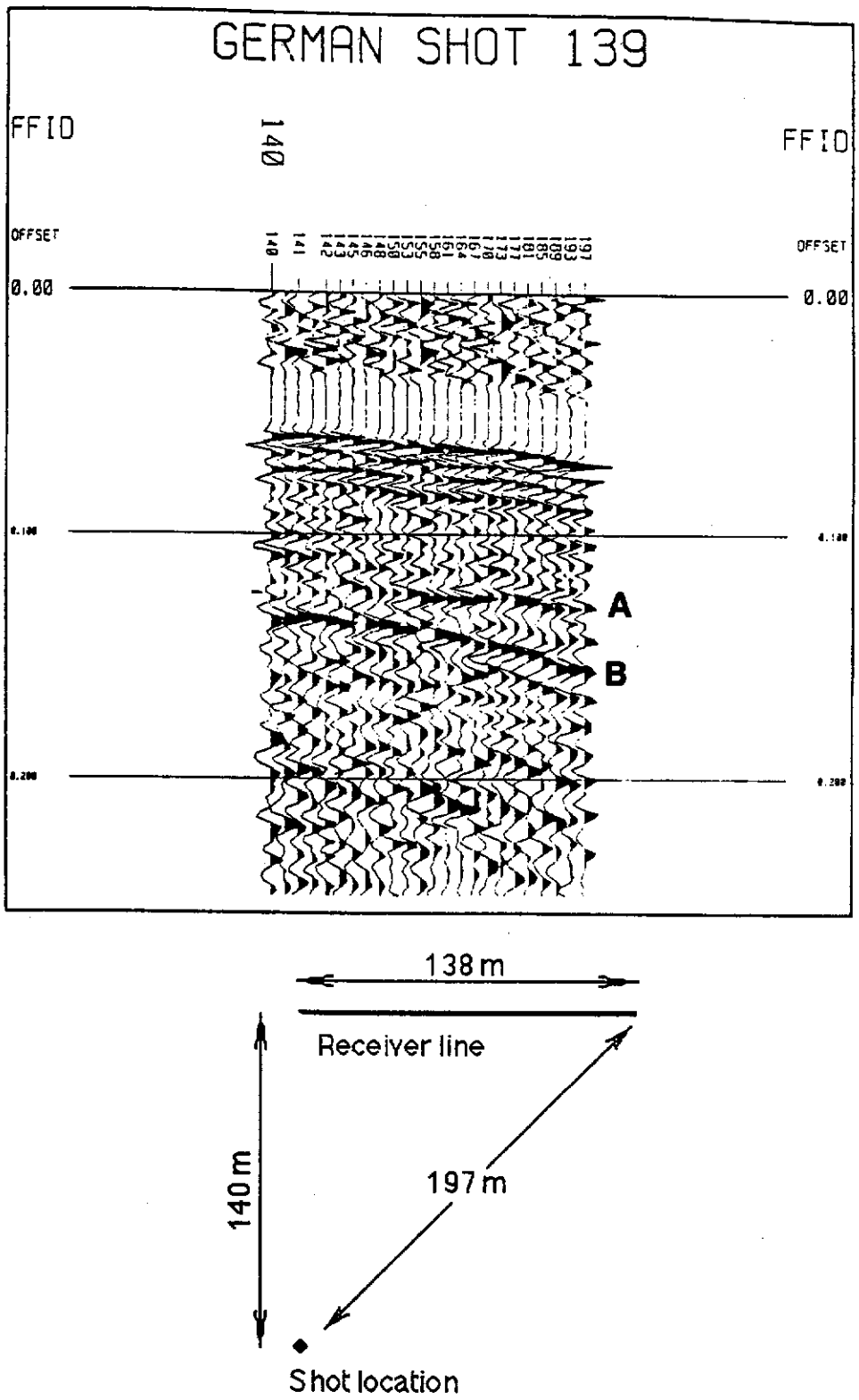

Figure 2.6. German Creek 3-D shot record and lay-out plan view. The near source/receiver offset was 140 m and the far source/receiver offset was 197 m. The in-line station interval was 6 m and the line length was 138 m. The shot lateral offset distance was equivalent to the line length. In the shot record, a surface wave at 'B' and a weak reflection at 'A' are similarly positioned on the record. They have similar frequency content and move-out.

Another common approach is the use of an f-x transform where t-x data are transformed into the frequency and offset domain (Goebel and Evans, 1987). Again, such transformations do not work well if the frequency content of reflections and surface waves is similar.

One solution could be the application of the tau-p transform (Diebold and Stoffa, 1981). This operates on 2-D in-line data along linear trajectories in t-x space to produce reflections with an ellipsoidal shape in the tau-p domain. Surface wave data concentrate at a point in the intercept time-slowness domain. However, this technique does not cater for the constantly changing curvature of surface waves, which change the appearance of wave arrivals on shot records, due to the changing source/receiver offset increments and azimuths used in 3-D surveying. An alternative method is desirable which can cater for record by record changes.

2.3 Conventional 3-D land seismic compared with LOFOLD3-D.

The conventional approach to recording land 2-D seismic data is to align the source and receivers along the desired profile. The source may be located in the centre of the receiver line, symmetrically or asymmetrically positioned in split-spread manner or off one end of the receiver spread.

In 3-D land surveying, the source may be placed anywhere with respect to the receiver line, provided the location of each is known. For example, a vibrator may be moved along a few receiver lines laid on the ground parallel to each other as shown in Figure 2.7. When the vibrator moves parallel with the dominant receiver line direction, this configuration is known as the 'in-line' recording approach (Lansley and Gonzalez, 1992). Because most receivers are along the same line direction as the vibrators, the dominant raypaths from source to receivers are in-line. Consequently, the in-line approach generally produces oblong single fold volumes from each cable lay-out as shown in Figure 2.8. Single fold is shown as a result of the first shot point, then additional fold occurs when the source moves along the line to the next shot point, and so on. Fold increases in-line at first, then it increases across the line direction ('cross-line') as more parallel receiver lines are added.

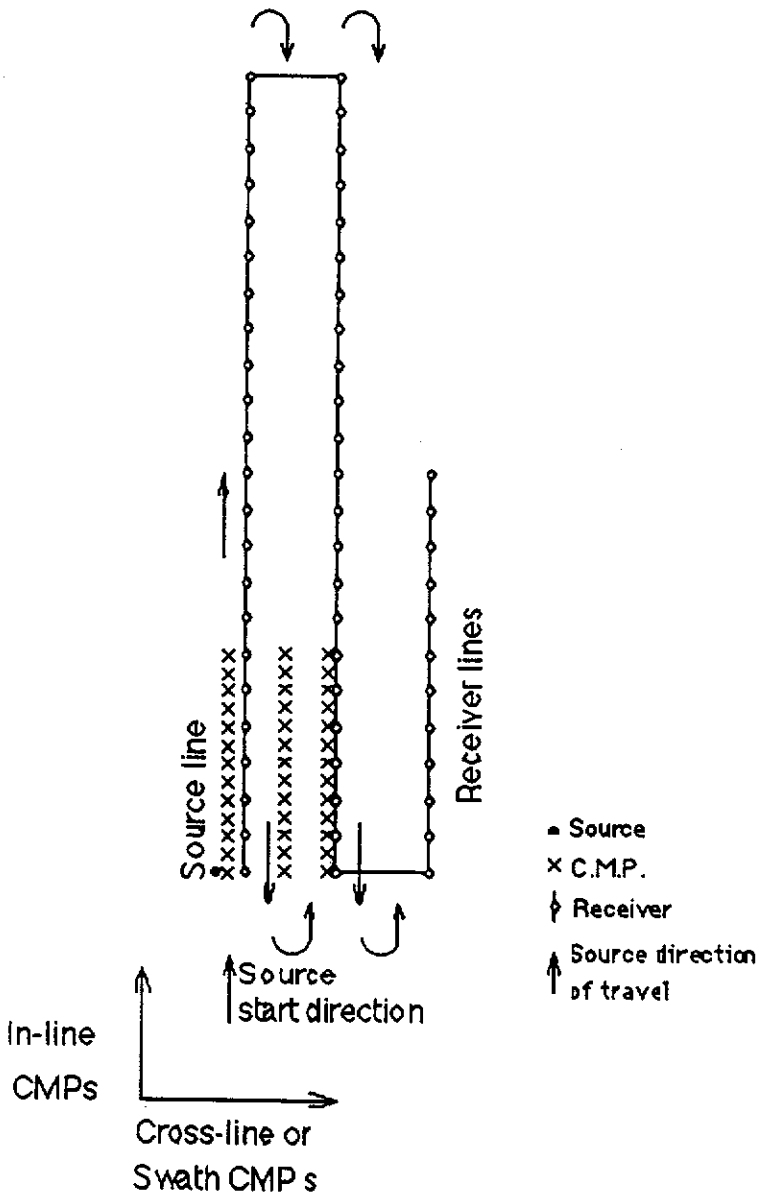

Figure 2.7. Land in-line 3-D recording in which the source moves parallel with the receiver line direction. This produces CMP lines in the in-line and cross-line directions. The source travels from the start point, moves up the line to the end, and turns around to move down the line, as shown by the arrows. The number of receiver lines depends on the number of recording channels available in the recording instruments. As the source moves in the in-line direction, in-line CMPs increase. When more receiver lines are added, the source generates more 'cross-line' or swath CMPs.

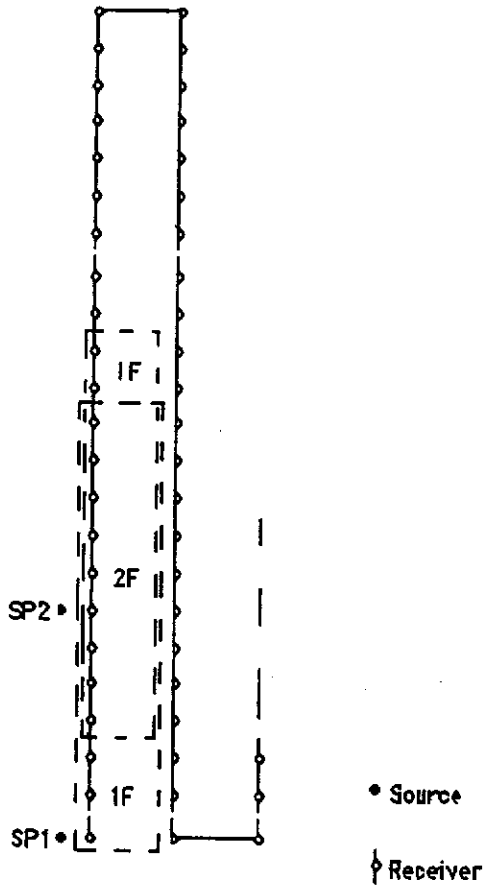

Figure 2.8. The build up in fold as the in-line recording method moves from shot point 1 to shot point 2. Each shot point produces a single fold volume (1F), which overlap near shot point 2 causing the fold in the overlapping area to increase to two fold (2F). Overlapping in this manner, the in-line method builds up fold to the required level. Azimuths are still dominantly in the in-line direction. The resulting CMP volume from a single shot point is of oblong shape as shown, with source to receiver azimuths dominantly in the in-line direction from the shot location.

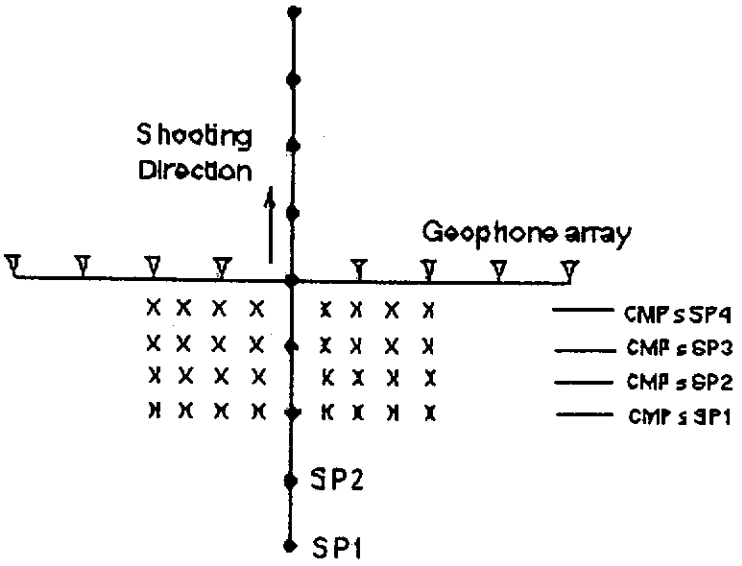

Figure 2.9(a).Crossed-array recording in which the source line direction is orthogonal to the receiver line direction. Each individual shot produces a single fold CMP line parallel with the receiver line. Firing all shot points on the source line, produces a single fold volume which is rectangular in shape. In this case, shot to receiver azimuths are in all directions.

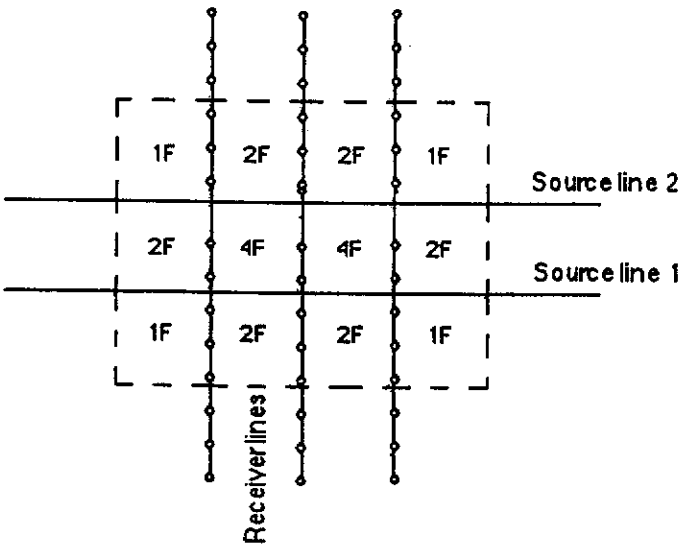

Figure 2.9(b). If a second source line were fired into three receiver lines, then a LOFOLD3-D volume ranging in fold from 1 to 6 is built.

Alternatively, when the source moves orthogonally across the receiver lines, as shown in Figure 2.9(a), this is the 'crossed-array' approach. The crossed-array technique (which is most often used when there is a small number of channels) has been compared to the in-line approach (Walton, 1972), and both methods give equivalent results at comparable cost. In crossed-array data collection, the raypaths have a broader range of azimuths since in-line as well as cross-line CMPs are recorded for each individual shot point. When the source moves across such receiver lines, square single fold volumes are produced from each cable lay-out, and as more receivers are added, the fold increases, as shown in Figure 2.9(b).

The preferred method for commercial vibroseis operations using many recording channels has been the in-line approach, since it offers a minimum number of seismic cables laying on the ground to be crossed compared with the crossed-array approach (cables are laid out in long parallel lengths). The in-line method also allows the normal roll-along sequence to occur, because the roll-along switch may address two receiver lines at a time, and after each vibrator has moved to the end of each receiver line, the roll-along switch then rolls one line of stations. Such a sequence is very familiar to 2-D recording crew operations.

In-line recording therefore lends itself to faster field operations than the crossed-array method, and therefore more profit for the contractor. Because there is a large build up in fold in the in-line direction when the source is rolled along the line from one end to the other, the in-line recording method allows the application of 2-D stacking and 2-D DMO processing along the in-line CMP lines (Lansley and Gonzalez, 1992), which is not readily applied in the crossed-array approach.

The basis of the LOFOLD3-D method is to reduce the cost of recording and processing 3-D data, while retaining the same final interpretation integrity as that for a high fold method. A reduction in the number of instrument recording channels also results in a cost saving. The LOFOLD3-D method therefore favours the use of the crossed-array approach, in which squares of single fold overlapping volumes are built over a smaller area than that commonly associated with the in-line approach. In mining applications, explosive is a commonly used and an available commodity. Consequently, the crossed-array approach using explosive as a source, is the most commonly adopted LOFOLD3-D method in mining 3-D surveys.

The crossed-array method results in a greater range of azimuths per CMP trace than that of the in-line technique, which is good for improved data quality. Comparisons of land 3-D data sets using various arrival azimuths have shown that when there is a large range of azimuths in 3-D CMP bins, the signal-to-noise ratio is higher than that using a restricted range of azimuths (Lansley and Gonzalez, 1992).

2.4 Field experiments

The original concept of recording a low fold volume of data was discussed by McDonald et al. (1981), where a single fold survey over a horizontal model containing an acoustic anomaly was successfully used to delineate the areal extent of the anomaly. The method was extended to image a pinnacle reef in a carbonate sequence in Northern Michigan (McDonald et al., 1981).

During 1984, funds were obtained from a consortium of exploration companies and a Western Australian Government instrumentality to perform field experiments, to test the applicability of LOFOLD3-D to Australian oil field development. The first published field test of the LOFOLD3-D method used four fold data to partially delineate a fault between two wells over the Woodada gas field, Perth Basin (Frey, 1986). The major problem was that of weak reflections caused by near surface limestone and sand dunes, but the data were adequate to form an interpretation (Evans et al., 1987). Learning from that experience, another field experiment was later performed north of Moora in the Perth Basin, where neither near surface limestone nor sand dunes were present. The data quality was better than at Woodada, and a comparison of the two surveys provided an indication of the minimum signal-to-noise ratio required for a confident interpretation (Evans, 1988).

The major difficulties of the LOFOLD3-D method:

There were two major difficulties associated with the LOFOLD3-D method:
(i) The average coherent signal-to-noise ratio required enhancement to a minimum level of 2.5 : 1 (Evans, 1988). Such enhancements could be performed in the field or processing centre by processing enhancements which were possible through the use of linearization filtering (Jervis et al.,1987) and by the improvement in residual statics corrections.

(ii) The problem of performing a velocity analysis on a small number of traces in a bin, when dip is present. The problem is that when dip is present, the apparent dip changes with source to receiver azimuth, and this can change the stacking velocity of each source/receiver pair in a bin. This problem may be overcome if a normal move-out expression is determined which separates the medium velocity from dip in the NMO equation, for each pair.

Subsequent to the research project testing the use of the LOFOLD3-D method over deeper oil exploration regions, a Federal grant allowed the application of the method on shallower, higher signal-to-noise ratio data in Australian coal fields. Coal has a higher reflection coefficient than most other sedimentary horizons (therefore providing a stronger reflection signal than other geology), and the application of low fold seismic to such geology had the potential to yield higher signal-to-noise ratios.

However, other problems became apparent with the application of LOFOLD3-D to higher resolution recording. In high resolution recording, changes in weathering lithology (such as high velocity lenses) or structural alterations (such as near surface faults) cause delays to or dissipation of the seismic energy as it travels from the source to the receivers. While this "statics" problem is partially resolved in multifold 2-D recording, something more was necessary to overcome the reduction in signal-to-noise ratio when using even less traces adopted by the LOFOLD3-D method. A method was required to improve the residual statics corrections.

The LOFOLD3-D method was thereafter tested at the Appin colliery site in the Sydney Basin (amongst others), and at the German Creek mine (amongst others) in the Bowen Basin. Different processing steps were applied in each case history, with the optimum case history being at Appin where a complex scissor fault was interpreted. Subsequent drilling at Appin mine site confirmed the fault interpretation. These surveys were conducted by the author, and provide case studies from which data will be shown later in this thesis.

2.5 The effect of 3-D dip on 3-D surveying

If the dip increases beneath a linear profile in the direction of the profile, the reflection points, which were midway between source and receiver, move

up-dip (Figure 2.10). To quote Sheriff (1991), "NMO corrects for the time delay on an offset trace assuming horizontality; DMO moves the data to the correct zero-offset trace for a dipping reflection; migration further moves it to the subsurface location".

When the dip of the reflecting layer is no longer in the plane of the profile, the stacking process moves traces along some other profile line. Thus, the dip of a reflection displayed on a stacked section is not necessarily the true dip of the reflecting horizon but an apparent dip. The true dip cannot be obtained from a single profile, since the assumption is that the reflection takes place in the plane containing the source, receiver and the normal to the reflecting surface. Thus, for out-of-the-line profile reflections from dipping planes, the displayed dip cannot be correct.

To resolve this problem, a different approach to recording out-of-the-line profile reflections is to record CMP lines resulting from using parallel source and receiver lines (Figure 2.11). In what is known as 'swath recording' of seismic data (Sheriff, 1991), each source/receiver pair in a particular gather has a different azimuth.

As pointed out above, when the dip is in the direction of the profile, the reflection points move up-dip (Levin, 1971). If a swath line has source and receiver lines in the true dip direction, reflection points move up-dip. They lie in a plane orthogonal to the reflector containing each source and receiver (Figure 2.12).

If the true dip is orthogonal to the receiver line, the reflection point would move up-dip between each source/receiver pair (in plan view, towards the source line in Figure 2.13).

For in-line recording where the reflecting horizon is horizontal, the reflection points are mid-way between source and receivers. But if the reflecting horizon is dipping, reflection points move up-dip by an amount dependent upon the true dip. This can be shown by a simple diagram adopting the method of images, and constructing lines from the image point to each individual receiver (Figure 2.14). The reflection point increment δx increases in the up-dip direction.

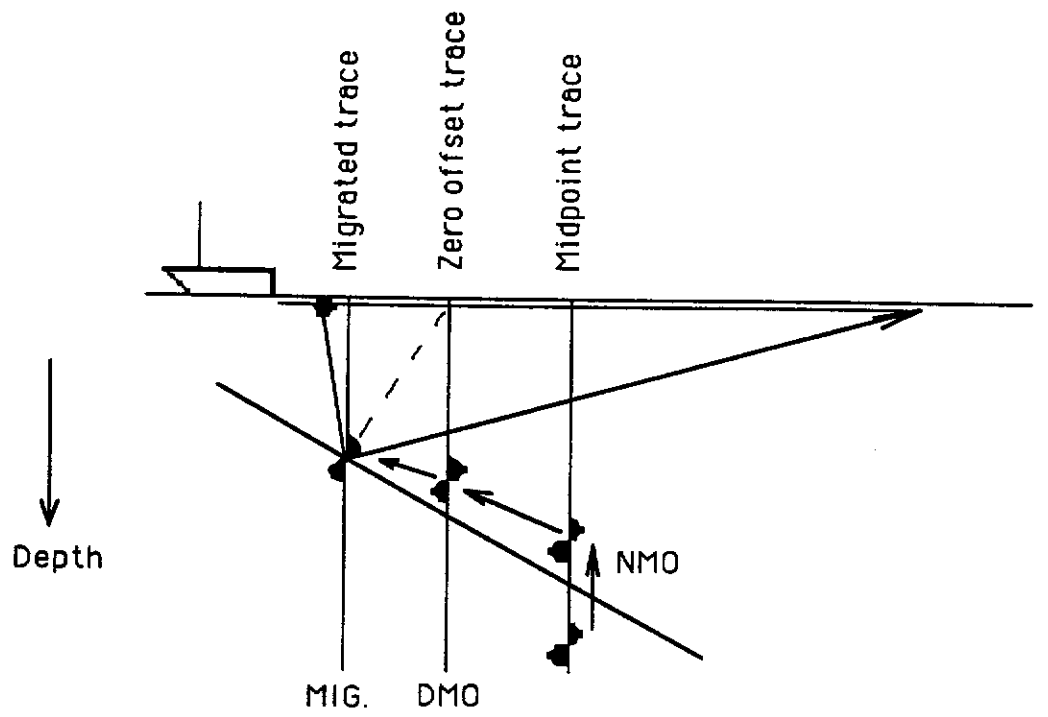

Figure 2.10. Dip Moveout (DMO) processing. The single lines with peak and trough pairs represent seismic traces. After application of NMO corrections, DMO application moves data to the correct zero-offset trace for a dipping reflection; migration further moves it to the correct subsurface location (after Deregowski, 1986).

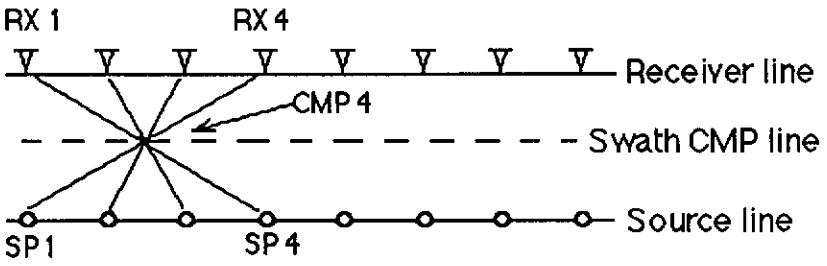

PLAN VIEW

Figure 2.11. Swath CMP recording. This uses parallel source and receiver lines to generate a CMP line mid-way between source and receiver locations. CMP bin traces for example, would be those traces recorded by firing shot at SP1 into the receiver at RX4, SP2 into RX3, SP3 into RX2 and SP4 into RX1 to produce a four fold CMP 4 gather as shown.

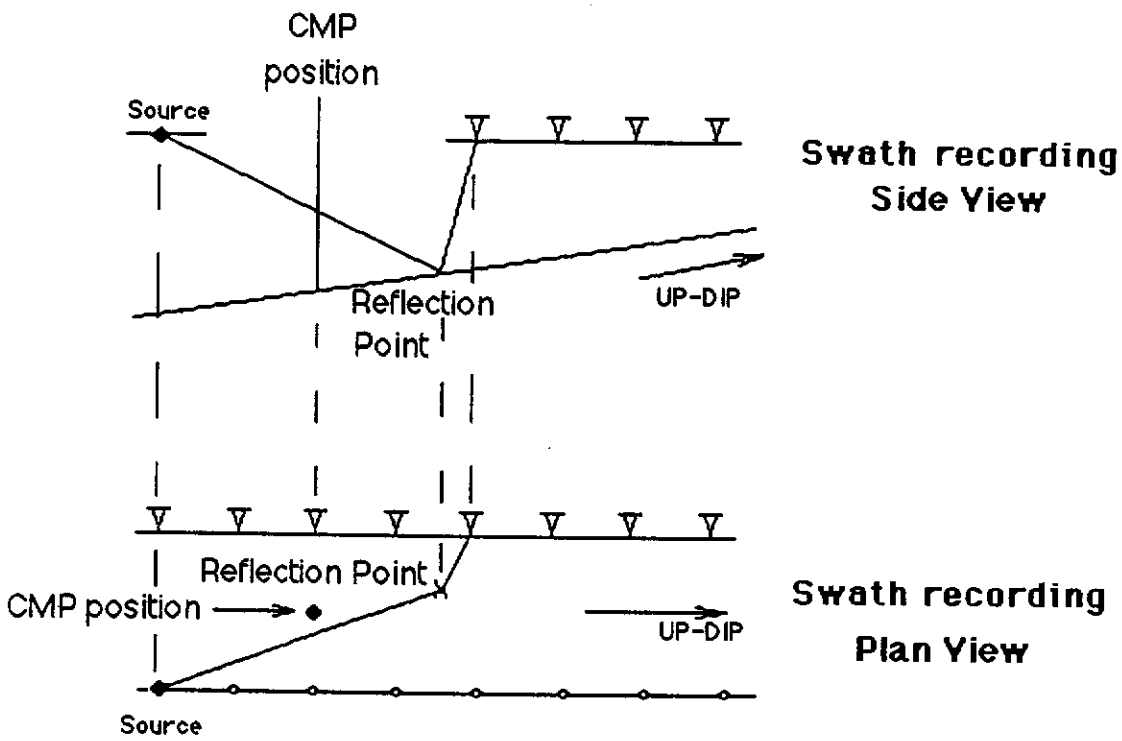

Figure 2.12. Raypath for up-dip swath recording, showing the side and plan views. In such swath recording where there is a variable azimuth between the source and each receiver, the reflection point between each source/receiver pair has a component in the up-dip and strike directions. Consequently in the above case, the reflection point moves up-dip and strike towards the receiver.

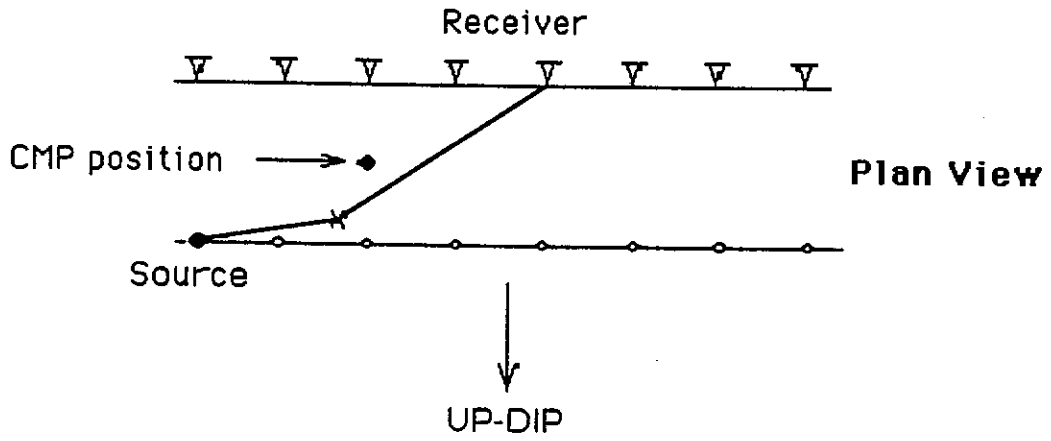

Figure 2.13. Raypath showing the reflection point movement up-dip, when the source/receiver pair are positioned along a plane orthogonal to the true dip direction. The reflection point moves up-dip towards the source line.

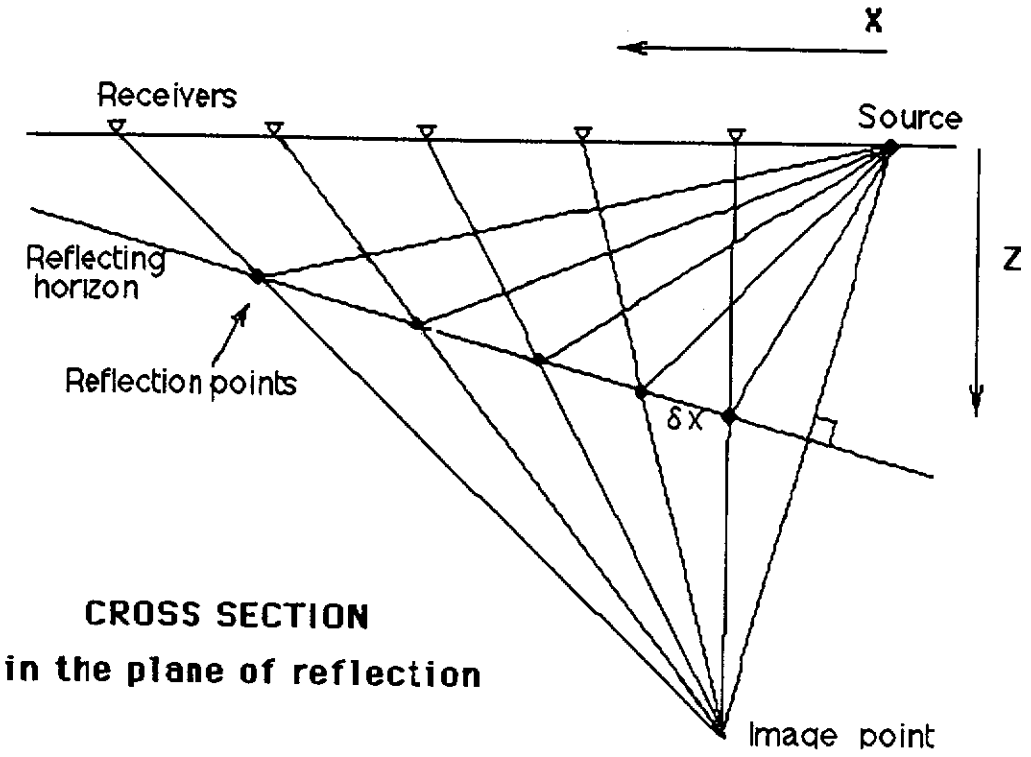

Figure 2.14. The reflection point moves up-dip in different increments. This is shown by an increase in δx from right to left, increasing the farther up-dip the reflection location.

In both swath and LOFOLD3-D recording, the reflection point line for any single shot into many receivers will therefore no longer be parallel to the source line, but could be positioned as shown in Figure 2.15.

The net product is a line for each shot gather which is not parallel with the CMP line (Figure 2.15). Consequently, reflection points are no longer located at common mid-points, resulting in a slight variation in stacking velocity per binned trace. In practice, it is common to perform a velocity analysis on all of the binned traces to determine a single optimum stacking velocity to align all of the traces. However, LOFOLD3-D cannot perform such an analysis using just a few traces, and therefore needs some other approach.

It is accepted that if the true dip and its azimuth could be obtained prior to conducting a 3-D survey (assuming that the dip does not change a great deal over the survey area), then survey lines could be positioned in a direction for optimum data collection (such as parallel with the maximum dip direction). If the true dip and azimuth are known, it may then be feasible to include the three-dimensional term in a generalised moveout correction for each separate CMP trace in a CMP bin. The moveout correction may then have a constant stacking velocity, allowing the application of a moveout which accounts for a variable source/receiver location, thereby removing the problem of variable stacking velocities of traces in each bin. The LOFOLD3-D method requires such an approach, particularly since there are very few CMP traces with which a velocity analysis can be performed.

2.6 An approach to resolving these problems.

The problems facing the LOFOLD3-D technique for the acquisition of cost effective 3-D data are:

(i) the inability to attenuate strong surface wave arrivals which have a curved profile on shot records and resemble reflections on shot records, and

(ii) the inability to obtain accurate statics corrections using a small number of traces. This is of greater importance in shallow, high resolution recording than in deeper data recording where frequency content is lower, and

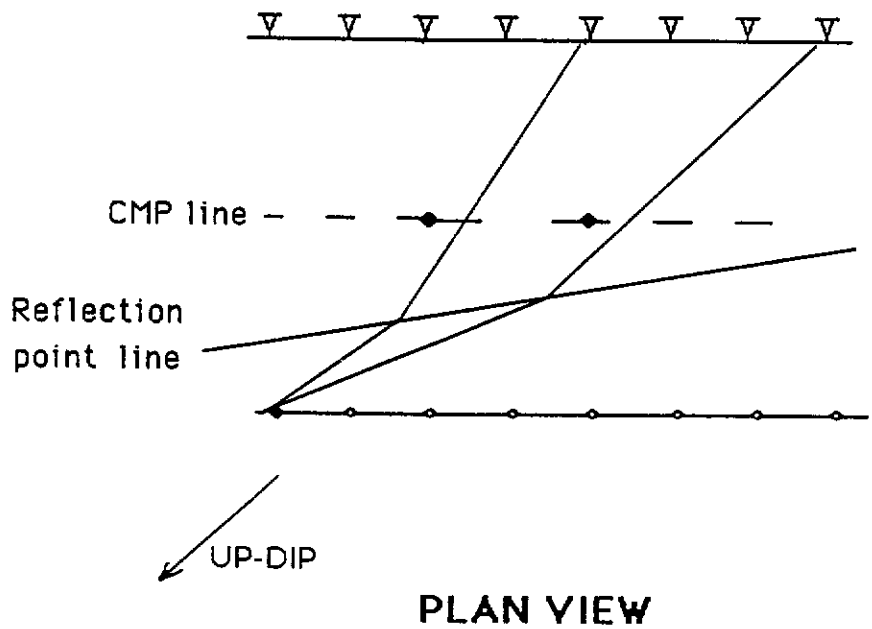

Figure 2.15. Raypaths for a swath line recording, in which the reflection points move up-dip for two chosen shot/receiver pairs. The reflection point line is no longer along the CMP line, as each individual reflection point moves up-dip.

(iii) the inability to determine stacking velocities because of the small number of traces in each bin, and their variation in azimuth.

The solutions to these problems and advancements in the method of LOFOLD3-D surveying developed in this thesis are as follows. First, a transformation of shot record data is proposed that could allow for the curvature of the recorded surface wave events (Figures 2.5 and 2.6) in 3-D or swath surveys. Then it may be possible to filter the data in the transform domain to separate, attenuate or even eliminate the surface waves from reflections on shot records. This would produce a shot record with an improved signal-to-noise ratio ready for further processing. Subsequent chapters will use the stacking technique of the τ-p transform, but modifying it to accommodate the non-linear curve of surface wave arrivals on shot records.

Second, a method for improving the statics estimation is devised which works on the basis that the refracted wave path is similar to the reflection wave path. Then processing techniques customarily used for improving reflection continuity may be applied to align refractions, and in so doing, may align reflections also.

Third, if the true three-dimensional dip and its azimuth could be determined in the field prior to or during recording, then the value of dip could be included separately in a generalised moveout calculation for each source/receiver pair. A single stacking velocity function independent of dip may then be used to correctly image the gathered traces.

In order to test the transformation of surface wave data, numerical and field data sets were used. It was not readily possible to test the dip and azimuth prediction method in the field since it was expensive to record field data. Partly for this purpose, a physical modelling facility was built in which the various field recording configurations could be tested. Because the physical modelling method was used to test both the surface wave transform and dip detection advancements, it is now necessary to describe the modelling system, which was specifically built by the author for such tests.

CHAPTER 3
The use of Physical Modelling.

This Chapter provides the background history and development of physical modelling of geological structures. It compares the physical modelling approach to that of numerical modelling, and then describes the physical modelling system built by the author. Physical model parameters, such as scaling of models is discussed, as well as seismic wave characteristics in models and a terminology convention for describing the manner in which models would be tested.

The physical modelling approach was chosen to test 3-D concepts, because model data possess accurate three-dimensional wave-field propagation effects, and physical modelling more closely simulates field data than numerical modelling. As such, physical model data provide a better test of new techniques than numerical model data do. Furthermore, physical models can be constructed with known three-dimensional structures and velocity parameters, so that structural and velocity information is better known than in field situations.

This Chapter therefore provides a description of experimental methods for obtaining synthetic field data, which would act as a test data set replacement for field data otherwise difficult to obtain under controlled experimental conditions.

3.1 Background

The first recording of the physical modelling of seismic wave propagation was performed at the Institute of Theoretical Geophysics in Russia, during 1945. An overview is provided of that work by Riznichenko (1966), since previous publications were inaccessible to other researchers (they were in Russian). The initial models used weights to impact discrete rubber nets, but these were abandoned since it was difficult to understand the wave propagation patterns of the generated waves. Riznichenko (1966) states that in 1951, he replaced the nets with liquid/solid layering, and using ultrasonic transducers, produced analog records of seismic arrivals. This was followed soon after by the first papers in English by Howes et al. (1953) and Northwood and Anderson (1953), describing their similar analog work with ultrasonic transducers. Most of such research was directed at

understanding seismic wave propagation with a global setting, and consequently much of the work simulated solid crustal boundaries (using metal plates glued together) with liquids beneath. Other Russian researchers moved on to use epoxy resins and rubbers, and to study wave passage through thin layers and wave-guides.

Ivakin (1966) provided a short introduction to 2-D and the use of 3-D models, along with the problems of modelling using different transmission frequencies. O'Brien and Symes (1971) provided the basic approach to the model building and recording methods used.

Maginness (1972) published the first numerical analysis of waves using physical modelling methods. He offered a numerical solution to integral equations, describing the wave motion. Walton (1972) demonstrated the possibilities of 3-D data acquisition of seismic data, while French (1974) was the first to apply the modelling approach to seismic exploration over 3-D physical models representing simple structures. He showed that the diffractions or reflections that emanated from points beneath the line of profile could be collapsed or imaged reasonably well by two-dimensional (2-D) migration, but reflections originating from outside of the line of profile could not be properly imaged.

The basic principles of physical modelling have been described by McDonald and Gardner (1983). Pant et al. (1988) provide a good introduction to 2-D modelling, Menke and Dubendorff (1989) provide good amplitude studies, while the most comprehensive overview of physical modelling papers was provided more recently by Ebrom and McDonald (1994).

In 1991, a three-dimensional physical scale modelling system (Evans and Urosevic, 1993) was built at the University of Houston and shipped to Curtin University, where it was reassembled in 1992. The system uses ultrasonic transducers to transmit and receive seismic waves. The transducers are in physical contact with the models which may be made of any suitable solid. The transducers are computer controlled in space in terms of x, y and z position. All measurements are automated for temporal and spatial efficiency and accuracy.

3.2 Physical versus numerical modelling.

Physical modelling of seismic data has definite advantages over numerical ray theory modelling. The benefits of physical modelling are as follows.

(i) Physical modelling in this system is always three-dimensional, whereas numerical modelling is generally two-dimensional. Three-dimensional numerical modelling takes prohibitively long computer times even on the world's fastest computers.

(ii) Physical models generate all of the waves resulting from wave-field conversions at interfaces, whereas numerical modelling programs often require the input of wave types and locations where conversions are expected to occur (finite difference models offer alternative methods).

(iii) Physical modelling allows the use of polarised sources and receivers, which can be physically rotated to observe their transmission effects through media such as fractures. This is prohibitively expensive and not commonly available with numerical modelling.

(iv) Physical models naturally produce refractions and diffractions. In contrast, most commercial software requires a decision on whether or not to compute refractions or diffractions in numerical models, since their production requires major computer power and often takes an inordinately long time to compute.

(v) Physical modelling allows the source to be immersed in liquids to model marine seismic recording realistically, and enables the realistic simulation of sea-bed wave-field conversions, which is not readily matched by numerical modelling simulations.

(vi) Physical modelling more accurately simulates wave transmission in the real world, whereas numerical modelling may truncate transmission effects to improve the speed of computation (such as limiting the ray capture radius in ray tracing).

(vii) Physical models generate all the noise problems, such as surface waves, typical of real world seismic data acquisition, whereas numerical models produce simplistic noise free data.

(viii) Transmission effects such as absorption and scattering occur naturally in physical modelling, whereas in numerical modelling absorption has to be estimated whereas scattering is frequently ignored. Consequently, numerical modelling often yields data having excessively high signal-to-noise ratios, beyond those encountered naturally.

(ix) The three-dimensional radiation pattern inherent in field sources and receivers is prevalent in physical modelling too, whereas they are commonly ignored in numerical modelling.

3.3 Physical modelling equipment and recording procedures.

The data acquisition system comprises ultrasonic source and receiver transducers. Those used in this research, had an operating centre frequency of 450 kHz. The impulse response of the Curtin system changes with transducer type, and the pair used for this research could duplicate the response of a zero phase wavelet. However, since only traveltime was of interest in this research, phase relationships were not a concern.

As shown in the schematic diagram of Figure 3.1, a transmit trigger is passed from the personal computer to a pulser transmitter amplifier, which supplies a positive-going leading voltage level at 125 volts to force the piezo-electric crystal transmitter to vibrate. The receiver crystal transducer is connected to a receiver amplifier. The personal computer also supplies the trigger to a 12-bit Nicolet analog-to-digital (A/D) converter oscilloscope. Thus, when the computer triggers the pulser transmitter amplifier, it also triggers the Nicolet to commence sampling and A/D conversion of input received data from the receiver amplifier. The source/receiver firing sequence is therefore controlled by the computer, which ensures that the transmitter fires at the same time instant as sampling and digitisation commences. The received digitised data is then displayed on the Nicolet oscilloscope and also on the computer video display terminal (for quality control checks of the recorded data).

The transducer movement is computer controlled by the use of robotic indexers controlling stepping motors. The computer executes movement sequences after a geometry program has specified where the transducers are to be positioned in space. The geometry program allows the user to input required positional information for both source and receiver transducers. Once the geometry program is activated, the main program provides logic voltages to six motor controllers. The controllers provide 110 volts to six D.C. motors, which rotate steel screws connected to the transducer holders.

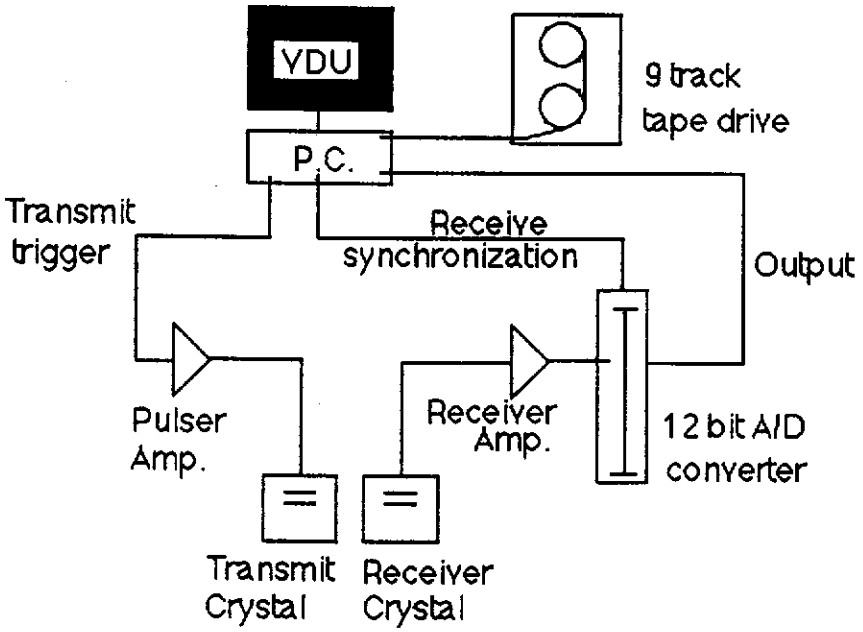

Figure 3.1. Schematic diagram of the recording design of the physical modelling system. The personal computer (PC) controls the seismic wave initiation, and recording of the physical model data. A real time display of the collected data is shown on the visual display unit (VDU) for quality control purposes. The transducers are positioned on the model.

The transducers are positioned in physical contact with the solid model enabling the generation of elastic waves. Prior to commencement of seismic data acquisition, the two transducers are manually placed at the initial desired locations. The geometry program is then set to call the motor indexers to drive the transducers to their subsequent locations away from the starting locations. Due to random noise occurrence, it is sometimes necessary to stack recorded data vertically. This is readily achieved through the geometry program (positioning accuracy around 5 m scaled).

Having loaded the geometry program and positioned the transducers at their starting locations, it is then possible to commence recording. The general procedure is as follows:

1. The geometry program requests the recording program to trigger the pulser unit.
2. The pulser transmits a voltage to the source transducer which then emits a 450 kHz pulse into the physical model.
3. The piezo-electric receiver transducer crystal undergoes strain caused by the arriving seismic wave. The resulting electrical signal is then amplified and passed on to the Nicolet oscilloscope.
4. The analog data are displayed on the oscilloscope screen and the computer terminal, during which time the data are also converted from analog to digital and recorded on disk.
5. Further shots may then be fired and displayed with the transducers in the same location to allow for later vertical stack summation processing.
6. Having completed a suite of shots at one location, the geometry program then commands the motor controllers to move the transducers to their next location. The system has two x, y and z-axis drive screw sets (one for the source transducer and the other for the receiver transducer), which allow movement of transducers, up in the z direction, and along in x and y directions.
7. The geometry program may then direct the x-axis motor to step the source transducer along either x or y-axis direction by the programmed source interval distance.
8. The vertical source transducer motor controls the transducer contact with the model. The transducer is normally raised during lateral repositioning.
9. After each shot is fired, sources and receiver transducers are re-positioned as pre-determined by the geometry program. In this way, an

entire seismic survey may be automatically recorded. After survey completion, the geometry program terminates the recording sequence.

The digitised data may either be written to tape using a flat-bed 9-track tape drive connected to the computer and the converter, or transmitted across the network to a workstation disk (the network is a recent development so for this thesis, all data were written to tape). During recording, the converter accepts the 12-bit data, and writes it in SEG-Y format on tape, including geometry information.

3.4 Scaling of physical model parameters

The concepts of scaling for seismic physical modelling have been discussed in detail by McDonald et al. (1983). Typically, experiments which have a length scale of 1:40,000 and a time scale of 1:10,000 would have a velocity scale of 1: 4. Throughout this dissertation, only "real" units will be quoted; for example, 1 cm in the model world is equivalent to 400 m in the "real" world and similarly a "model" frequency of 450 kHz would be 45 Hz in the "real" world. High model frequencies necessitate a short sample interval of 0.1 microseconds, which corresponds to 1 millisecond.

When written to tape in SEGY format the scales in length and time become invisible to the seismic processing software. At this time all data appear to be "real" world data.

3.5 Propagation of waves in a physical model

Provided that the chosen modelling material is relatively elastic and has low attenuation, it will transmit all of the seismic waves expected under field conditions, exhibiting similar seismic behaviour to those found in elastic geological structures.

A common model material used is an acrylic resin with the brand name 'Plexiglas'. In Plexiglas, the actual compressional (or P-) wave velocity is 2,666 m/s, whereas the surface wave velocity is 1,300 m/s for an air interface, which is similar to the shear (or S-) wave velocity. By placing a shear wave transducer (polarised in the vertical direction) at one end of a Plexiglas slab, the retrograde elliptical particle motion of surface waves appears as vertical motion on the end of the slab. Similarly, S- waves can

be detected by placing a shear wave transducer oriented radially or transverse, on the upper surface of a Plexiglas slab.

Converted waves (P to S) are also detectable by their particle motion, and it is possible to transmit shear waves from the surface by the use of a compressional transducer source. Consequently, different events can be recognised by their velocity and particle motion.

The objective with the modelling system in this thesis was to generate a representative 3-D data set with defined characteristics, on a model of known dimensions, in seeking the solution to the problem of azimuthally dependent stacking velocities. As a result, a Plexiglas model was used to simulate typically desirable field characteristics, such as reflected waves. However, such a model can also simulate undesirable characteristics, such as surface waves. For the purpose of this research, surface waves were unwanted effects. This research therefore utilised the same physical model to carry out experiments to observe the attenuation of surface wave noise in data recorded over the model, prior to application of other transformation methods.

3.6 A specific model and sign convention

For the purposes of this research, a simple model was required of a suitable scale to be manageable in the laboratory, while having realistic field proportions. A reflection from a depth of 2 km was a desirable attribute to simulate real world geology, and the model block had to be sufficiently large to obtain vertically reflected arrivals before unwanted arrivals horizontally reflected from the sides of the Plexiglas block. The reflecting horizon had to be dipping, to satisfy the demands of this research. A block with the dimensions of 30 cm by 25 cm by 7.8 cm was used. Using a length scale factor of 1:40,000, this represented real world dimensions of 12 km by 10 km by 3.12 km thick. The model had a 5 degree dip machined in its base (Figure 3.2).

In order to observe reflecting waves from different dip directions, it was possible to physically rotate the model by a nominated amount, in order to repeat the recording sequence over models of different dip. It was not possible to rotate the transducer positioning system, due to the supporting steel structure of the transducer movement mechanism.

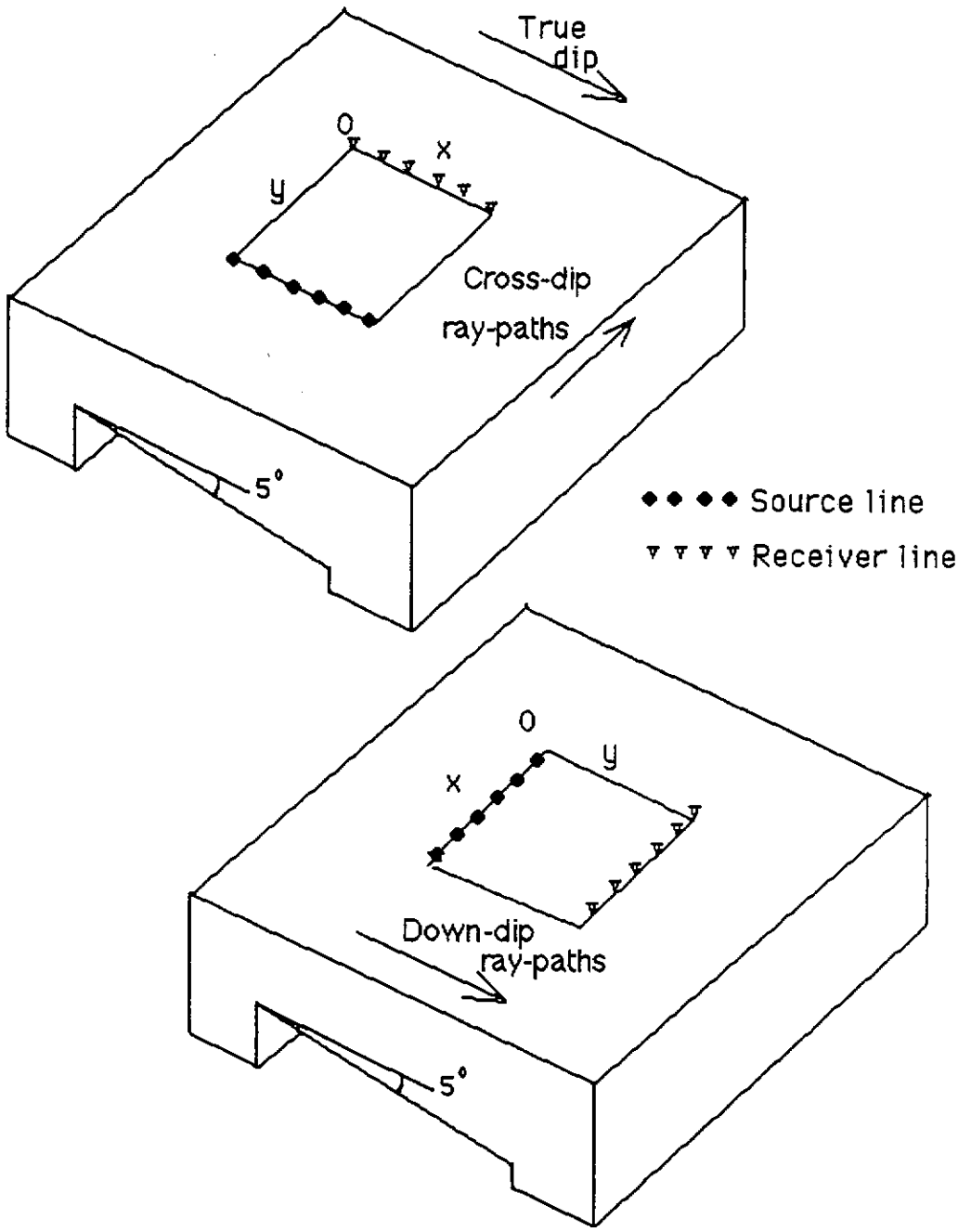

Figure 3.2. Physical model made of acrylic used for data acquisition. The model had a 5 degree dip machined into its base. 'Cross-dip' recording occurred when the source and receiver lines were positioned along the true dip direction, in which most ray-paths were across the dip direction (i.e., generally along strike). 'Down-dip' recording was orthogonal to cross-dip, and occurred when the source and receiver lines were positioned along the strike direction so that the dominant ray-path direction would be in the down-dip direction.

A typical field layout would have a maximum offset from source to receivers of 2400 m. That is, if 48 receiver stations were recorded with a separation of 50 m, then the near to far receiver offset would become 2350 m. Initial testing with the source and receiver lines 2350 m apart, corresponded to a separation of 5.875 cm on the model. After recording a number of test shots, it was realised that the surface wave totally masked the reflection, and rather than cut a trench in the model, it was decided to increase the source/receiver offset. The source/receiver separation was therefore doubled to 4700 m, which was 11.75 cm on the model. The surface wave was now found to arrive after the main reflection of interest which was acceptable for the research.

This research required the use of swath geometry, in which all source points would be along one line which was parallel with a line containing all receiver points. A point of origin was then required for all measurements in an initial set of tests, just as in conventional land recording where all x, y and z coordinates in a seismic survey are referenced to a surveyed bench mark origin.

This coordinate system origin '0' was taken as being located up-dip at the model's top corner point (Figure 3.2), and the vertical distance from the '0' point to the dipping base (normal to the base), was measured as 2540 m. In the field (for example in the shallow coal mining environment), this distance and the average velocity would be ascertained by the use of an up-hole or a zero-offset shot being recorded. Data could be acquired as previously described.

In order to specify the three-dimensional geometry, a set of conventions were devised for the experiments to be carried out on the model. With the large amount of data to be recorded in different directions, it became necessary to perform the tests in a logical sequence, commencing with a known dip direction, so that confidence could be established in the test and analysis procedure. After the establishment of such confidence, it would become possible to ignore the general orientation of source/receiver placement (provided they retained a swath geometry).

Therefore, the initial convention established that when the source and receiver lines were positioned parallel to each other and in the direction of maximum dip, as shown in Figure 3.2, the *majority* of raypaths were

approximately across the dip direction (i.e. in the approximate strike direction). It was unreasonable to refer to this configuration as 'strike' recording, since only a few raypaths would travel in the true strike direction. Consequently, I refer to this direction of recording as the 'cross-dip' direction, which indicates that a majority of raypaths are across the dip direction. As a result of such a swath recording configuration, a CMP line of scattered trace locations would result within bins which would be aligned in the general dip direction.

The swath configuration could be rotated 90^0 by rotating the physical model 90^0. This allowed recording in the direction in which the majority of rays were travelling down-dip to their receivers, so that the CMP line would be aligned generally in the strike direction. I refer to this direction as the 'down-dip' direction. A strike CMP line would then be recorded, the CMP traces being reflected from a scatter of points on the reflector's surface.

Where the reflecting plane intersects with the x-z plane, the angle between the reflecting plane and the horizontal was termed α, while that on the y-z plane between the reflecting plane and the horizontal was termed β as shown in Figure 3.3(a). The adopted sign convention conforms with Sheriff and Geldart (1982).

Having defined the specific physical model which will be used for recording synthetic field data under controlled conditions, and having determined the sign conventions for use with the model, the next step is to introduce the first advancement in processing LOFOLD3-D data.

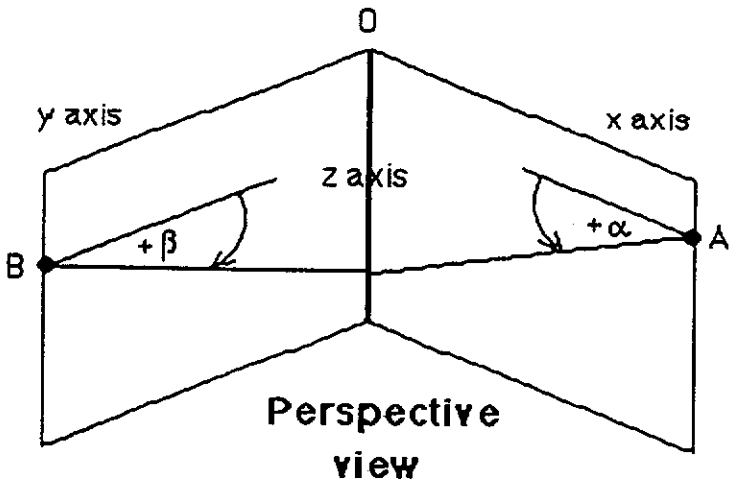

Figure 3.3(a). Perspective view for angles α and β on x and y-axes, respectively. The view shows the origin 0 on the z-axis, and the positive values of α and β when the reflection horizons are dipping from A and B, down towards the origin. This convention was adopted for consistency with previous published literature (Sheriff and Geldart, 1982).

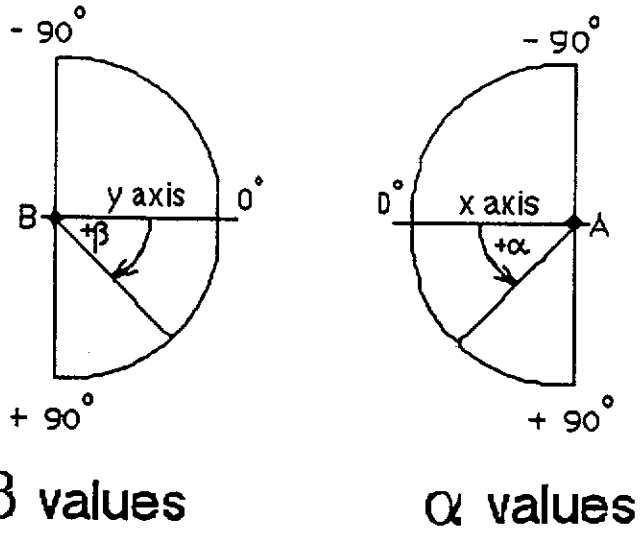

Figure 3.3(b). Angular values for angles α and β. The values are positive when they dip down from hinge points A and B towards the origin.

Chapter 4
The Radial Transform

Chapter 1 earlier discussed the problem of the attenuation of surface waves in seismic data. Surface waves are generally of a high amplitude compared with reflections, and travel at such a velocity that they frequently mask the more useful reflections. In 2-D collinear seismic recording, surface waves appear as a linear event on a shot record, and one approach to their removal is the application of the τ-p transform. However, in variable azimuth 3-D recording, surface wave arrivals appear as curved events so conventional approaches are no longer applicable.

This Chapter therefore commences with an explanation of the application of the conventional τ-p transform to 2-D data. It then discusses a linearization approach for the removal of surface waves from 3-D data, and offers an alternative linearization approach using the τ-p transform, called the 'Radial' transform. This transform is further modified to allow the use of swath offsets as an additional aid to the elimination of surface waves. Numerical, physical and field data are used to show the transform's application on different data sets.

4.1 The τ-p transform

The τ-p transform sums in the time-offset space along a specified direction to transform data into the intercept time-slowness domain. The application of Tau-p transformation of 2-D data is a discretized version of the Radon transform (Radon, 1917). It has been used as a tool to decompose plane wave-fields into their component waves (Diebold and Stoffa, 1981). Other applications include inversion of seismic data (Bessenova et al., 1974; Kennett, 1977; McMechan and Ottolini, 1980), multiple removal and velocity estimation (Gerver and Markushevich, 1966; Schultz, 1982; Young, 1987).

The τ-p transform has been used on 2-D data sets, where data are recorded as a function of traveltime t and source/receiver offset x. The data may be represented in the domain of intercept time τ and slowness p. As with all transforms which have discrete versions (eg. the Fourier transform), there are limits to which discretization may be applied. The τ-p process works well when there is an adequate number of input seismic traces (eg. 30 traces) which are adequately sampled in time, and these must be

transformed into a minimum number of traces in the τ-p domain (eg. 50 traces). Attempts have been made to limit the effects of such minimum aperture and time series constraints, since they can produce artefacts which can severely affect the data (Tatham et al., 1983). Compressional and shear wave-fields have been successfully separated (Tatham et al., 1983; Dietrich, 1988), while CMP stacking and migration in the τ-p domain have been investigated (Ottolini and Claerbout, 1984; Bisset and Durrani, 1990; Miller et al., 1987).

The minimum data aperture produces artefacts and truncation effects (Harding, 1985) during the forward transform, and methods to suppress such effects have been tested. These include semblance weighting with offset tapering (Brysk and McCowan, 1986), and frequency with offset weighting functions (Mithal and Vera, 1987), with varying degrees of success. Forward modelling using a limited aperture simulation process has been described (Dobbs et al., 1990) to simulate the artefacts produced by the forward transform. Mute functions and automatic gain corrections have been applied in an attempt to partition energy (Tatham et al., 1983), and a method to determine the incidence angle of arriving waves (Treitel et al., 1982) has been tried. To date, there has been little research into the τ-p transformation of 3-D or swath recorded data. The data processing industry generally assumes that the source/receiver combination is in-line rather than in a swath format. Standard transforms are not applicable for this situation.

4.2 Surface wave linearization

Jervis et al. (1987) applied a method they named 'linearization' to separate the swath recorded surface waves from reflections by initially linearizing the curved surface wave event with a temporal shift on each trace, and then filtering the data using standard f/k or τ-p transforms (after which data linearization was reversed). This was particularly successful using numerically modelled data in which surface wave apparent velocities were of a single value, but was time consuming when used with real field data having dispersive waves of variable apparent velocity values.

The conventional τ-p transform sums samples from each recorded seismic trace along a given slope of $p = \delta t/\delta x$ in the time domain. The output trace

has a summed value at slowness p, with data points in τ resulting from the intercept time value τ of the slope used. The value of τ is then given by:

$$\tau = T - px.$$

A linear event will sum to a single value in the conventional τ-p domain. It follows that a curved reflection will remain curved in that domain (Figure 4.1). If the linear arrival (which may be a surface wave) is to be removed from the data, this is performed by zeroing the affected Tau-p domain region (or point), and performing the inverse transform into the t-x domain without including the affected slowness values (Tatham et al., 1983). The linearization approach (Jervis et al., 1987) is to apply a temporal shift δt to each trace in order to linearize the surface wave as shown in Figure 4.2, before the application of conventional τ-p or f-k filtering is performed.

The shift value is computed using distances and two velocity values- the velocity of the medium and an arbitrary velocity. The precise value of δt is therefore velocity dependent and is a function of the degree of linearity required by the transform to be applied (f/k or τ-p) in the processing sequence.

After linearization of the surface wave, reflections lose their NMO curvature and take up a new location on the record, as shown in Figure 4.2. Before the application of the filtering transform, the linearized data must be checked to ensure the correct velocities have been used, and this can be time consuming if surface wave apparent velocities change from shot record to shot record. Consequently, the drawback of the linearization approach is that the medium velocity must initially be known, followed by the application of an arbitrary velocity.

An alternative method is now proposed which overcomes the requirement to know the medium velocity.

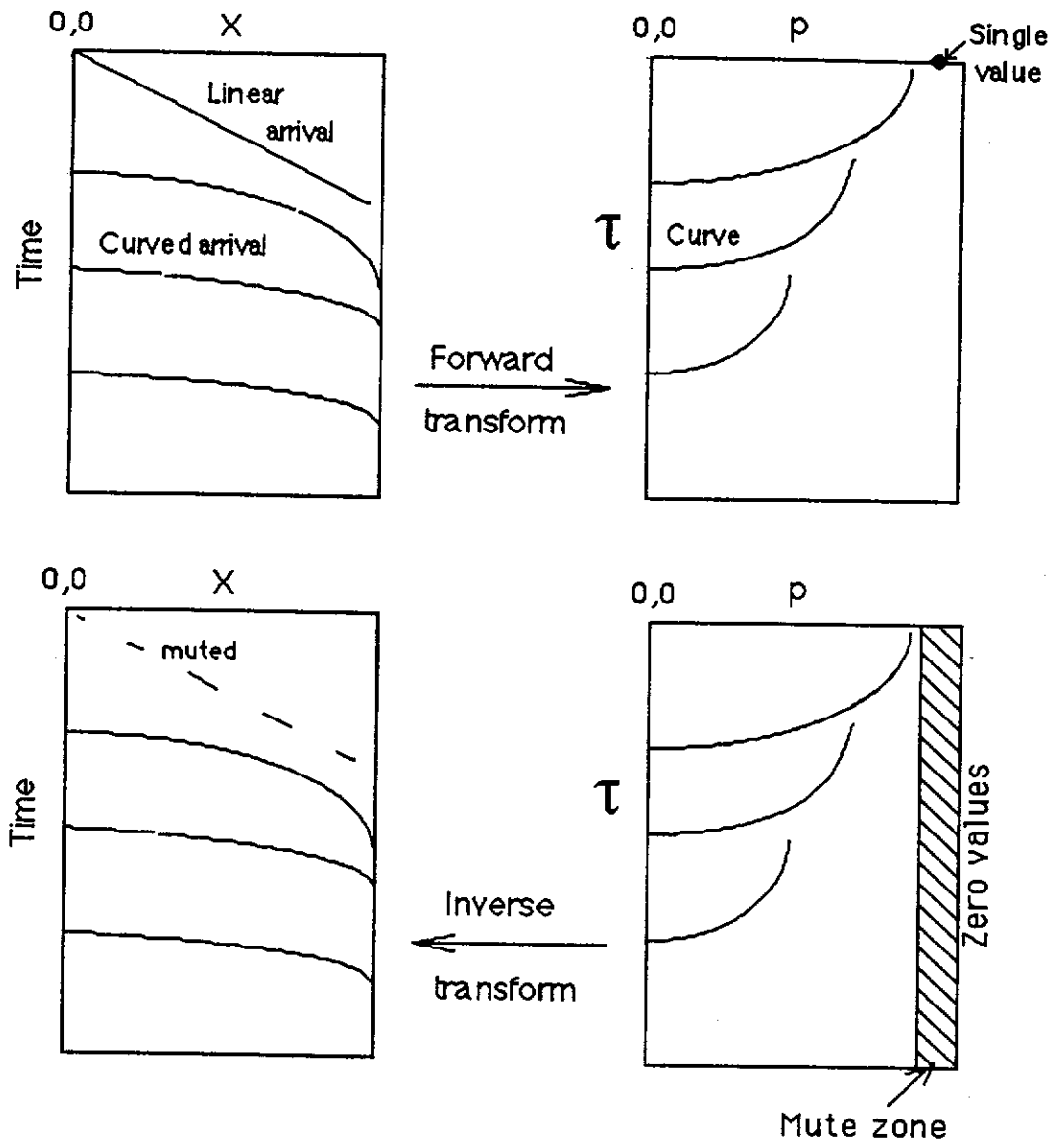

Figure 4.1. Forward and inverse τ-p transformations of t-x seismic data. After forward transformation, filtering may be performed in the τ-p domain by zeroing data, before inverting back into the t-x domain. The effect is to mute-out the linear arrival in the t-x domain, as shown by the dotted line.

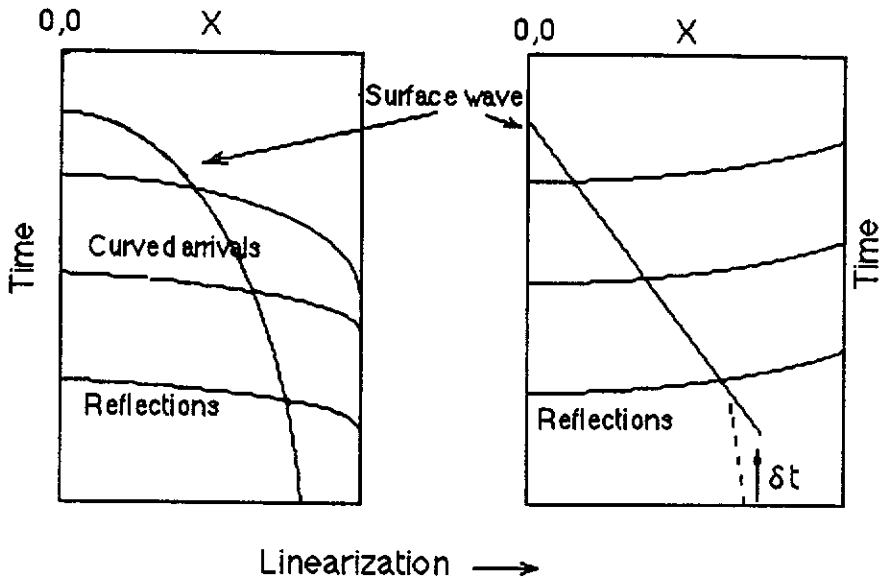

Figure 4.2. The linearization method of separation of surface waves from reflections. The method applies a time shift δt to individual traces, to linearize the surface wave, so that thereafter conventional f/k or τ-p filtering may be performed.

4.3 The Radial approach

In Chapter 2.6, I indicated that an alternative to the τ-p transformation process could be to sum data along curved events. While the conventional τ-p transform sums along linear trajectories in the time-offset domain, it is possible to modify the forward transform to sum along curved trajectories in the time-offset domain (Evans, 1991a, 1991b). Figure 4.3 shows a surface wavefront arriving from a source laterally offset at distance R from the receiver line. As the wavefront appears to travel along the receiver line, offset distance S_n from the source determines the time of arrival of the surface wave.

The wave may be considered to be arriving at a time given by $t = \frac{S}{V}$,where t is the one way traveltime, S is the radial distance (offset) from source to each receiver, and V is the surface wave velocity.

The moveout time δt from receiver 'n' to receiver 'n+1' may be computed using the surface wave's true velocity V.

$$\delta t = \frac{S_{n+1}}{V} - \frac{S_n}{V} \quad . \tag{4.1}$$

Thus, the normal moveout time between any two receivers for a surface wave is the difference in radial distance between the two receivers divided by the medium velocity.

In terms of slowness p (reciprocal velocity):

$$\delta t = p\,[(S_{n+1} - S_n)]\,. \tag{4.2}$$

In contrast to the linearization approach, a different method has been devised which avoids the need to pre-determine surface wave velocity. Surface wave data may be linearized by either moving traces up or down along the time axis to make the curved surface wave linear, or alternatively by shifting traces laterally along the x offset axis, prior to the τ-p transform.

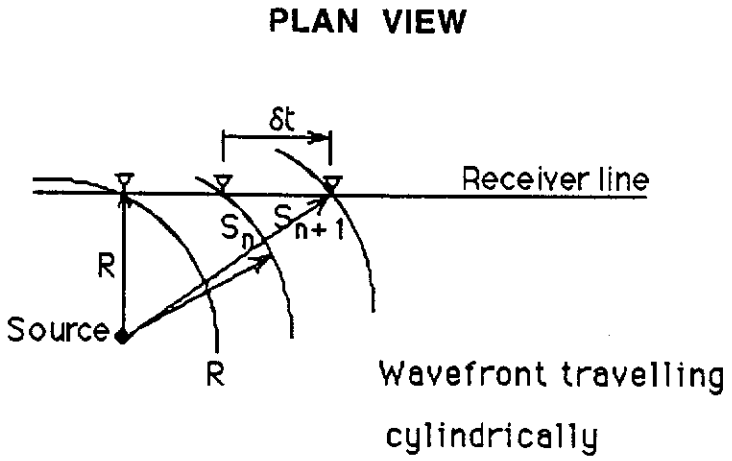

Figure 4.3. Radial geometry of swath recording. The wavefront has changing apparent velocity as it arrives at receivers in the receiver line. The offset distance from the source to the nearest receiver is R. The distance to a chosen receiver is S_n, and the distance to the next receiver further away is S_{n+1}. The time taken for the surface wave to pass from one receiver a radial distance S_n to the other receiver at S_{n+1} is δt. This is the time shift applied by the linearization method, which is dependent upon the selection of a defined surface wave velocity value. (Jervis et al., 1987)

Consider the swath source/receiver geometry, as shown in Figure 4.4. Such a geometry produces the schematic shot record shown on the left side of the figure, which has receivers equally spaced because the record is displayed with traces separated by an equal in-line distance. The distance from the source to any receiver is the offset distance as if the source were located in-line at 0,0.

If the in-line offset distances were now replaced with the radial distances from the source to each receiver S_n, this would change the appearance of the record, to appear similar to the schematic radial distance against time record, shown on the right side of Figure 4.4.

In that record, the radial distance R to the nearest receiver causes the near trace to be offset a distance R, which is large by comparison to the in-line separation between traces. The nearest trace to the source appears farther away from the 0,0 point than it was in the previous record. The separation distance from receiver 'n' to receiver 'n+1' is $S_{n+1} - S_n$. This separation distance $\delta x'$ changes with radial offset distance as shown in Figure 4.5. This change is slow at the near offsets, but increases with increasing source to receiver radial distance. At far offsets and those towards infinity, this distance becomes very similar to the normal in-line separation distance δx.

Consequently there is a blank region between 0 and R, followed by an apparent compression of traces in the record thereafter, as shown on the record on the right in Figure 4.4. The surface wave becomes linearized, but the reflections are also modified by a value dependent upon their offset. In some cases, it may be possible that reflections curve slightly down at near or middle offsets.

The conventional τ-p transform may now be applied to the linearized record in Figure 4.4. When transformed in this two step process, the τ-p transform may be considered to be applied along curved trajectories in t-x space.

I name this transform the '*Radial*' transform, in which all data are effectively summed along curved trajectories on the shot record, not along linear trajectories. Data are said to be thereby transformed into the '*Radial*' domain, which is not the conventional τ-p domain.

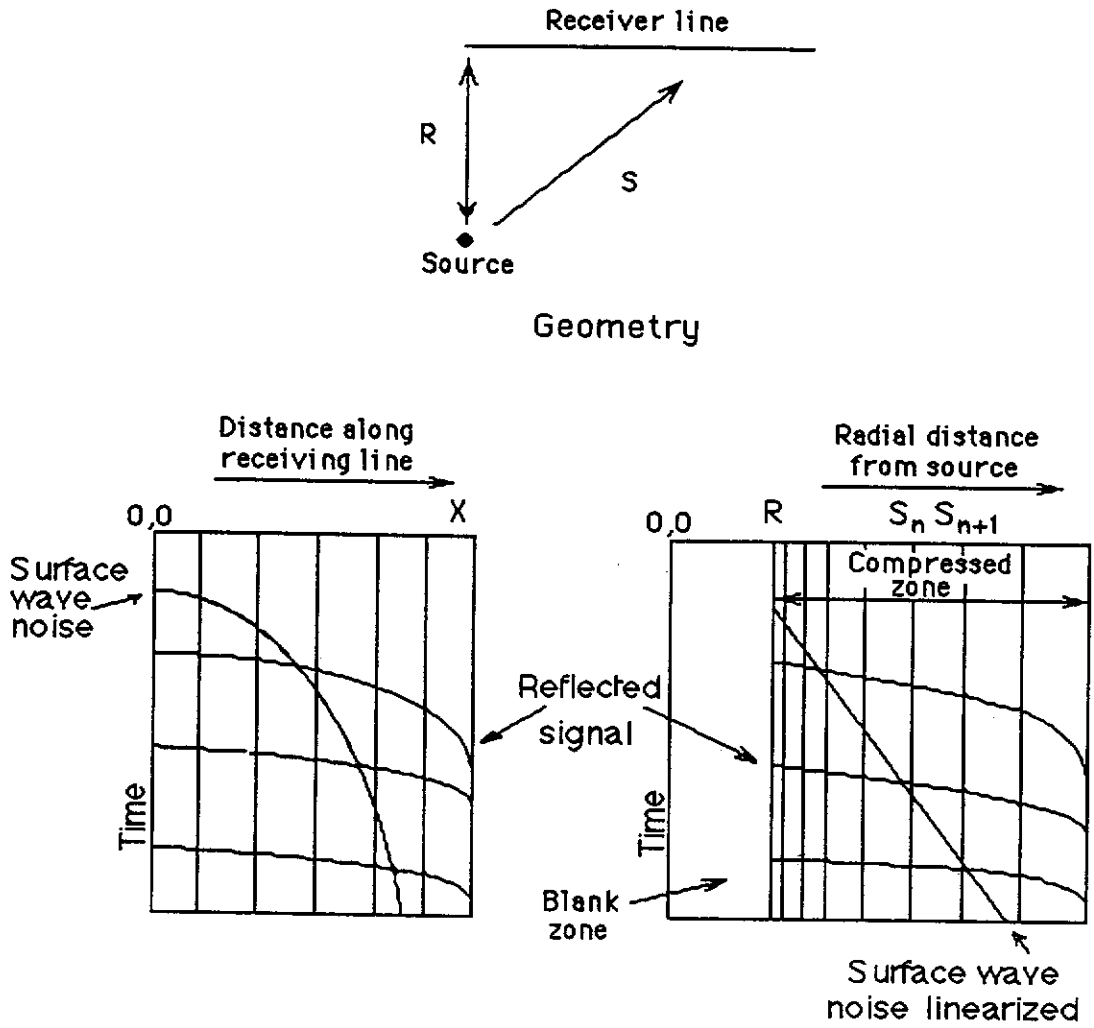

Figure 4.4. Shifting trace offsets prior to τ-p transformation. The left side shot record shows the curved surface wave arrival passing across a series of equally separated 3-D receivers, with the source/receiver geometry shown. The distance to the nearest receiver is R, and S_n is the radial distance from the source to the n th receiver, shown on the right side shot record where the equal distances between receivers are replaced with radial distances S_n. The distance from receiver 'n' to receiver 'n+1' is $S_{n+1} - S_n$. The receiver separation becomes compressed, with shorter separation at the near offsets, gradually increasing towards the linear station interval at the far offsets. A blank zone results between 0 and R, and the resulting record reflections change shape, becoming more linear at the near offsets.

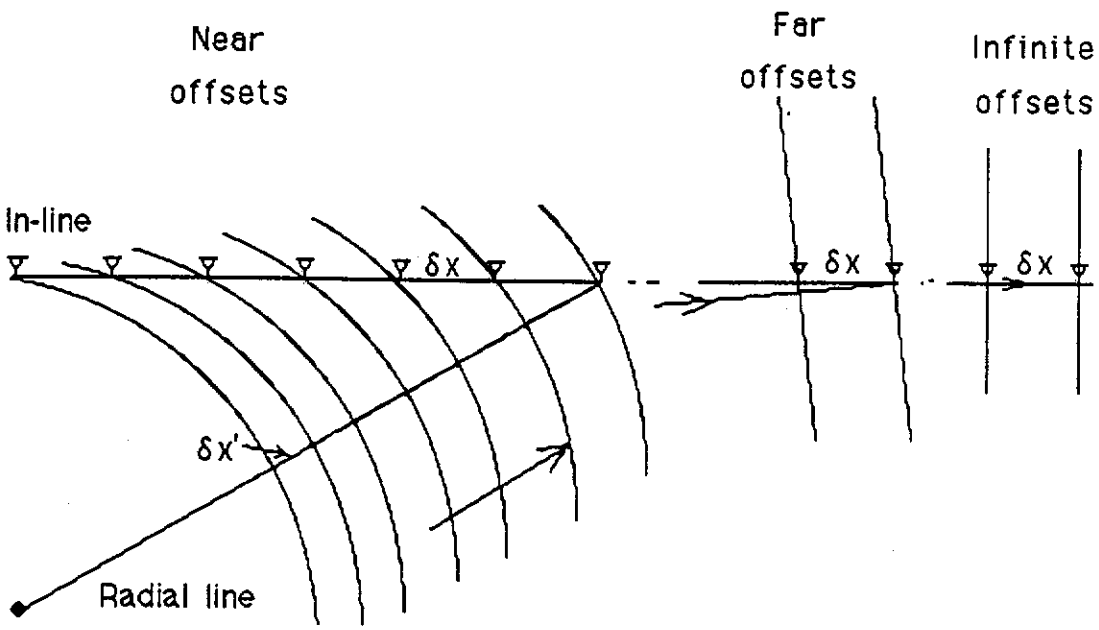

Figure 4.5. Variable receiver radial offset increment. There is an increase in apparent radial receiver interval δx' with offset, where δx' tends to δx at an infinite distance from the source.

The initial velocity term of the medium plus some arbitrary additional velocity term for the temporal shift is required by the Jervis et al. (1987) linearization approach. However, these velocity terms are already built into the data summation method of the *Radial* τ-p transformation process and are therefore not a prerequisite of the *Radial* transform. In practice, transformation to the radial offset is performed by replacing the receiver trace header coordinates with the desired radial offset distance from the source, then performing the conventional τ-p transform.

In Figure 4.6, the *Radial* transform is shown schematically, operating on the shot record in Figure 4.6(a) produced by the geometry shown. Reflection A and surface wave B are shown before and after changing the offsets from their linear value to their radial value, resulting in the t-x radial record of Figure 4.6(b). A conventional τ-p transform is now performed resulting in the plot of Figure 4.6(c), which causes the curved reflection A to become curved in the *Radial* domain, while the linear surface wave sums to a point at B.

The *Radial* domain reflection displays a shift to lower τ values because the reflection intercept time 't' projected from the intercept time at R to the time axis (shown by a dotted line) is less than the value of 't' at R in the time domain. However, the *Radial* domain surface wave B is concentrated at a τ value at zero, because the intercept of the surface wave will be at zero time before transformation.

The curved length of the reflection event in the *Radial* domain is short because the amount of reflection curvature in the time domain is small, covering a small range of intercept time values. The diagonal lineations from the reflection in the *Radial* domain are a truncation effect, the gradient of which is determined by the t-x coordinates of the truncation in Figure 4.6(b).

If the radial distance R were to be shorter in t-x space of Figure 4.6(b), the gradient of the diagonal lineations for waves A and B in the *Radial* domain would be more horizontal than is shown, so shortening the radial distance has the effect of rotating this component of data in the *Radial* domain. Consequently, a second approach to transformation may be considered in which the radial offset to each receiver is S_n-R .

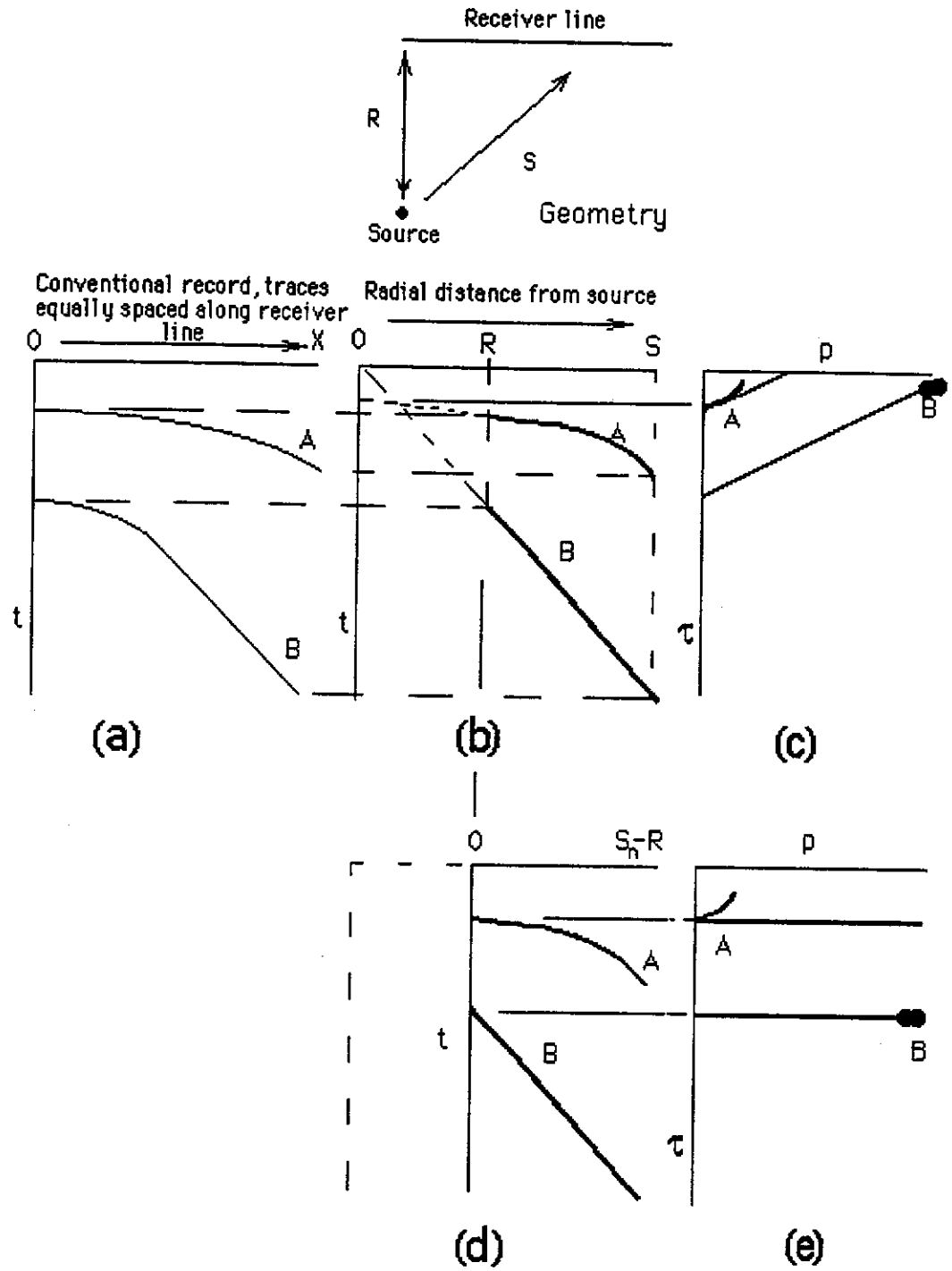

Figure 4.6. Schematic of the application of the *Radial* and *Extended* transforms. With the geometry shown, shot record (a) shows a curved reflection A and surface wave B. Application of radial offsets causes wave compression in (b). τ-p transform results in curved events in (c) where strong energy concentration is shown at high p-values. Replacing offsets with S_n-R shifts offsets in (d) and the *Extended* transform moves data to locations in (e).

4.4. The *Extended* Radial Domain

The radial offset shot record of Figure 4.6(b) shows a blank zone between 0 and R, and traces having a radial offset value S where S is greater or equal to R. Reflection A is shown terminating at near offset R, as is the linearized surface wave B. During subsequent τ-p transformation, the surface wave B would be summed back to an offset and τ value of zero.

If radial offsets S_n were now replaced by a value of S_n-R (that is, subtracting the radial offset value R from each individual value of radial offset distance), the blank zone would be removed as shown in Figure 4.6(d). A subsequent τ-p transform of these data would result in a curved reflection, positioned at the same τ as the intercept of the reflection on the time-axis, shown in Figure 4.6(e). The linearized surface wave now sums to an intercept value in time which is the same value in τ. The reflection is still curved in the τ-p domain, and the diagonal artefact lineations of Figure 4.6(c) are now horizontal in the transform domain, because the waves are now truncated at zero offset in t-x space.

The data are now vertically separated in Figure 4.6(e) rather than diagonal in Figure 4.6(c), allowing retention of the reflected energy by the application of a surgical mute to the artefact lineations. This has been referred to as the '*Extended*' transform of three-dimensional data (Evans, 1991b).

As with the previous *Radial* transform in practice, the receiver trace header coordinates are replaced with the desired radial offset distance from the source. Either the *Radial* or the *Extended* radial transform are considered to be summing data along curved trajectories, the curvature of which is dependent upon the slowness (or velocity) range across which the τ-p transform to operates.

4.5 The inverse *Radial* Transform

If a conventional 2-D inverse τ-p transform is performed on data which was generated in-line, the receiver interval will be equally spaced. This is not the case for a swath recorded configuration, where the increment in radial receiver offset δx changes with radial offsets, as explained earlier.

The inverse transform must also allow for any lateral offset changes used during forward transformation. Therefore in practice, a subroutine is run within the inverse τ-p program, which computes the required radial distances to each trace, so that inverse transformation can be performed to produce an output set of traces equally separated in x space (equal receiver separation). (Trace offset computation was necessary before the inverse τ-p transform because Disco software always displayed traces with equal separation, so a display showing a variable trace spacing after conventional τ-p transform was not possible.)

To eliminate the surface wave therefore, the forward transformation process may be run using a limited set of p-values (not including the surface wave velocity), followed by the inverse transform in a single Disco job file. The result of submitting this file was to produce displays of the input shot record, followed by the τ-p domain map, and the output shot record after inverse transformation. Results of such work are shown later in this Chapter.

A further point is that, once data are transformed, and *assuming the reflections are from flat horizons*, then it is feasible that an inverse transform could be applied using a source to near receiver offset distance R of zero. This could generate a synthetic in-line record, which could be useful in crooked-line processing.

4.6 Operation of the *Radial* transform

In this research, the *Radial* transform program *shotet.for* takes the input shot data traces from t-x space into the radial τ-p space. The output is displayed as a *Radial* time-slowness domain representation of the data. Slowness filtering (to remove surface waves) may be performed by limiting the high slowness values during the forward transformation from the t-x domain, as suggested earlier. Alternatively, further filtering such as muting of data, may be performed in the *Radial* domain, prior to inversion. The inverse transformation is performed by running a Fortran program *shotinv.for* which computes the correct offset header values after which the inverse *Radial* transformation is performed. In both forward and inverse operations, the user may apply either the *Radial* or *Extended* radial alternatives.

Apart from filtering data by muting in the transform domain, another option for application as a filter is to change the manner in which the forward data

are summed. This is executed by applying an excessively large offset distance (such as 10,000 m) from source to receiver line during forward and inverse transform, which limits the range over which slowness values are summed.

4.7 Testing the *Radial* transform using numerical modelling.

The first step was to generate numerical data representative of typical field data. Consequently as a trial of the forward *Radial* transformation, numerical records were generated using Sierra Geophysics *QuikRay* and *Slipr* software (Evans, 1991b). A four layered 3-D model was constructed, with an initial 10 m thick weathered layer of velocity 500 m/s. (Since Sierra ray tracing software did not have the ability to model surface or direct waves, the solution was to use an initial thin 10 m layer from which could be ray traced a reflection, which was a close approximation to a surface wave). The weathering was overlaying a 2,500 m/s layer, a dipping layer of 3,200 m/s, and a wedge-shaped layer with opposite dips with a velocity of 3,500 m/s, overlaying a half-space with a velocity of 8,500 m/s and is shown in Figure 4.7(a). The receiver line consisted of 48 geophones with a 15 m station spacing. The orthogonal source line had 10 shot point locations, denoted as SP1 to SP 10. Two examples of the resulting shot records are shown as SP 2 and SP 10 using a 30 Hz Ricker wavelet in Figure 4.7(b). The initial orthogonal offset at SP 1 was 65 m, for SP 2 it was 130 m, and 650 m at SP 10 (the receiver line was 705 m long).

The layers were named A, B, C and D, and simulated the geology of Appin coal field in N.S.W. Consequently the numerical model was named *APPIN4L*. Reflections from the base of layers A and C are strong due to larger velocity contrasts, whereas the second reflection B from the interface of layers B and C is weak due to the poor velocity contrast (Evans,1991b).

The two shot records indicate how the events from each layer change shape with a change in orthogonal offset. In particular, the surface wave event of layer D is curved at the near offsets of SP2, becoming more linear with increase in offset. In SP10, the surface wave event has a pronounced curvature across the record. Reflection events from A, B and C do not change a great deal with the change in offset.

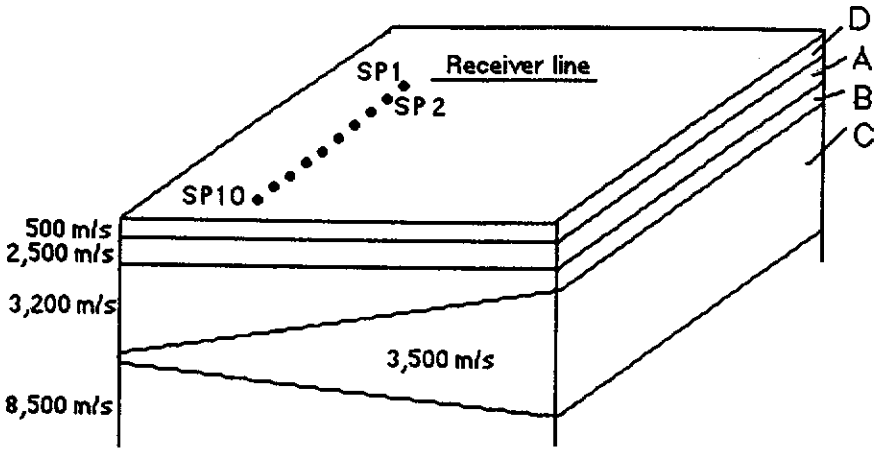

Figure 4.7(a). Four layer model *APPIN4L* over a half-space, having horizontal layers A and D, plus dipping layers B and C. There were 10 shots fired into 48 receivers spaced 15 m apart along the receiver line, with SP 10 used for further data processing (after Evans, 1991b).

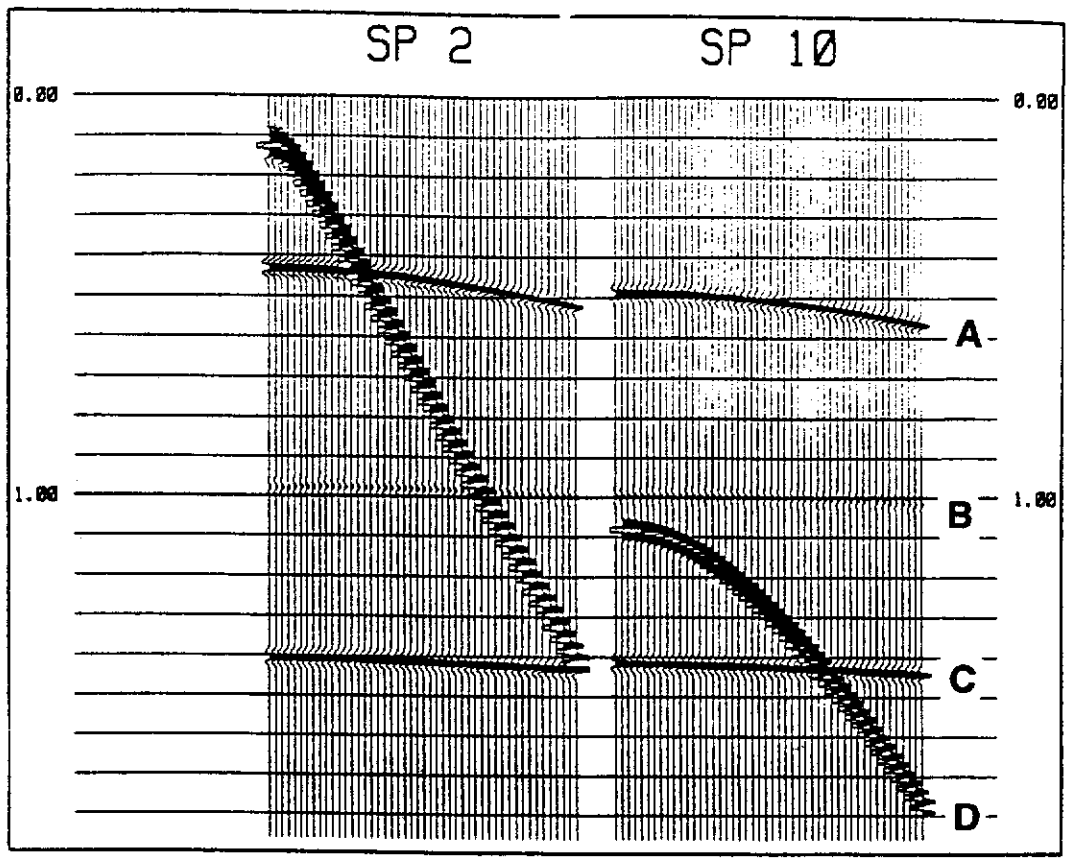

Figure 4.7(b). Shot records of SP2 and SP 10. The surface wave interferes with the reflections at different locations on each shot record.

Both *Radial* and *Extended* radial transforms were performed on the data of shot record SP10 of Figure 4.7(b) using a velocity range of 500 to 20,000 m/s (slowness range of 0.05 to 2.0 s/km.) and the result is shown as Figure 4.8(a). The vertical axis is the intercept time τ while the horizontal axis is slowness p.

The essential features in the *Radial* domain of Figure 4.8(a) from top to bottom are:

1. The three reflections show curvature as was predicted in the schematic of Figure 4.6(c), and the surface wave D is located at high slowness values.
2. Diagonal lineations are present which are due to truncation effects of the data, as discussed earlier.
3. A shift of approximately 25 ms on the reflections, due to the summation process summing to lower intercept values in the time domain as expected, but no shift from τ=0 occurred on the surface wave (as expected).

The essential features of the *Extended* radial domain of Figure 4.8(b) are:

1. The three reflections are still curved, though with marginally less curvature than previously. The surface wave D has been shifted down to a value on the τ-axis which it had in the time domain, as predicted in schematic Figure 4.6(e). Wave D has slight curvature at the centre of its area of most energy, resulting from the fact that it was generated as a reflection having similar moveout to a surface wave.
2. The diagonal lineations have now become horizontal, since the transform used a lateral offset R of 650 m for initial subtraction from the offset distances.

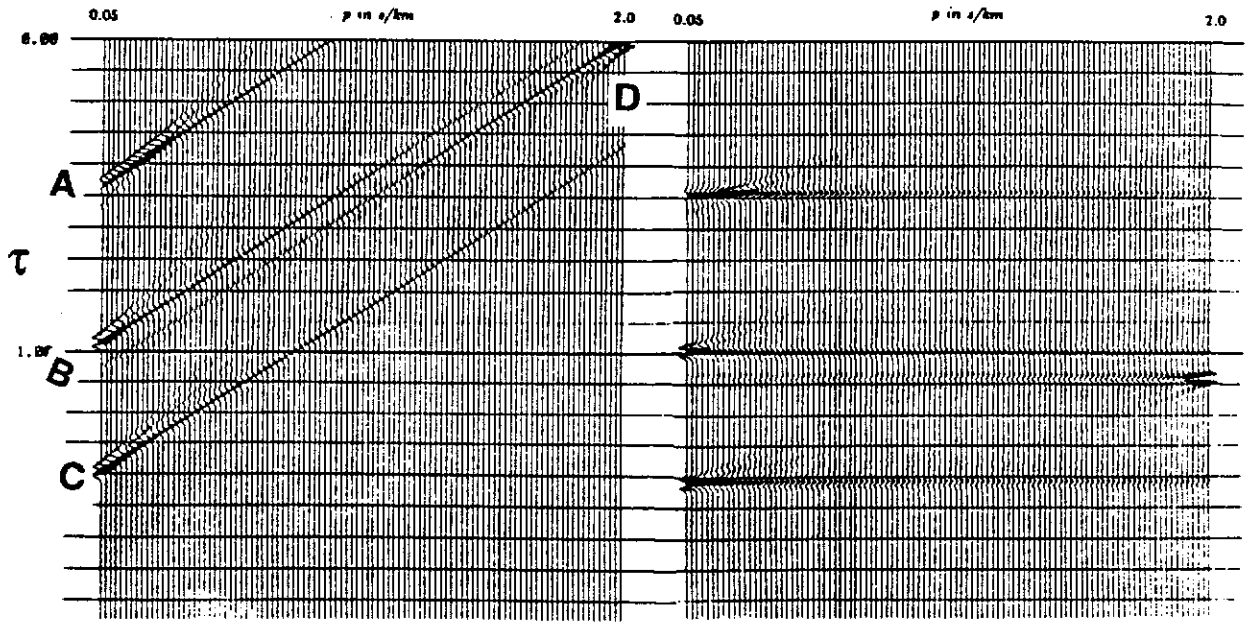

Figure 4.8(a). SP10 after *Radial* transformation. Reflections A, B, C and surface wave D are present with diagonal lineations. The reflection signal is at the lower p values, whereas the surface wave is at higher p.

Figure 4.8(b) is the data after *Extended* radial transformation which has resulted in the data becoming horizontal for easier filtering (after Evans,1991b). The reflections, the surface wave and their horizontal lineation artefacts are now positioned at the zero offset arrival time in τ, corresponding to the zero offset times expected from t-x plots.

The inverse *Radial* transform of SP10 gather was performed with a p-range of 0.05 to 0.5 s/km (2,000 to 20,000 m/s) is shown as Figure 4.9. The data show the strong events arriving at the expected times, while the weak reflector B at 1.0 s is present also. The surface wave D has been reduced at the far offsets, but an artefact E of the inverse transformation process is present which has resulted from reconstruction of the larger inner trace amplitudes of the surface wave using low p values. These data clearly show that the inverse *Radial* transform attenuates surface waves on swath records, simply by restricting the range of slowness values during inverse transformation.

In the *Extended* transform domain, the surface waves may be separated vertically from the reflections so that horizontal surgical muting is an easy task. However in the case of Figure 4.10, these data have been transformed on the basis of a false offset of 2,000 m (rather than the correct offset of 650 m), which is an additional filtering mechanism of the *Extended* transform, without the addition of surgical muting. The use of a large offset changes the origin artificially (Figure 4.6(d)). The intercept time now becomes negative. The range of gradients in the transform from the new origin no longer includes those for the surface wave event. This results in retention of the flatter reflection events in the *Extended* domain but not the surface wave event (although surface wave artefacts are now present). After inverse transformation, the result is that the surface wave has been further attenuated.

Without the offset subtraction, the *Radial* transform may be considered to be summing along curved trajectories across traces which have true radial offsets. With the offset subtraction, the *Extended* transform may be considered to be summing along curved trajectories across traces which have a radial offset which may be chosen arbitrarily. Any radial offset value may therefore be used in the *Extended* transform, provided that the inverse transform uses the same parameters as the forward transform. The *Extended* transform is therefore considered more versatile than the Radial transform and in Figure 4.10 has shown a successful application in removing the majority of the strong surface wave data.

Figure 4.11 was produced using a false offset of 10,000 m. It shows reflections present (and the weaker reflection at 1.0 s stronger) but now

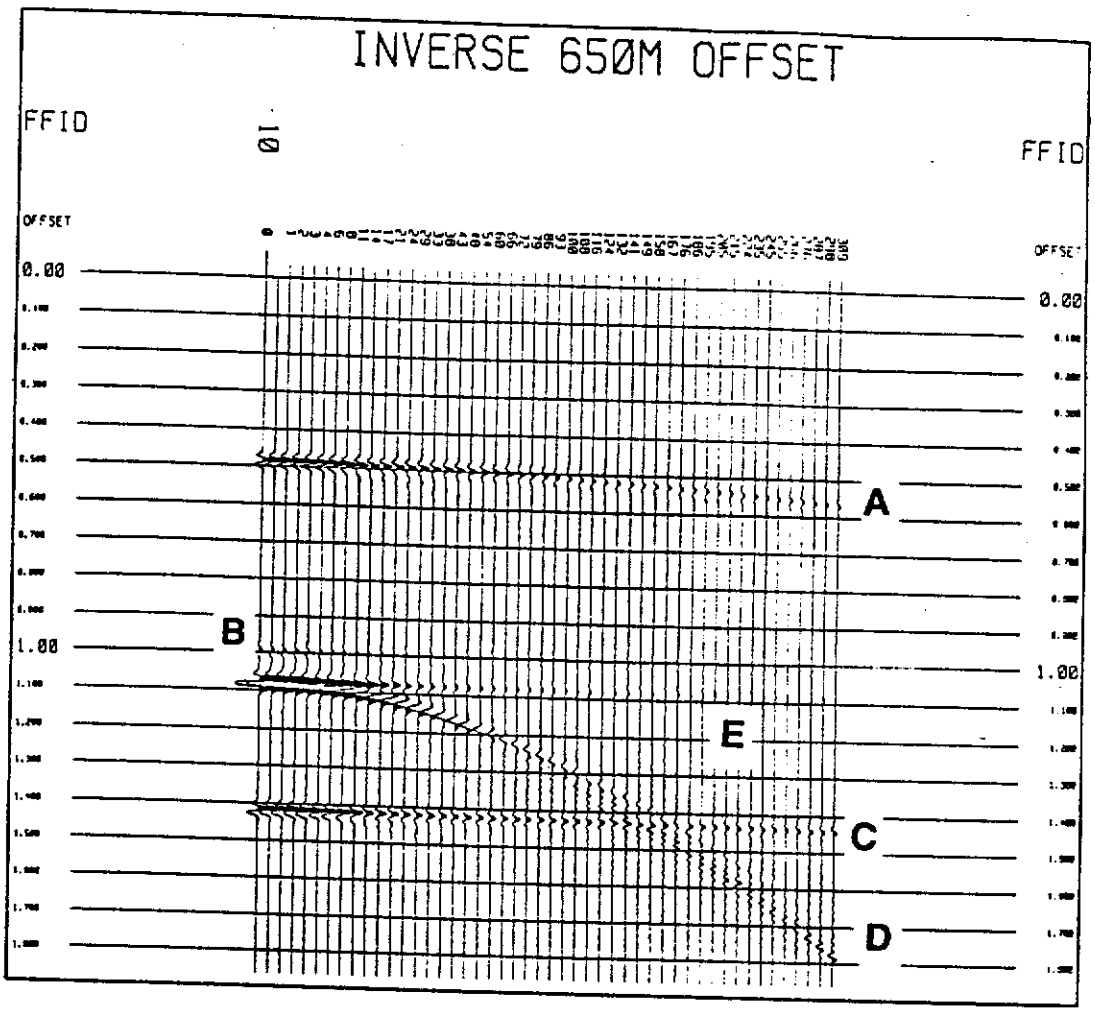

Figure 4.9. Inverse *Radial* transformation of SP 10, using the true radial offset of 650 m, and a restricted p-range of 0.05 to 0.5 s/km. The data shows the strong reflections A and B correctly positioned, while the weak reflector at C is present, but poorly resolved. The surface wave D is present with the expected curvature, but an artefact of the transformation process is present at E.

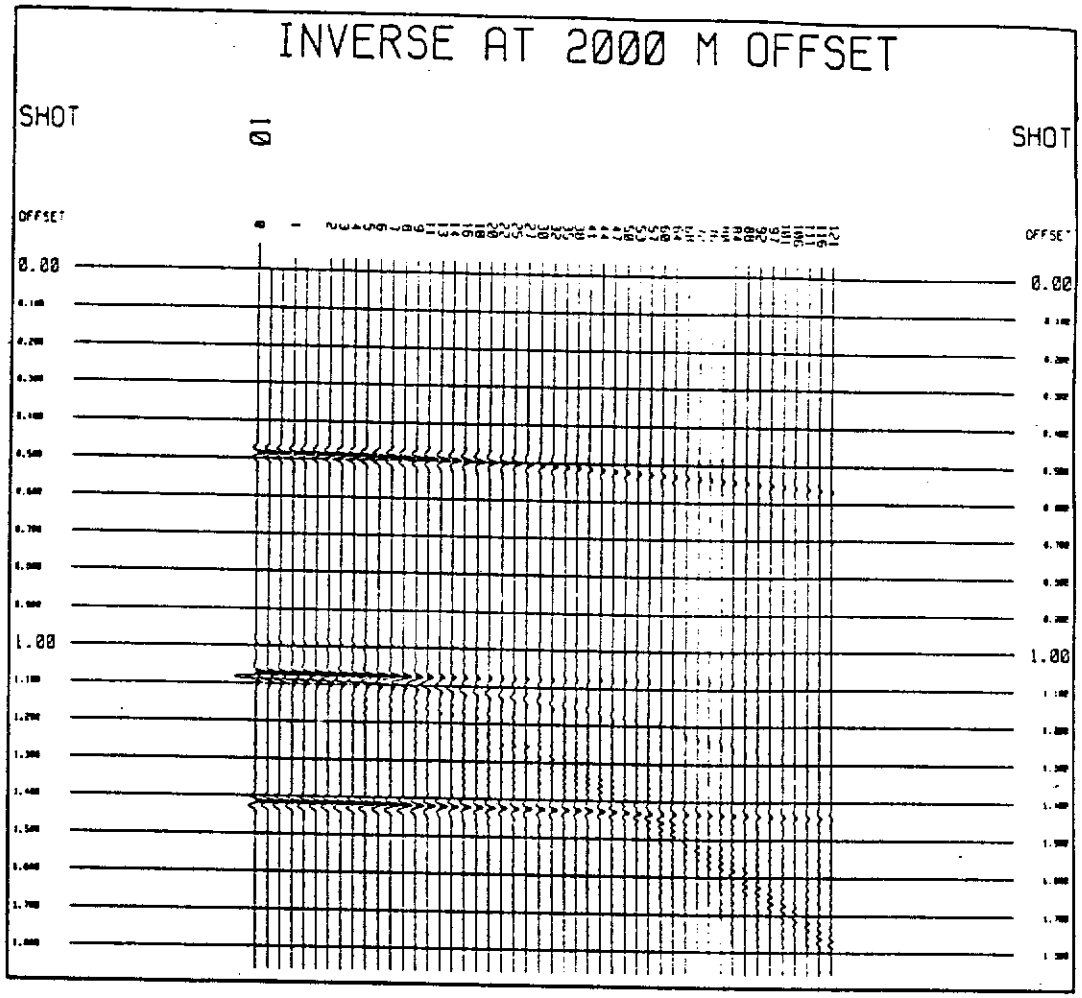

Figure 4.10. Inverse *Extended* transformation of SP 10, with a false offset of 2,000 m. The reflections have been retained and the surface wave has been attenuated significantly.

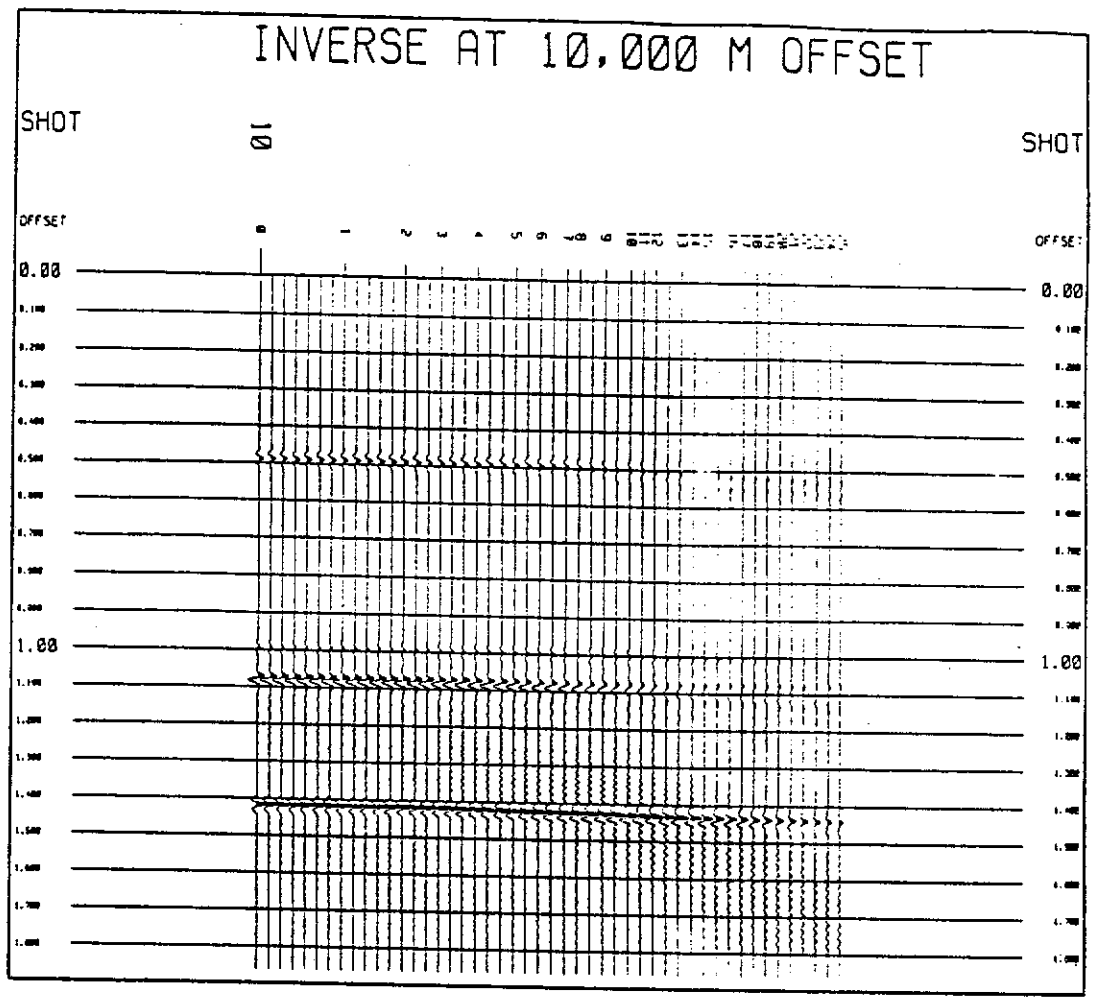

Figure 4.11. Inverse transformation of SP 10, with an offset of 10,000 m. The reflections have been retained, the original surface wave has been removed, but surface wave artefacts now appear as if caused by a reflection at 1.1 s.

causes the surface wave event to appear as if it were a reflection also. This is because an *Extended* transform with a very large offset will sum along the dominantly flat portion of events, which is the situation with both reflections and surface waves at the shortest offsets. The surface wave data could be removed completely by surgical muting in the *Extended* domain. Tests to observe if a greater number of p-traces could improve the transformation were performed, but there were no appreciable differences using more than 100 p-traces. This confirmed that the data were acceptably sampled during forward transformation.

4.8 Testing the *Radial* transform using physical modelling.

The simple physical model discussed in Chapter 3 and shown in Figure 4.12 was now used to test the *Radial* transform. Interfering surface and reflected waves were observed when transducers were placed on it, which is typical when shallow reflection 3-D seismic surveys are performed over coal fields. Shot records were generated by recording with the cross-dip swath source receiver configuration, as was discussed earlier in Chapter 3. The 24 receivers were positioned at a separation distance of 100 m and an orthogonal offset of 2,300 m. The acrylic velocity was 2,666 m/s so both the reflections and direct wave travelled at this speed. The first cross-dip shot record is shown in Figure 4.13.

Electrical crossfeed between source and receiver appears between zero time and 100 ms. The upper reflection from the plexiglas base is shown as event 'A' and has an average apparent velocity of 13,500 m/s, as does the second event 'B' (which is probably a converted PS reflection wave). Wave 'C' has greater curvature at near offsets but a flatter appearance with an apparent velocity of 4,000 m/s at the far offsets. This may be the direct wave. Wave 'D' may be a multiple at 7,200 m/s while linear wave 'E' (apparent velocity of 2,760 m/s) appears to be travelling directly along the receiver line. Other events appearing on the record are considered to be reflections from the various sides of the model.

These data were radially transformed, the objective being to observe the performance of the transform going forward and inverse using just a limited range of p-values (0.01 to 0.2 s/Km) on the five chosen waves A to E. For this exercise, the other waves were irrelevant.

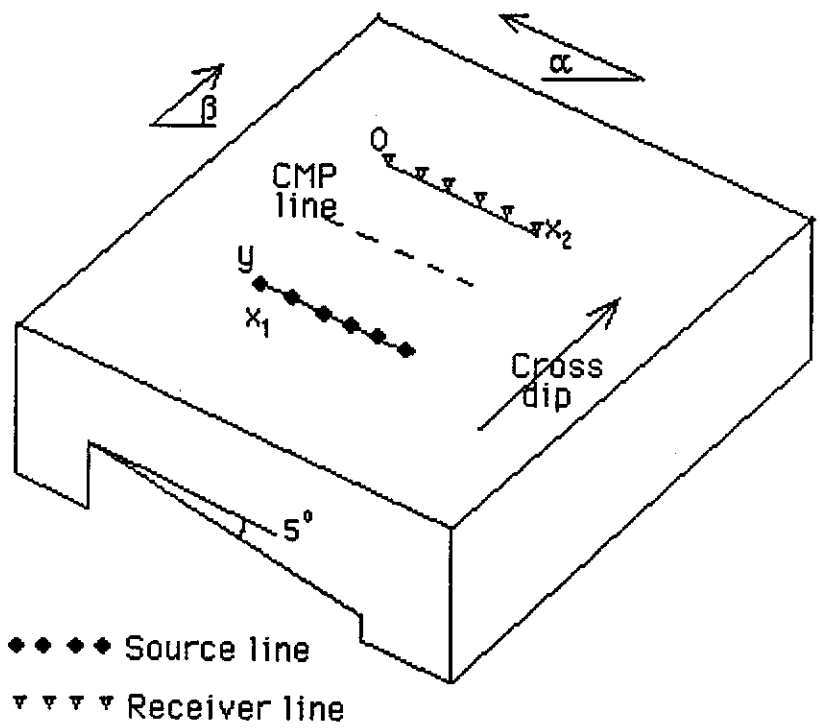

Figure 4.12. Physical model made of acrylic plastic, with a 5 degree plane cut in its base. When recording with the cross-dip recording configuration, the receiver line passes through the origin 0. The CMP line is recorded along the dip direction, and for the physical model, α is the dip along the receiver line in the true dip direction, while β is the dip along the strike direction.

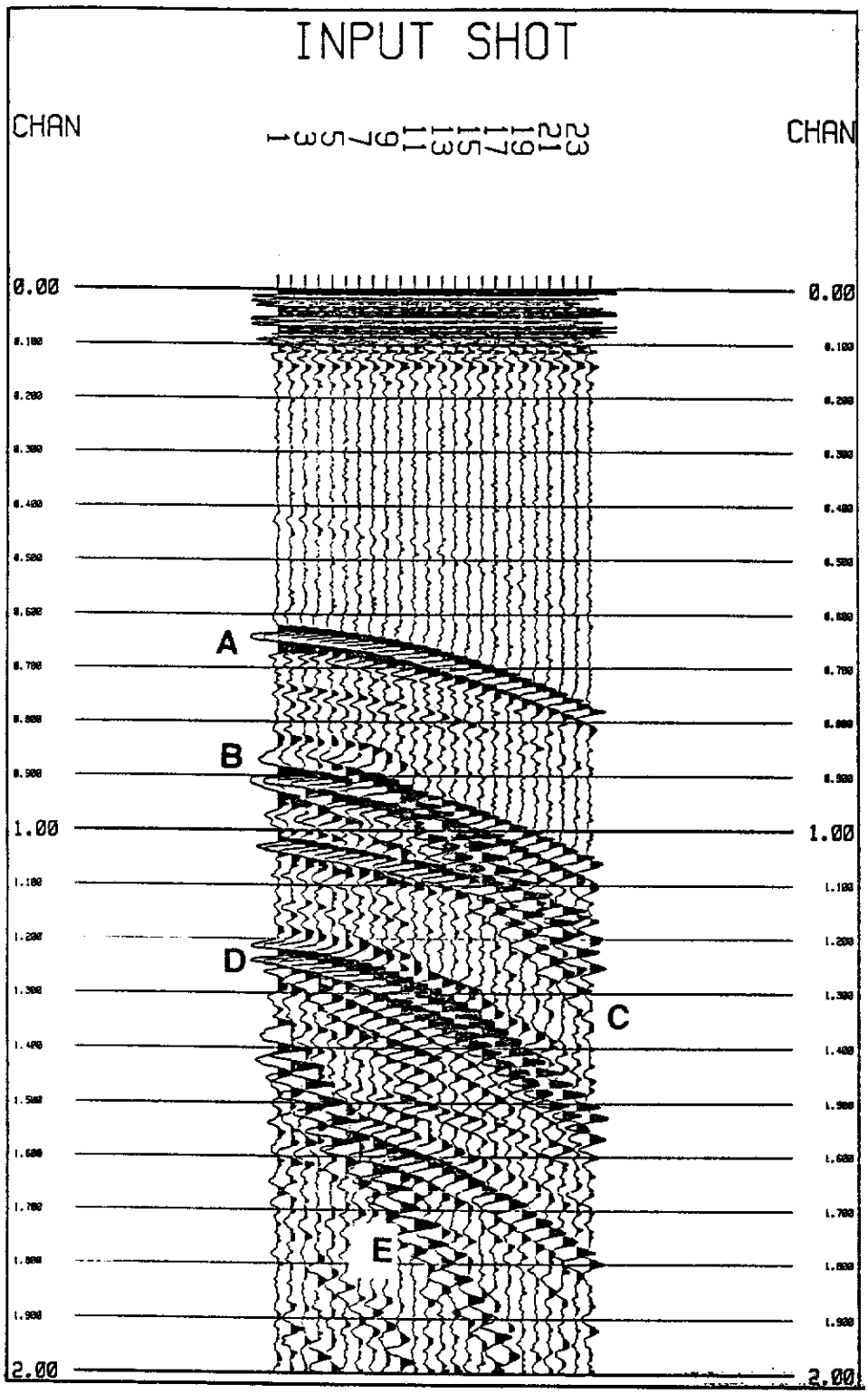

Figure 4.13. The input cross dip physical model shot record for *Radial* transformation. The first event 'A' is a reflection flattening off at a zero offset time of 620 ms; the second event 'B' flattens at 900 ms and interferes with the direct wave 'C' passing across it from 870 ms to 1.25 s. Linear wave 'E' passes along the receiver line with an apparent velocity of 2,760 m/s.

A forward *Radial* transform of the cross-dip record is shown in the *Radial* domain in Figure 4.14, using a slowness range of 0.01 to .2 s/Km (100,000 to 5,000 m/s). The parallel diagonal lineation form of the data results again from the truncation effects during forward summation, as was the previous case with the numerical data of Figure 4.8(a). The majority of the energy of Reflection 'A' is at the centre of the p-range. Direct wave 'C', with an apparent velocity of 4,000 m/s at the far offsets, would have the majority of its energy restricted to near offsets by the summation process (with a higher apparent velocity at the inner traces within the transform range). This should appear at the end of the plot at high p-values and result in attenuating much of the far offset energy of wave 'C' after inverse transformation. The inner trace energy should be retained. Wave 'E', with an apparent velocity of 2760 m/s, should be removed completely, since velocities lower than 5,000 m/s were not sampled.

The major waves are observed in the *Radial* domain of Figure 4.14 to have their energy concentrated across a p-range from 0.05 to 0.15 s/Km (20,000 to 6,666 m/s). Wave 'D' has a slowness value around 0.14 s/Km (2,700 m/s), while the linear wave 'E' is not present on the plot, because values as high as 0.36 s/Km (2,760 m/s) have not been sampled on this occasion.

Figure 4.15 shows the result of the inverse shot record, and it is clear that the far offset data of wave 'C' has been attenuated as predicted, while linear wave 'E' has been completely removed. Event 'B' at 900 ms has been preserved. Wave 'D' is still strong. Artefacts due to the transformation and inverse data sampling are apparent as indicated on Figure 4.15. The strong artefact at 1.4 seconds (top arrow) results from the forward transform summing the high inner trace amplitudes of linear wave 'E', while the other artefacts result from summing other noise arrivals in the inner trace region.

These artefacts appear curved because the forward *Radial* transform sums along curved trajectories and performs the inverse by reconstructing waves along curved trajectories. Consequently, artefacts may appear as curved events at later times, when reflection signal strength is weak and there is only noise upon which the transform can operate. The artefacts are easily recognised as distinct from reflections, because their curvature is greater than reflections would be at such late arrival times, while their spectral content is much higher than later arriving reflections would be expected to exhibit.

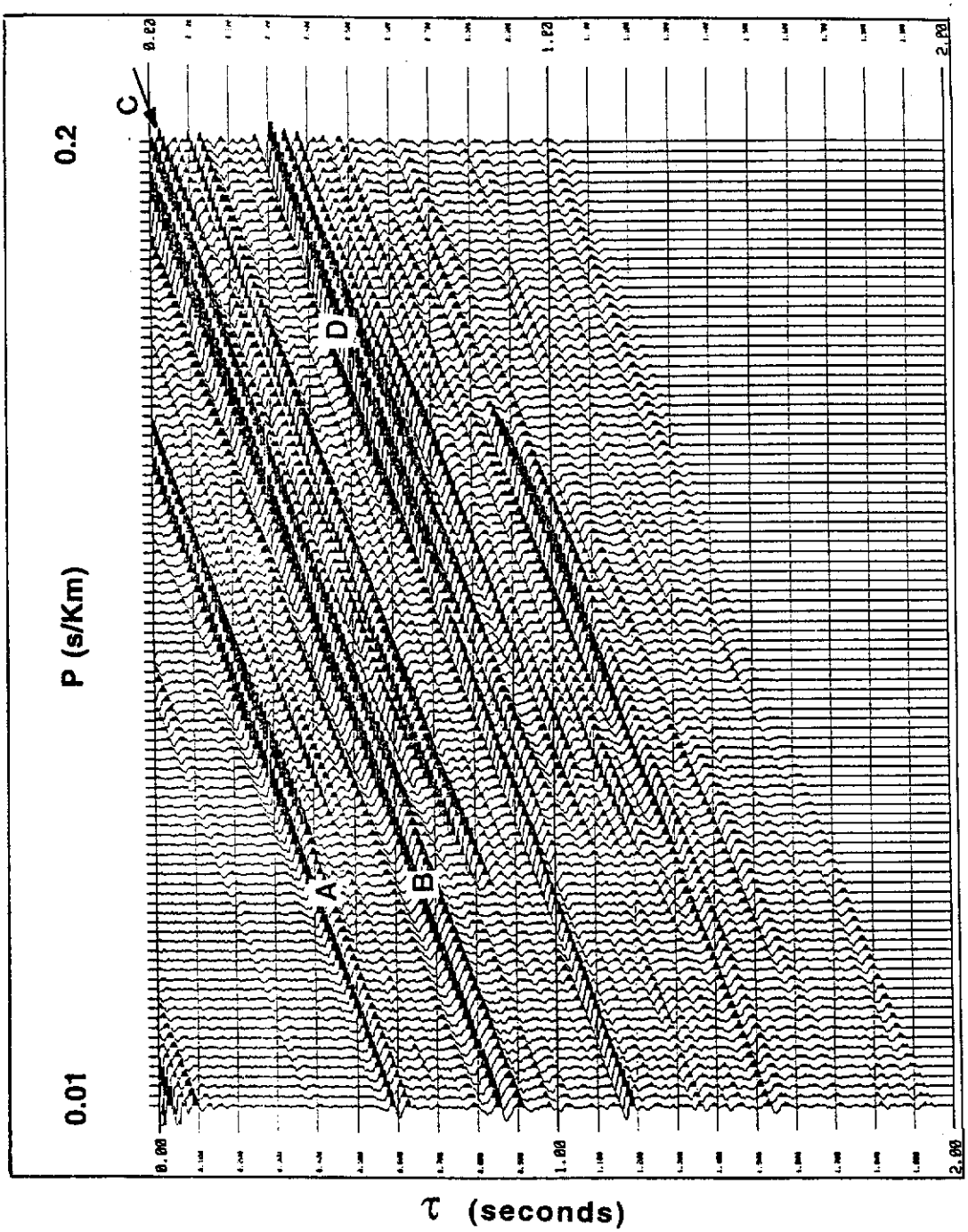

Figure 4.14. The *Radial* domain transform of Figure 4.13, using a p range of 0.01 to 0.2 s/Km (100,000 to 5,000 m/s). Reflection 'A' and converted reflection 'B' are shown with waves 'C' and 'D'. Wave 'C' has not been sampled adequately, partially appearing at the highest p values, while 'D' has most energy in the higher p values also. Wave 'E' is not present because its p value of 0.36 s/Km (2760 m/s) has not been sampled during the forward transform.

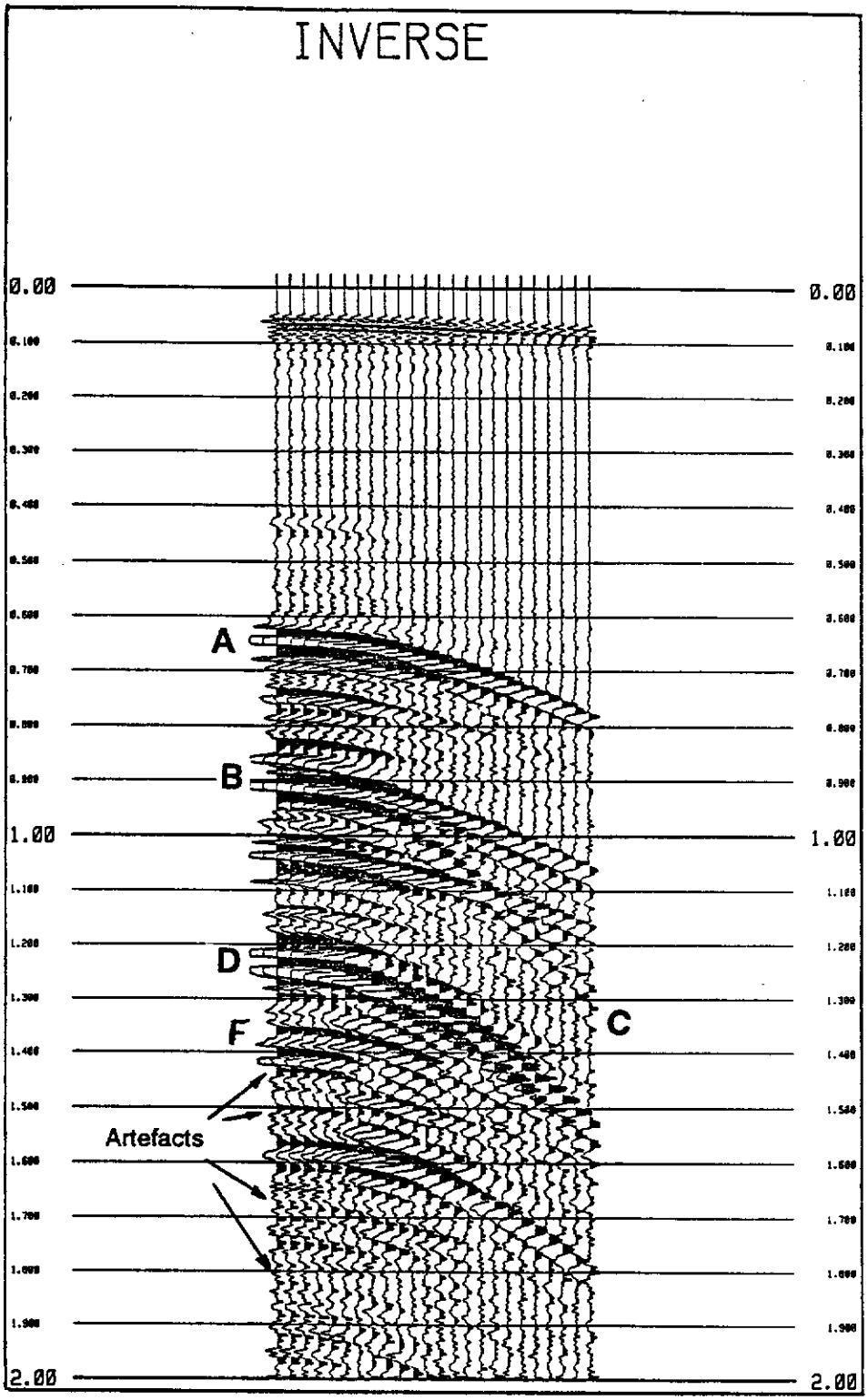

Figure 4.15. The inverse transform of the data. Reflections 'A' and 'B' have been maintained while waves 'C' and 'D' have been attenuated. Wave 'E' has disappeared from the shot record, but there are inner trace artefacts now apparent at the later arrival times, as shown.

4.9 Application of the *Radial* and *Extended* transforms to field data.

In this section, I present two case histories. The first case history is the application of the *Radial* and *Extended* transformation process to a deep reflection record from a LOFOLD3-D survey recorded at Moora, W.A. The second case history is the *Extended* transform's application to a shallow reflection record from a LOFOLD3-D survey recorded at German Creek coal mine, Queensland, in which muting was applied in the *Extended* domain.

Moora Case History. A LOFOLD3-D survey was recorded in 1987 at Moora W.A., over a thick sedimentary sequence of sands and shales. The survey had a receiver line length of 1598 m (48 receiver stations 34 m apart) and used the orthogonal crossed array approach in the LOFOLD3-D method. Figure 4.16 shows an AGC field record (*MORA1.dsk*) from a swath 3-D shot recorded during that survey, in which the source was 411 m orthogonal to the recording spread. The radial offset from the source to receiver is shown in the offset location at the top of the figure.

The first arrival wave 'A' in Figure 4.16 has an apparent velocity of 2,000 m/s at the far offsets. The curved surface waves 'B', 'C' and 'D' clearly mask the reflections, with a marked curvature at the near offsets. At the far offsets, these low frequency waves have apparent velocities of 740 m/s, 500 m/s, and 370 m/s, respectively. Higher frequency shallow reflections can be seen to arrive between 300 ms and 2 s, and from 4 s onwards after the onset of the surface waves. Note that the near offset surface waves can have similar curvature to the shallow reflections. The input record had AGC applied which resulted in making the random line noise apparent before the first arrivals.

The first step was to observe the effect of the *Radial* transform by applying it over a limited range of slownesses. These data were forward radially transformed within a range of 0.02 to 2.0 s/Km (i.e. 500 to 50,000 m/s), and the *Radial* domain profile is shown as Figure 4.17. The far offset data of the first arrival 'A' appear to overlay higher frequency reflections in the region of 0.056 s/Km (1,786 m/s), while the higher frequency reflections are concentrated in the low order values of p between 500 ms and 1.2 seconds. In the Radial domain, surface waves 'B' and 'C' are evident as strong interfering events at the high slowness end of the plot.

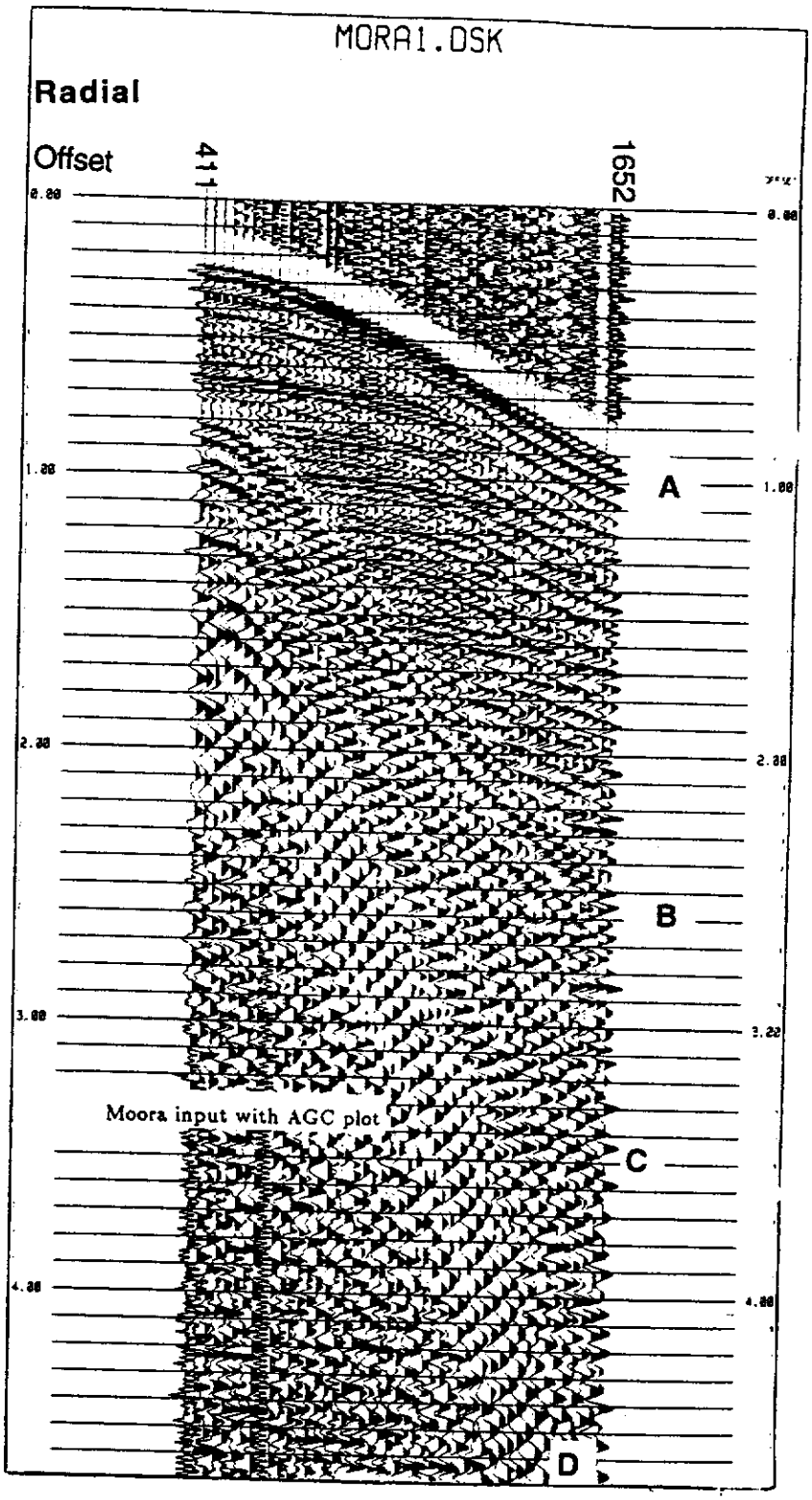

Figure 4.16. Moora shot record showing strong surface waves.

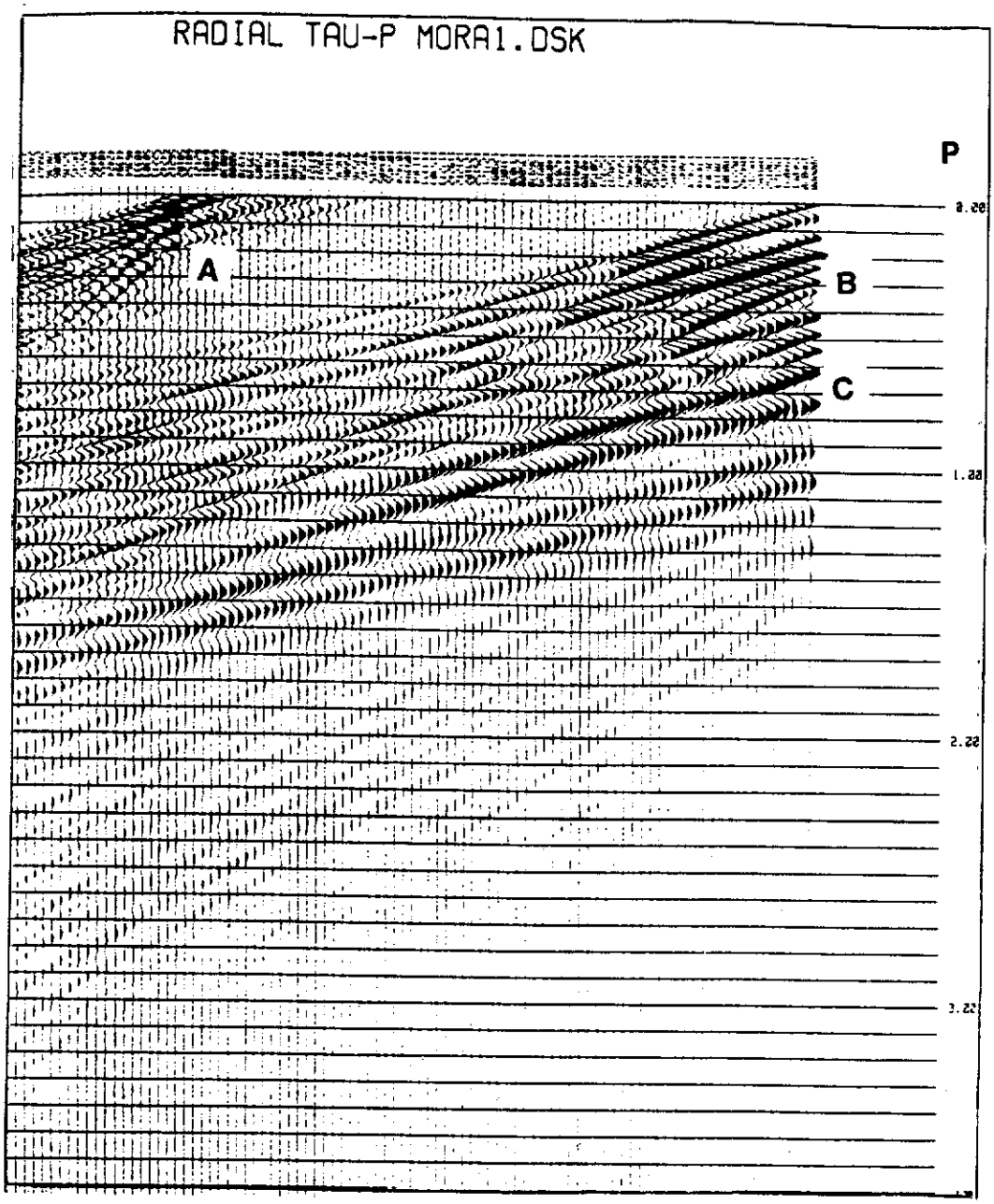

Figure 4.17. *Radial* transform of Figure 4.16.

An inverse *Radial* transform record having AGC applied to it and using the same geometry as the forward transform is shown in Figure 4.18. A comparison of input with output data shows almost identical shallow reflections but the deeper reflections have been clearly enhanced across the record (although there may be artefacts present also). Surface wave 'C', which had an apparent velocity of 370 m/s has been eradicated, since it was not in the forward transform range of 0.02 to 2.0 s/Km (500 m/s to 50,000 m/s). However, once again near offset trace artefacts have been manufactured by the transform summing across high amplitude surface waves, resulting in high amplitude strongly curved events being generated across the near offset traces between 1.0 and 3.0 seconds.

The input record random noise (prior to the first arrival) now appears similar to high frequency reflections, while consistent high frequency noise on the near offset trace of the input record has now been spread across the inner four traces. Overall however, the general improvement in reflection signal due to the *Radial* transform is welcomed, particularly the improvement in the deeper reflection continuity resulting in an improved signal-to-coherent noise ratio.

It was of interest to observe the result of applying the *Radial* transform to the same record with a reduced slowness range. A p-value range from 0.05 s/Km to 1.0 s/Km (1,000 m/s to 20,000 m/s) was selected, which would not sample surface waves B, C and D. The inverse *Radial* transform is shown in Figure 4.19 alongside the input record (Evans, 1991b). The inverse record appears to show a marked improvement over the input record, having improved the reflection continuity both in the upper section and at later times, with the surface waves no longer evident. The inner trace noise is present once again. Clearly, raising the low velocity end during the forward transform has a great impact on the attenuation of the surface waves (this is not unexpected, since it is also the case with the conventional τ-p transform when the summation process does not include surface wave slopes). Reducing the high velocity end of the slowness range does little to alter reflection continuity, since changing the high velocity from 50,000 m/s to 20,000 m/s would mean sampling only a few more values at the lower end of the slowness range.

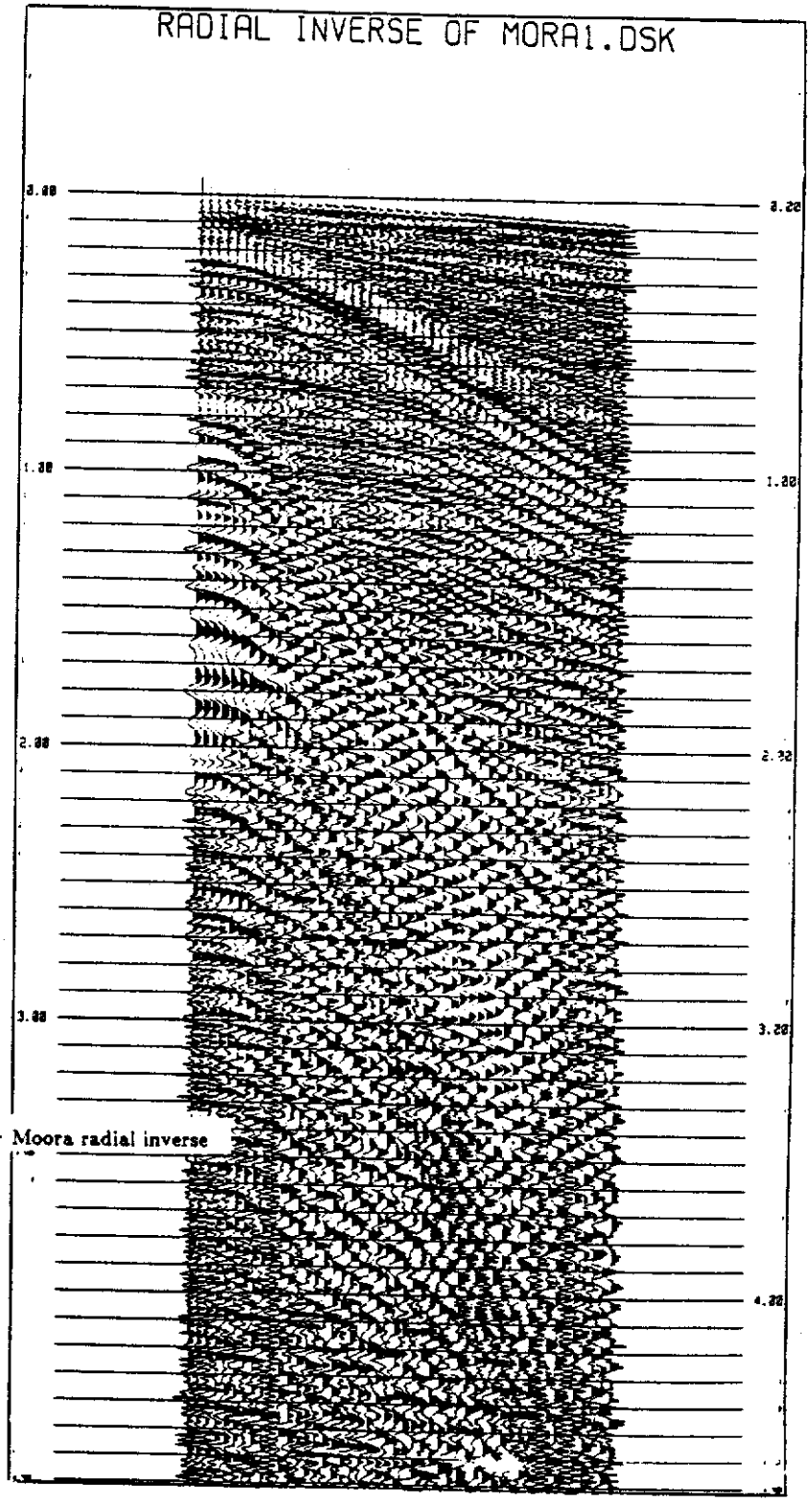

Figure 4.18. Inverse *Radial* transform of Figure 4.17.

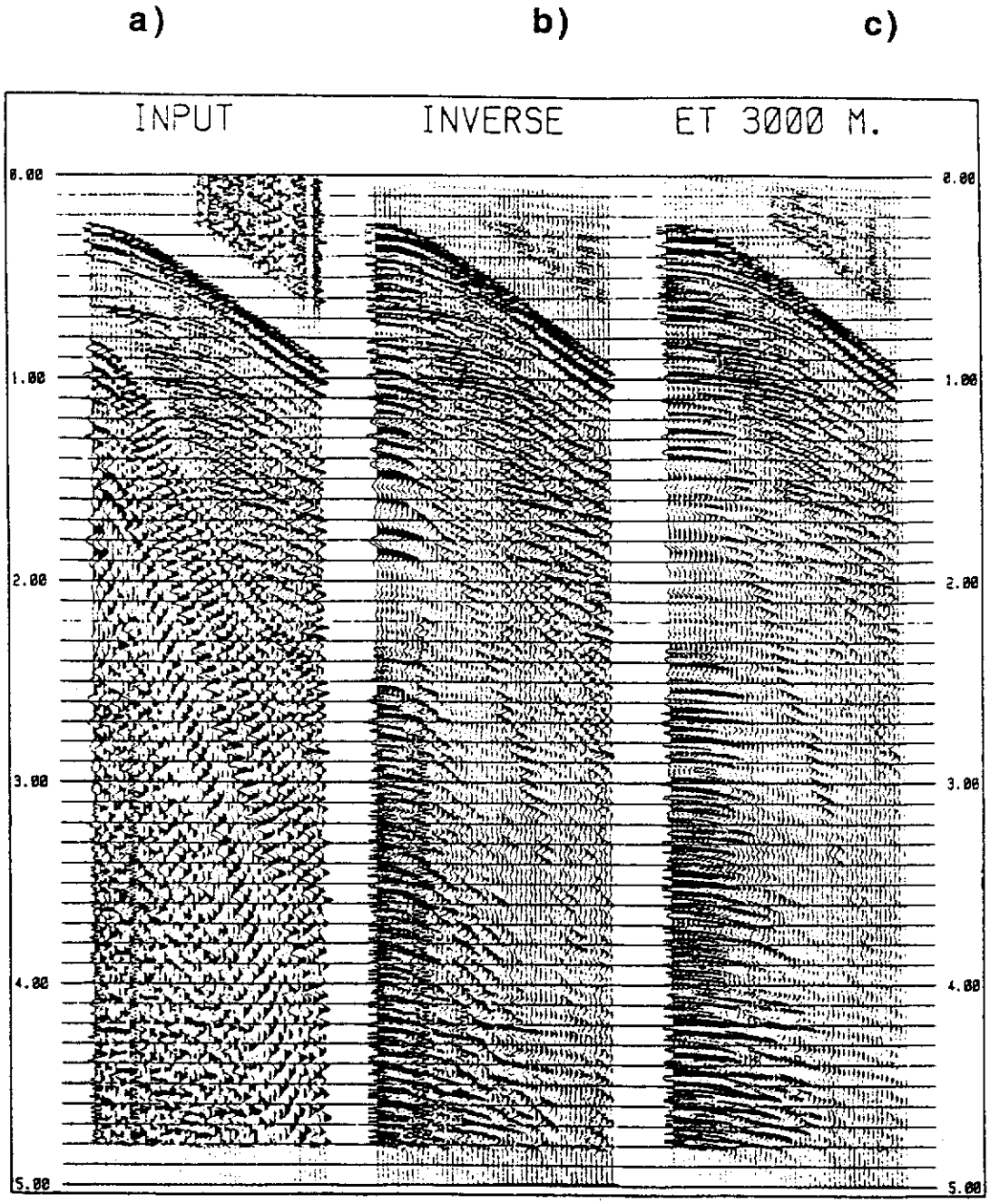

Figure 4.19. Comparison of input record (a) with *Radial* transformed record (b) and *Extended* transformed record (c). The Radial record transform was performed across a range of 0.05 s/Km to 1.0 s/Km (1,000 m/s to 20,000 m/s), while the *Extended* transform was performed across a range of 0.05 to 2.0 s/Km (500 m/s to 20,000 m/s). There is an improvement in reflection signal-to-noise ratio in both transforms.

The *Extended* transform was now applied to the same input record, using a slowness range of 0.05 to 2.0 s/Km (500 m/s to 20,000 m/s), in order to see if the *Extended* transform could provide further improvement in signal-to-noise ratio over the *Radial* transform, without the need to limit the lower velocity end of the slowness range. An arbitrary offset of 3,000 m was chosen (the actual radial offset being 411 m to the nearest trace), and the *Extended* transform run forward and inverse. The result is shown in Figure 4.19c).

There is a further improvement in shallow reflection continuity, particularly the reflection at 1.0 seconds which is now seen to be continuous to the nearest offset trace. The deeper reflection events are enhanced while the inner trace artefacts which were a problem with the *Radial* method are no longer present. The transform summation curvature is now a function of offset, so that different offsets result in different summation curvature. The *Extended* transform using an offset of 3,000 m has now summed data over a much flatter trajectory of shot record data points than that of the *Radial* transform, which has resulted in the failure to sum along surface wave trajectories (allowing their attenuation). This has resulted in an enhancement in reflection continuity, and a general improvement in signal-to-noise ratio.

The conclusion is that the *Radial* and *Extended* transformed records have improved the general quality of the input data. In these records, the most important reflections were those down to 1.5 seconds. In 1987, the forward and inverse transform (using the VAX mainframe computer) took a total of 28 minutes per record. With this in mind, and the fact that only the long offset data suffered from such noise patterns, it was decided that the radial transform approach would not be applied to the full 3-D volume. Instead, a band-pass filter was used to remove the lower frequency surface waves (Stewart and Evans, 1989). However, the transforms operated successfully.

German Creek Case History. A second case history of the application of the *Extended* transform is now provided but this time muting is tested. In this data set, the surface wave was of similar frequency to the reflections so it was not possible to apply a simple band-pass filter (as was applied to the Moora 3-D volume). A LOFOLD3-D survey was recorded in 1989 at 'German Creek' coal mine, Queensland, in an effort to delineate shallow coal seams.

Figure 4.20 shows two AGC shot records in which 24 channels (at a 6 m station interval) were recorded at different lateral offsets. Shot 512 has a lateral source offset of 41 m and radial far offset of 143 m. Adjacent record 514 has a shot offset of 55 m but far radial offset of 148 m. The first break arrival is shown as event 'A'. Reflection 'C' is observed to arrive between 80 and 100 ms, whereas the surface wave 'B' arrives between 60 and 140 ms, cutting across the reflection. If such data are restricted in frequency bandwidth (which typically they are using small surface vibratory sources like MiniSosie Wackers), the separation of reflection from surface wave noise becomes difficult using conventional frequency or f/k type transforms.

As an example of the use of muting as a filter, the data of shot 512 were transformed using the *Extended* transform with a p-range of 0.05 to 2.0 s/Km and the *Extended* domain is shown as Figure 4.21. The tight band of energy in the 0.2 to 1.0 s/Km region represents arrival 'A', surface wave 'B' and reflection 'C'. Selective surgical muting was performed after application of AGC and shown in Figure 4.22, where reflection 'C' is weak. (AGC after muting has enhanced the reflection's presence in Figure 4.22.)

The inverse *Extended* transform of Figure 4.22 resulted in Figure 4.23. This shows a great improvement in reflection continuity compared with the input record data of Figure 4.20. The far offset reflected coal seam events are now clearly passing across the record at 'C', unobscured by the surface wave. Wave 'A' has remnant moveout associated with near offsets only. (Linear wave 'D' appears at the far offsets due to the summation of far offset noise during the forward transform.) Muting in the *Extended* transform domain is shown to improve reflection continuity in data where the application of frequency transforms may be limited.

Conclusions The *Radial* transform worked acceptably well on the physical model data. It worked better on the Moora field data where strong surface waves masked deeper reflections, requiring a limited range of slowness values to remove surface wave energy (as is expected of the conventional τ-p transform). The *Extended* transform worked even better than the *Radial* transform on the Moora data, using an arbitrary radial offset as a filter instead of a restricted slowness range. The surgical mute in the *Extended* domain on the very shallow German Creek data showed the *Extended* transform could be used with all forms of field data.

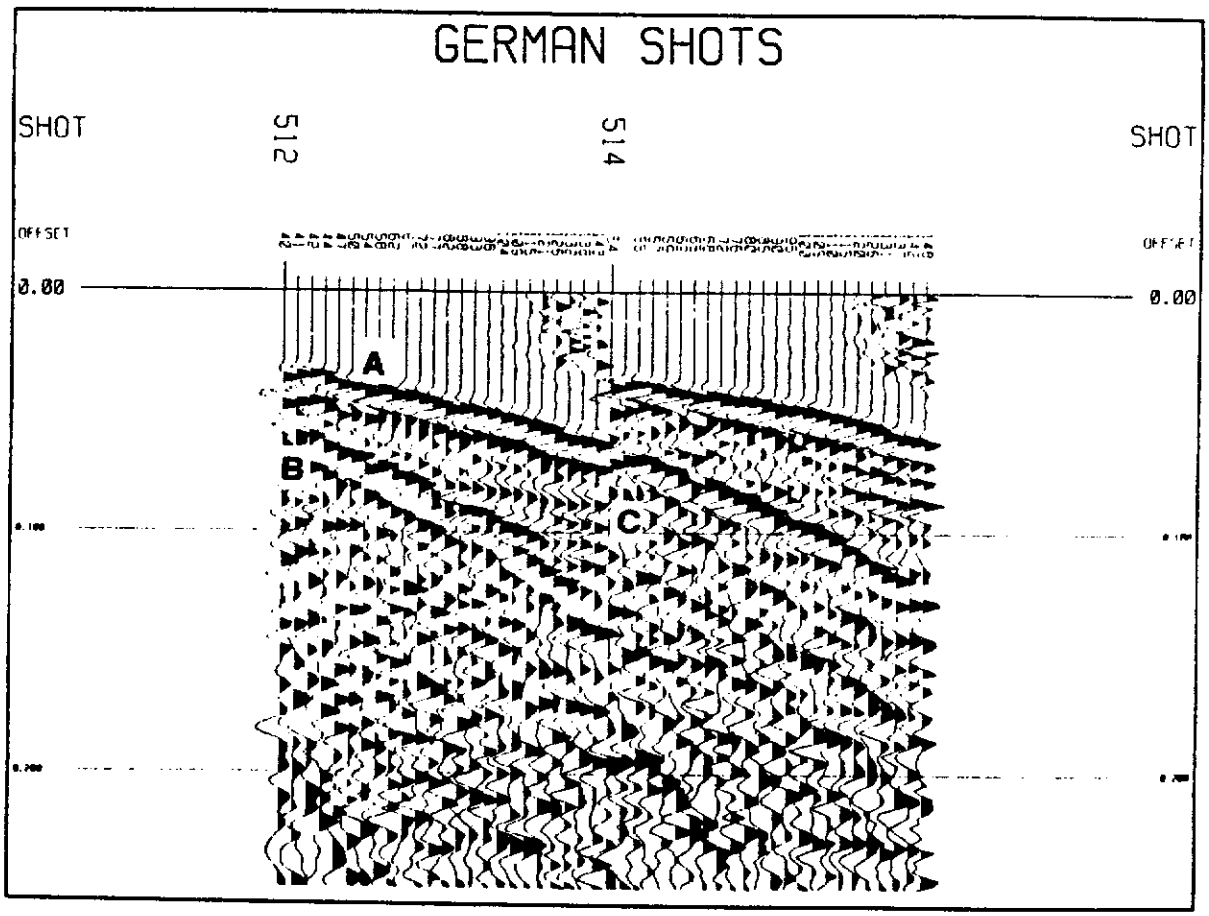

Figure 4.20. Two German Creek shot records 512 and 514 with AGC applied. Shot 512 shows direct wave 'A' (apparent velocity of 3,560 m/s), the surface wave 'B' (apparent velocity of 1,270 m/s) and the reflection 'C' (apparent velocity of 11,800 m/s).

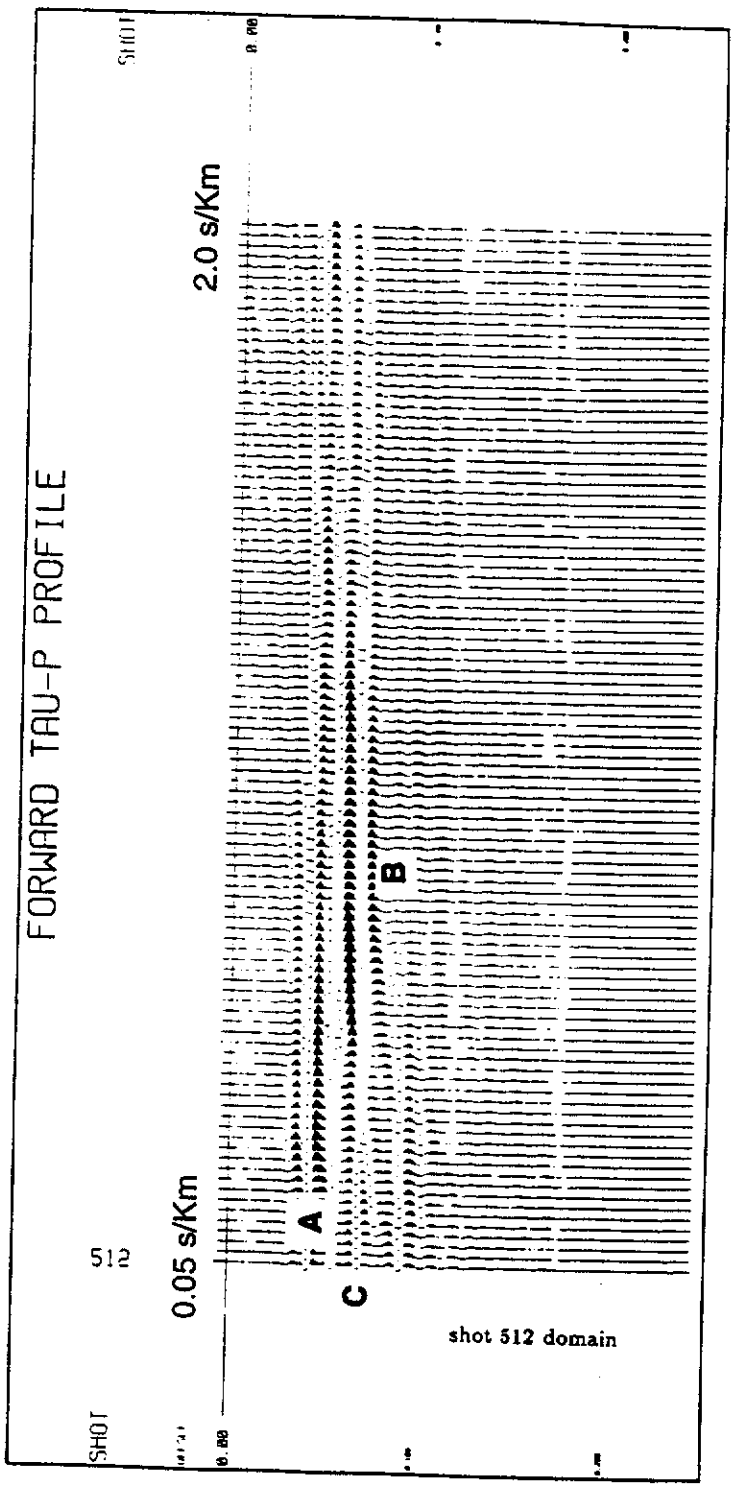

Figure 4.21. The *Extended* domain representation of Shot 512 of Figure 4.20, in which the p-range is 0.05 to 2.0 s/Km (500 to 20,000 m/s). The direct and surface waves ('A' and 'B') are strong relative to the weak reflection 'C'.

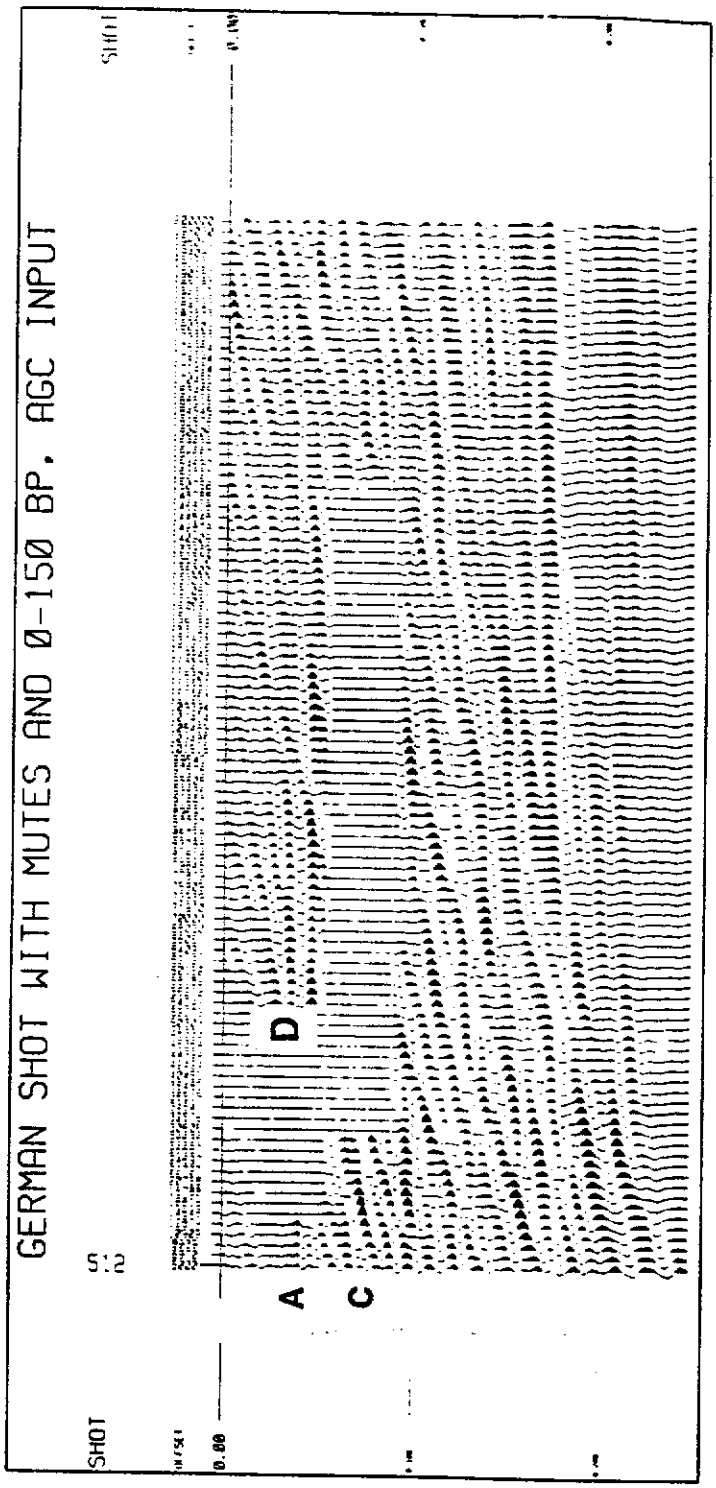

Figure 4.22. The *Extended* domain with a surgical mute, after AGC has been applied to the input data. Low p-values of 'A' while the majority of reflection 'C' remains after muting.

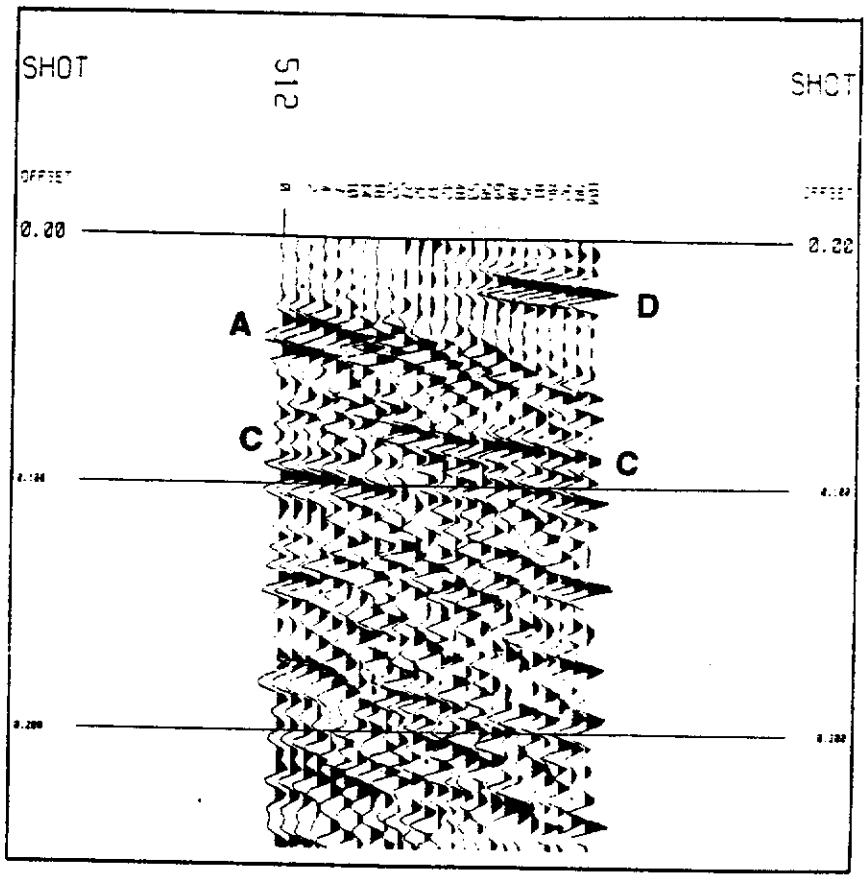

Figure 4.23. The inverse *Extended* transform of Figure 4.22 after AGC. Wave 'A' has been extensively muted (residual moveout results from not being totally muted in the *Extended* domain), surface wave 'B' has disappeared, and reflection 'C' clearly extends from near to far offsets. Lineation 'D' results from the summation of random noise on far offsets during forward transform.

CHAPTER 5
An approach to statics corrections

While surface waves cause major problems in masking high frequency reflections recorded by coal seismic data, another strong influence on the ability to obtain a good image with high frequency coal reflection data, is the problem caused by near-surface static errors. The higher the frequency of the data to be stacked, the more important that static errors are resolved early in the processing of data. In LOFOLD3-D where the number of binned traces is low, the correct application of statics corrections is even more important.

During 1990 it was noted that, after observing a considerable range of 2-D and LOFOLD3-D coal field seismic data, changes in the near-surface refraction wave were duplicated in later arriving reflection data (particularly where the topography was flat). This generally occurred where the sub-weathering layer velocity was much faster than the weathering layer velocity- a typical situation in the shallow coal mining environment. (It was accepted that the weathering velocity, structure and uneven topography affected such refraction arrival times.)

Consider therefore the fact that if both the refracted and the reflected waves pass through the weathering layer with very similar travel paths (Figure 5.1), then static corrections to remove the effects of weathering variations on the refraction traveltimes will be very similar to those required for reflections. If this were so, semi-automated processes to align refractions may be applied to make reflection waves become more continuous (Hatherly et al., 1994).

For example, if there is a velocity contrast greater than 3:1 between the sub-weathering and weathering, a refracted raypath through the weathering is less than 6 percent longer than a vertical raypath. A reflected raypath would therefore be expected to pass through the weathering between the refraction raypath and the vertical. Given this situation, static corrections calculated to remove the effect of the variations in weathering on the refraction traveltimes approximate those required for the reflections. To perform the refraction alignment, a linear moveout (LMO) correction is applied to data which is based on the refractor's velocity.

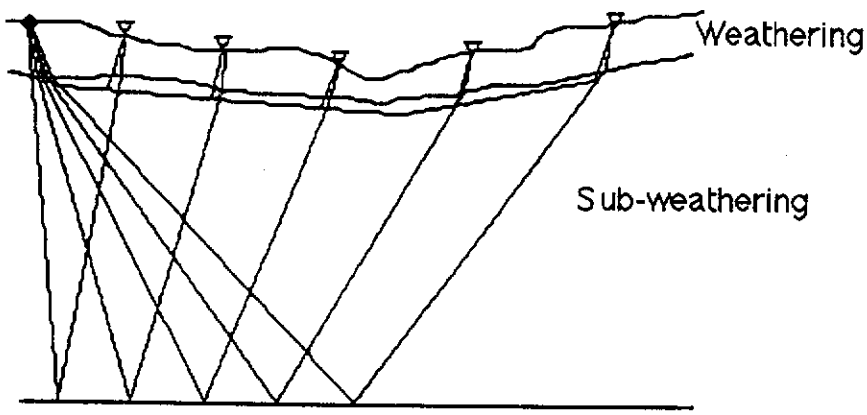

Figure 5.1. Refracted and reflected ray travel paths. The travel path lengths are very similar within the weathering if there is a velocity contrast of 3:1 or greater between the sub-weathering and weathering (after Hatherly et al., 1994). Consequently, static corrections to remove the effects of weathering variations on the refraction traveltimes will be very similar to those required for the reflections.

To then execute the refraction statics application, common shot traces containing refracted waves from the same horizon are used. (The method is not applicable where refractions are weak, discontinuous or when there is more than one refractor, and shot gathers have many more traces for use than in LOFOLD3-D). A pilot trace representing the average refraction break time across a half the receiver spread length is used to run along the (LMO) refracted wave. Corrections are then calculated using the surface-consistent residual statics program (such as the DISCO 'STATIC-R' program), calculating the correction required to flatten the refractor. This can be performed on either the common-shot or common-receiver gathers. A second statics pass may be needed, followed by elevation statics corrections. The mechanics of this approach is similar to that of Daly and Diggins (1988), but does not require the building of a refractor model.

Figure 5.2(a) shows shot records from the Sydney Basin, after LMO application. Figure 5.2(b) shows the statics variations in both reflections and refractions have been removed after such surface-consistent statics have been applied. Figure 5.3 shows the result on Bulli seam reflections from data recorded at Appin, N.S.W. Figure 5.3(a) is the set of raw shot records, showing the Bulli reflector at 300 ms and the first breaks are irregular. Figure 5.3(b) shows application of elevation statics, which makes little apparent difference. After LMO and the surface-consistent statics, Figure 5.3(c) is produced. The moveout on the first breaks is now linear and the reflection appears to be hyperbolic.

Figure 5.4 shows a stacked section with and without this procedure. Figure 5.4(a) shows the section with uphole and elevation corrections applied, whereas Figure 5.4(b) shows the statics application and a remarkable improvement in data quality and resolution.

In practice, it has been found that uphole times are unnecessary, since variations in shot timing due to weathering velocity variations are accounted for in the shot component of the statics calculation. This is useful when attempting to maintain low costs, as in the case of the LOFOLD3-D method. The method works best where arriving refractors are approximately linear and well defined. The method reduces in performance

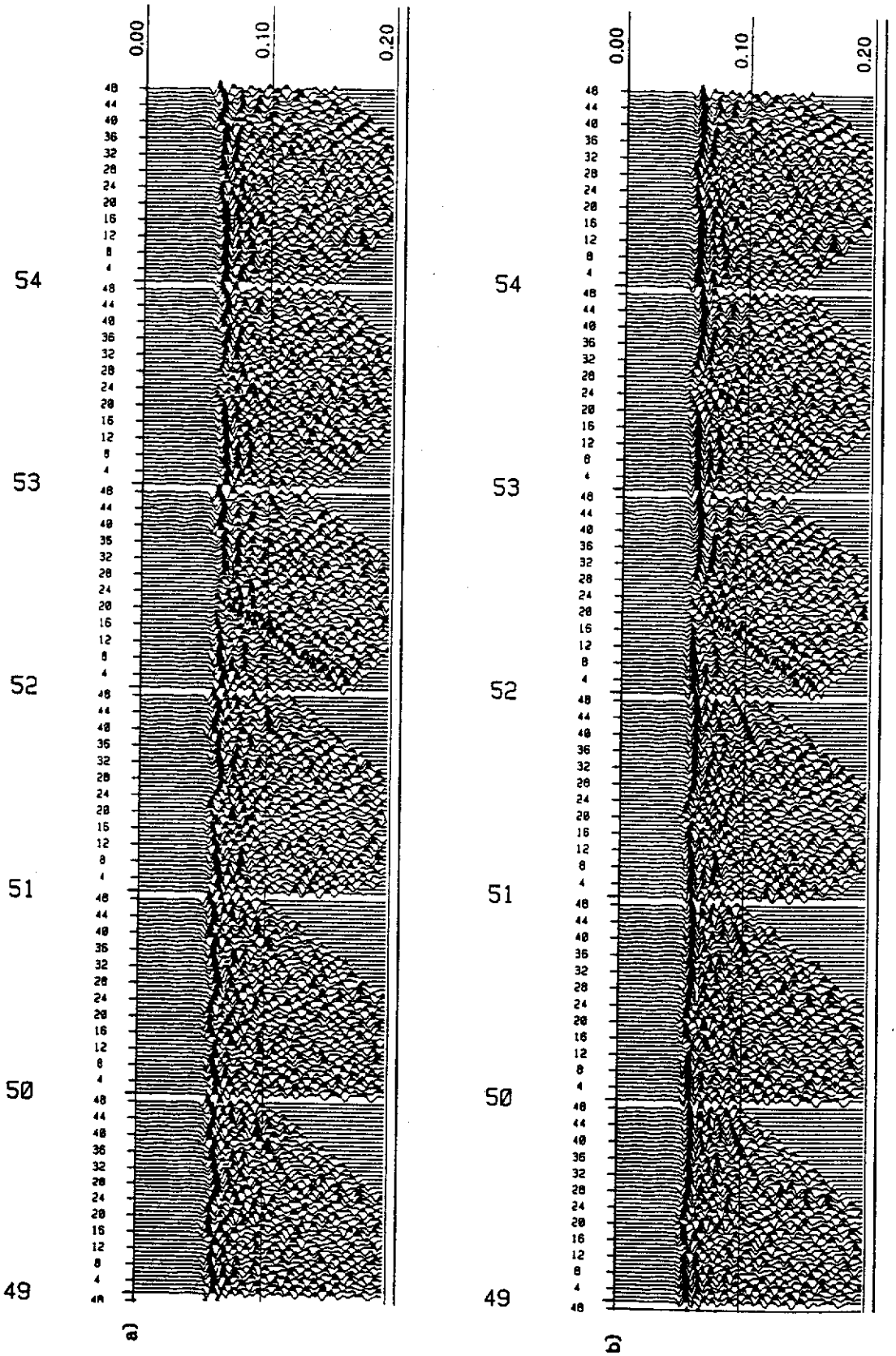

Figure 5.2(a). Raw shot records after LMO and before application of the refraction statics correction, and Figure 5.2(b) are the same records after application of residual statics (after Hatherly et al., 1994). The records after correction have continuous first breaks.

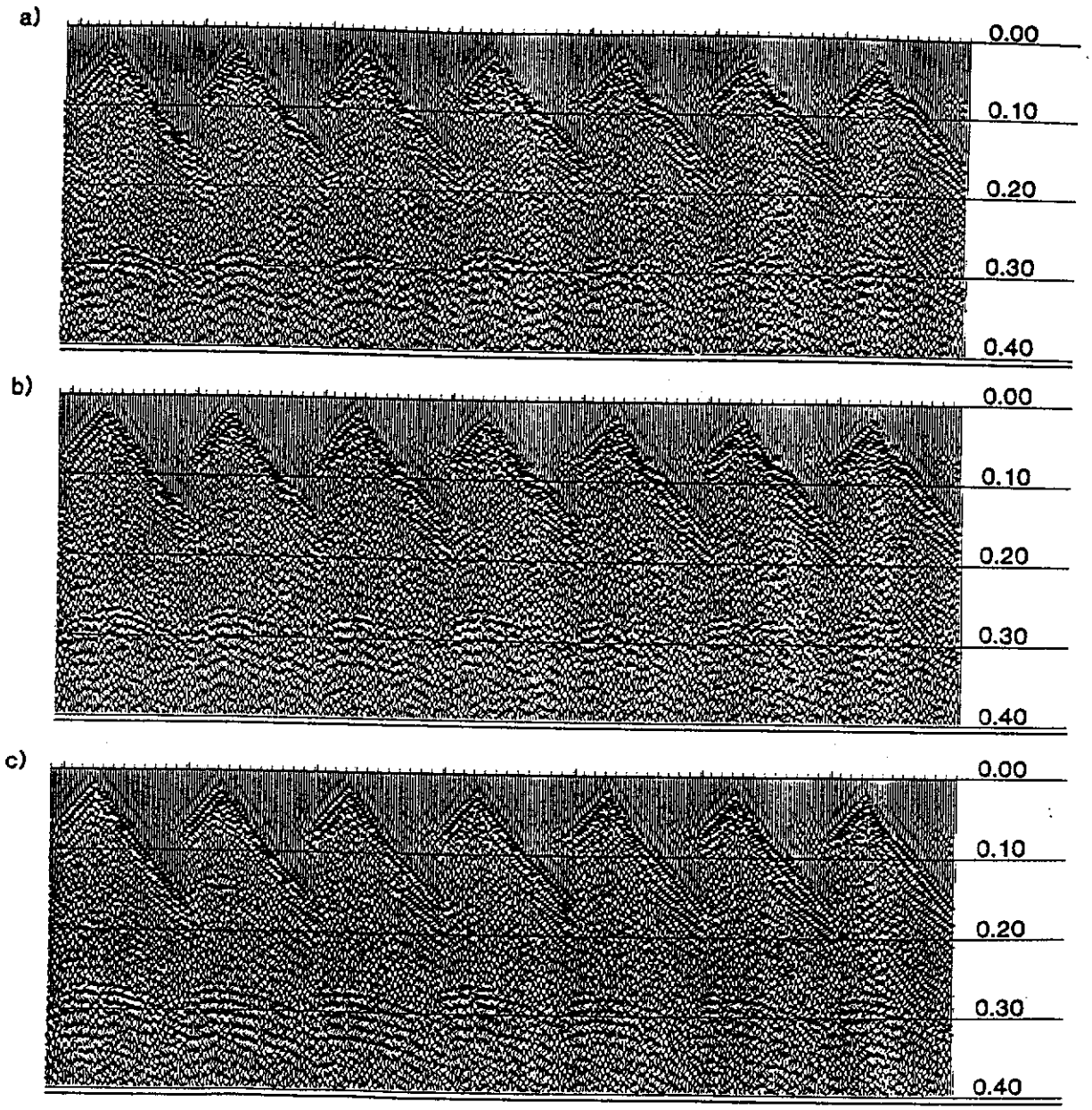

Figure 5.3(a) Raw shot records, (b) after elevation correction, and (c) after surface consistent refraction and elevation corrections (after Hatherly et al., 1994).

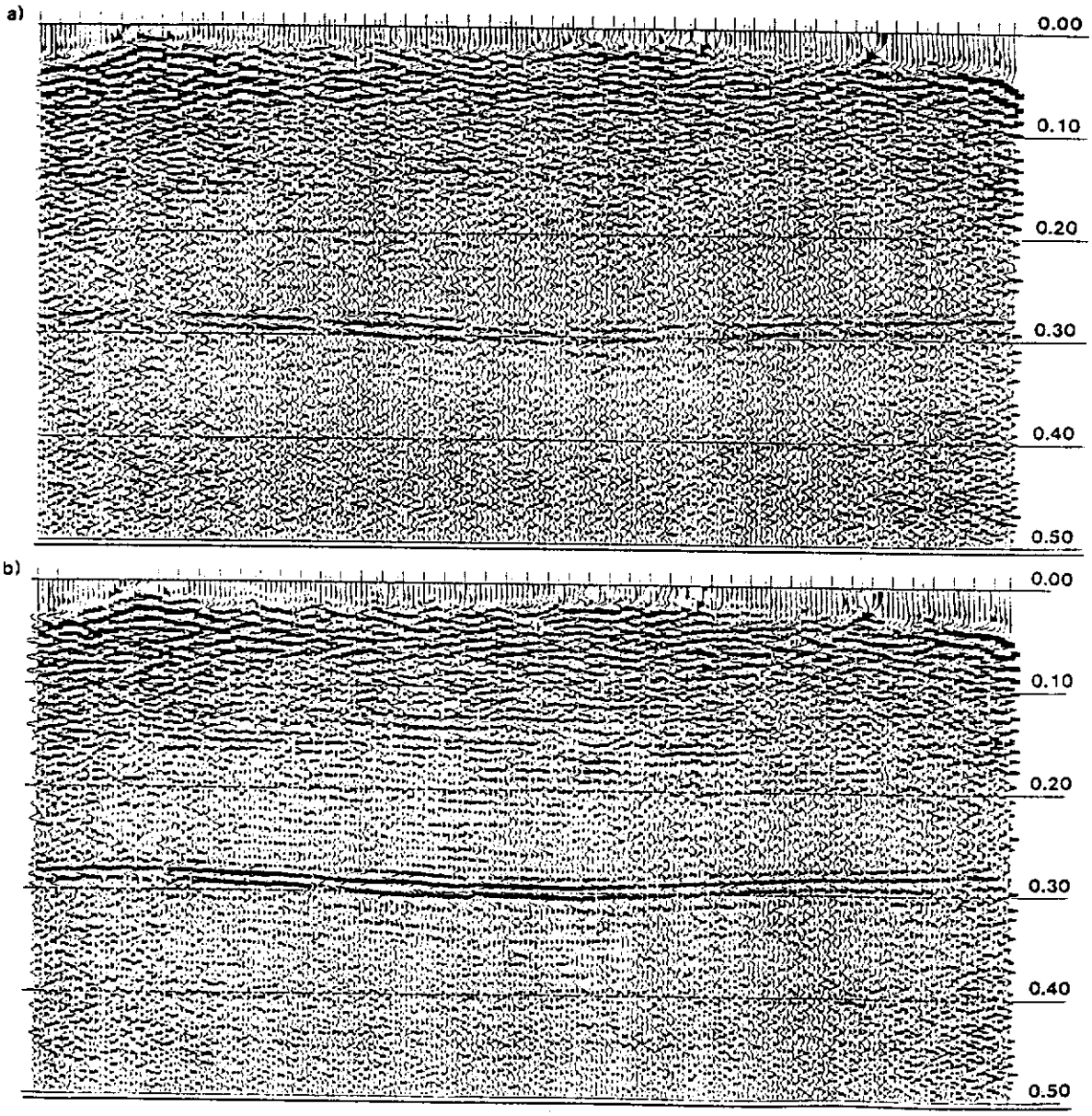

Figure 5.4(a) Stacked section of an Appin 2-D line with field statics only, and (b) after application of the surface consistent refraction statics correction (after Hatherly et al., 1994).

at near 3-D offsets where either refractions may not have developed well, or where reflections have their highest curvature. Consequently, the application of the method is easiest using the longer offset, more linear refraction data. The approach has been found successful in both 2-D and 3-D recording, providing consistently useful results in most cases.

The data shown in Figure 5.4 is derived from a 2-D explosive source survey at Appin, but the method worked equally well for LOFOLD3-D surveys at Newlands mine and at Tower Colliery (Lambourne et al., 1991). It did not work well at Collie where rapid short-distance changes in near surface velocities and overlapping refraction arrivals were encountered. Low velocity contrasts between the weathering and sub-weathering is a further problem compounding the difficulties with Collie data (Evans and Urosevic, 1995) .

The major advantages of this statics approach are that separate up-hole surveys are not necessary. There is no need to pick first breaks. Check shots and uphole times are not required. Only single pass velocity analyses have often been needed and surface consistent residual statics computations are often unnecessary in later processing. The major constraints on the method are that the refracted and reflected waves pass through the weathering layer with similar paths, and that the method does require a clearly defined continuous refractor on which to operate.

The approach discussed is commonly used in LOFOLD3-D processing for coal seismic surveys, and is also frequently adopted in conventional 2-D data processing. A patent for its use was approved (Hatherly and Evans, 1991). This advancement in statics corrections has gone a long way to improving the method of LOFOLD3-D surveying for coal seismic data. So far, the 3-D data have been improved by the application of the *Radial* and *Extended* transforms to enhance signal-to-noise ratios, and the application of statics corrections to improve alignment of high frequency reflections in a 3-D bin. However, the next major impediment to the LOFOLD3-D surveying method is that of performing an acceptable velocity analysis on a low number of binned traces. Chapter 6 will now develop a method to resolve this final impediment, as well as define a new method for the detection of three-dimensional dip, which is a prerequisite to resolving the velocity analysis problem.

CHAPTER 6
Three-dimensional moveout

It was explained earlier that one of the drawbacks to the LOFOLD3-D technique is that an acceptable velocity analysis using a low number of binned traces of varying source/receiver azimuth, cannot be performed when dip is present. The reason for this is that the stacking velocity for individual traces in a bin depends on their individual source/receiver azimuths. The three-dimensional moveout of a seismic wave travelling from a shot to any receiver changes as a function of the amount of dip, the shot to receiver azimuth, and the velocity of the medium.

If the value for the true dip of the horizon of interest and its direction were known, the apparent reflector dip between any source and receiver for any azimuth may be computed for that horizon. The velocity term in a three-dimensional moveout equation may then be separated from the value of dip, so that three-dimensional moveout corrections for binned traces may use a single velocity for all azimuths. In the following Chapter, I present the development of the generalised moveout equation (GMO). The application of this equation for moveout corrections is dependent upon having a knowledge of the reflecting horizon's dip in terms of magnitude as well as direction, and the medium's velocity. To obtain a value of true dip and its direction, I have developed a dip detection technique which utilises the swath recording method.

A knowledge of the medium's velocity is central to this work. Fortunately there are numerous methods available to obtain a medium's velocity such as recording up-hole surveys, bore-hole velocity tests (i.e. 'well shoots'), zero offset VSP recordings, sonic interval velocity computations, the use of the Dix equation, conventional τ-p transforms, and so on. (In coal field work, such shallow velocity information is not a problem to obtain in the field anyway.)

This discussion therefore commences with developing the mathematical expression for the GMO equation, after which a method is developed to determine true dip/strike and azimuth of a reflecting horizon. A case history (using a physical model) of the dip determination is then provided, and the Chapter finishes with a second case history showing the correct binning and stacking of LOFOLD3-D traces, without the use of a velocity analysis.

6.1 A generalised moveout equation (GMO)

Consider the plan view shown in Figure 6.1 in which an orthogonal coordinate system has horizontal axes X and Y, and vertical axis Z. Let a ray travel from a source point S located at (x_1 , y, 0) down to a reflecting interface and back up to a receiver R located at (x_2, 0, 0).

Let the receiver line be along a line from a position (x_1,0,0) to (x_2,0,0). In Figure 6.1, dip is down and positive along the X-axis from R to 0 while in the Y-axis direction it dips downwards (and is positive) from y to 0. (This follows the sign convention established in Chapter 3.3.) The 3-D true up-dip direction is from low values to high values of x and y. The reflection point therefore moves up-dip in both the X and Y directions, shown by the movement from directly below mid-point location M to some reflection point Q. The plan view shows the ray (represented by the dotted line) passing from source point S (x_1, y, 0) reflecting at M mid-way between S and R, and on to the receiver R (x_2, 0, 0). In plan view this is a straight line when the reflection plane is horizontal. However, when the reflection plane dips, the reflection point Q moves up-dip from M .

Since the reflecting surface dips three-dimensionally, the plane containing the raypath, which is normal to the reflecting surface, is not normal to the Earth's surface (the X-Y plane). In order to analyse the travel path of the reflected ray, a 3-D perspective view must be considered. Rays are reflected from up-dip positions, lines drawn normal to the reflecting layer are all up-dip from the vertical plane through S and R, and consequently the travel path analysis is more complex than the simple two-dimensional dipping layer analysis. In this thesis, I commence with the three-dimensional diagram of Sheriff and Geldart (1982), shown in Figure 6.2.

To compute the three-dimensional travel path length from a source to a reflection point and on to a receiver, the approach adopted is that of optics using the method of images. The distance from the source down to a reflection point and up to a receiver is the same as the distance from an image of the source to a receiver.

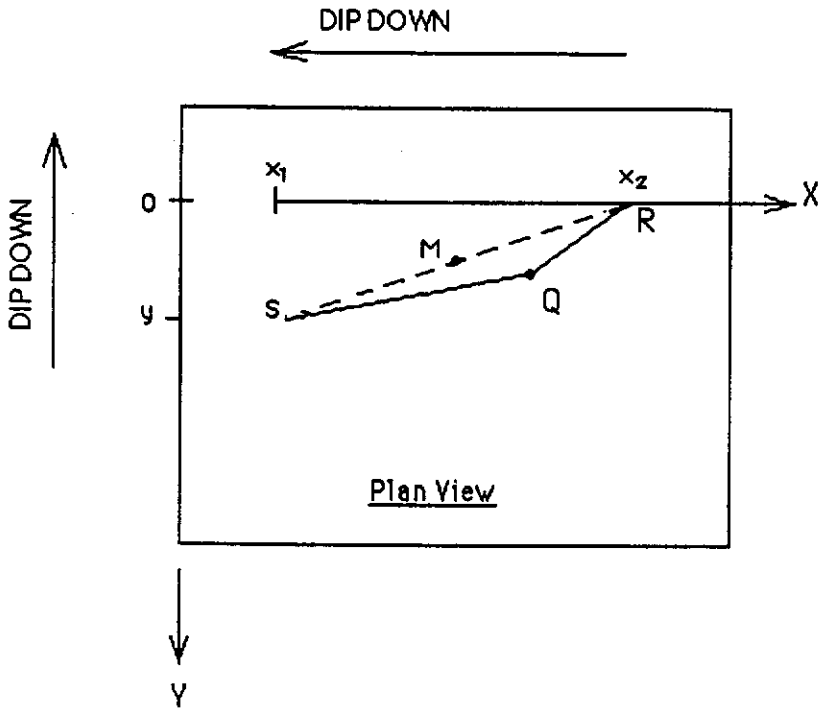

Figure 6.1. Plan view of the movement of the reflection point up-dip from M to Q when the reflecting plane is tilted. On a horizontal reflector, the reflection would occur at M (in plan view).

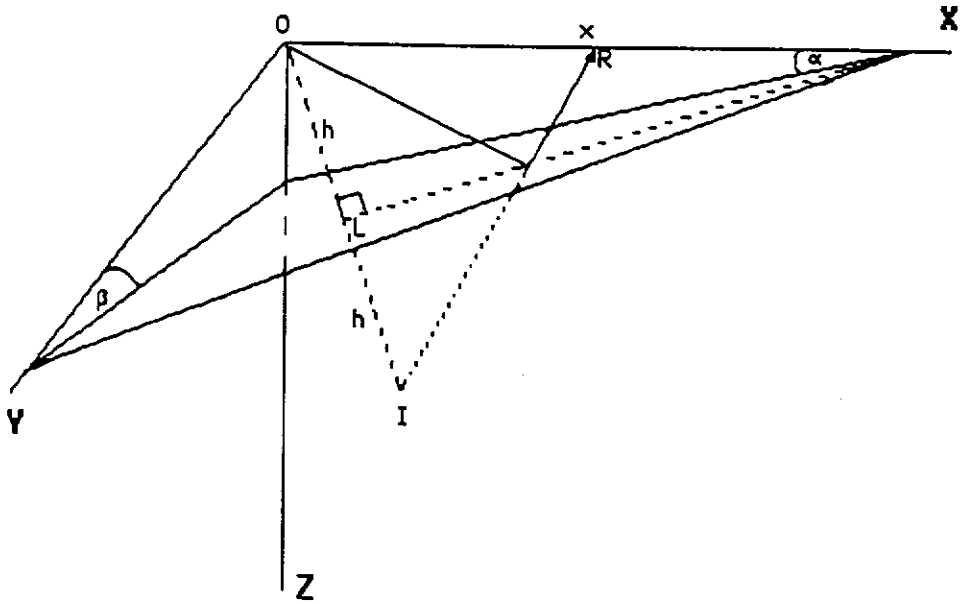

Figure 6.2. In-line reflection from an out-of-the-plane dipping layer (after Sheriff and Geldart, 1982).

Where x = Offset source to receiver
h = Zero offset length, perpendicular to reflector
α = Angle of dip along X-axis towards the origin 0
β = Angle of dip along Y-axis towards the origin 0

6.2 Determination of travel path length IR

Consider the three-dimensional box with coordinate axes X, Y and Z is shown in Figure 6.3 . The dipping reflection plane has dip angles of α in the vertical X-Z plane, and β in the vertical Y-Z plane. α and β have a positive value when the reflection horizon dips down towards the Z-axis, and a negative value when dipping upwards away from the Z-axis, as established in Chapter 3.3. X and Y are positive in the directions as shown, while Z is positive downwards.

The expression for the two-way travel path length where the source is at (x_1 ,y_1 ,0) and the receiver is at (x_2, 0 , 0), is given as follows (see Appendix A):

$$|IR| = \left((x_1 - x_2 + 2at)^2 + (y_1 + 2\,bt)^2 + 4\,t^2 \right)^{1/2} , \qquad (6.1)$$

where $a = \tan \alpha$,

$b = \tan \beta$,

$$t = \frac{d - a\,x_1 - b\,y_1}{a^2 + b^2 + 1} \quad , \; d = h\;(a^2 + b^2 + 1)^{1/2} \text{ , and}$$

h = the length of the normal from the origin of the coordinates to the reflector.

The two-way travel distance for every trace in a CMP gather is affected by three-dimensional dip. Equation 6.1 is dependent upon the value of dip α and β in two orthogonal directions, as well as lengths h, y_1, x_1 and x_2. For any set of CMP traces recorded from this reflection plane, x_1 ,x_2, y_1 , α, β and h are known values. The length of the normal to the reflection plane h, may be obtained in practice by a zero offset shot recording where the medium velocity is known (as explained earlier), or in shallow coal recording when a bore-hole is drilled to intersect the reflector orthogonally (with a knowledge of the regional dip).

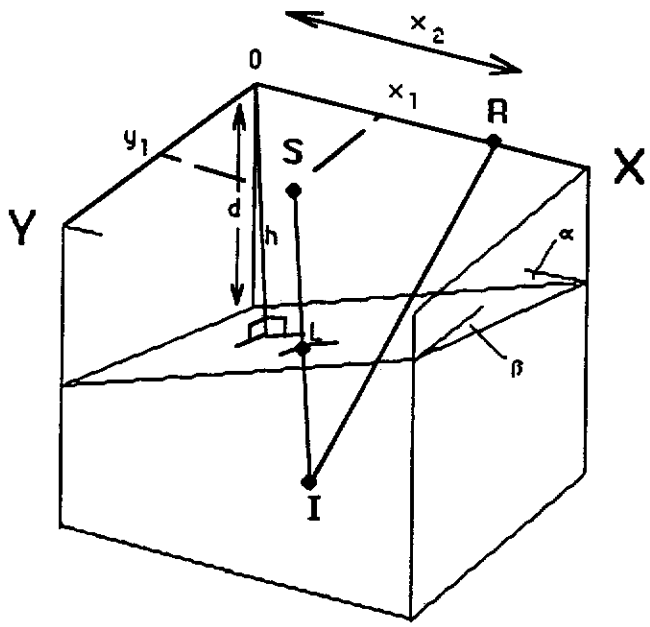

Figure 6.3. Source S and receiver R with image point I form triangle SIR. A line drawn perpendicular from S to I passes through the plane at L.

The generalized moveout equation (GMO) is the two-way time for each trace in a CMP bin gather and may be obtained by dividing equation (6.1) by the medium velocity, V.

The GMO equation is therefore:

$$\frac{IR}{V} = \frac{\left((x_1 - x_2 + 2at)^2 + (y_1 + 2\,bt)^2 + 4\,t^2 \right)^{1/2}}{V} \qquad (6.2)$$

If there were no dip, the application of the GMO equation could be used to align all reflection events along any chosen line of gathers. It would therefore follow that in the presence of dip, if the values of α and β were known, all the reflections in any gather in any direction could be aligned by subtracting the zero offset traveltime from the GMO corrected two-way travel time.

This knowledge becomes useful if used in reverse. If test values of α and β are used in the GMO equation for each trace, the alignment of the reflections along all gathers in a bin line will be an indication of the correctness of the values of α and β, irrespective of the azimuth or offset of the different CMP traces.

The two-way travel reflection time from the origin is $\frac{2h}{V}$ or t_0. The general GMO correction (δt) for the reflections in all gathers to be aligned is simply:

$$\delta t = \frac{IR - 2h}{V} = \frac{IR}{V} - t_0 , \qquad (6.3)$$

$$\text{or, } \delta t = \frac{\left((x_1 - x_2 + 2at)^2 + (y_1 + 2\,bt)^2 + 4\,t^2 \right)^{1/2}}{V} - t_0 . \qquad (6.4)$$

For simplicity, I leave the above equations as they stand, without the inclusion of the t_0 value, since although the zero offset two-way time can be separated out from the other terms, the general expression becomes very cumbersome and lengthy.

Once α and β are determined, the true dip and its azimuth can be obtained, resulting in the ability to use a single velocity term V in the GMO gathers

with an azimuthally variable dip factor. The next step now is to develop a procedure to obtain values of dip using equation (6.4).

6.3. A method for Dip Detection

Equation (6.3) can now be used to obtain an estimate of three-dimensional dip. In the field, the known variables will be x_1, x_2, and y_1, while the zero offset two-way traveltime t_0 will be known from zero offset tests (as suggested earlier) and the medium velocity is known (using the conventional well or bore-hole tests discussed earlier). The unknown variables are the dips α and β. By varying values of apparent dip in equation (6.3), it becomes possible to produce an optimum line-up of traces across all the gathers.

To ensure the optimum alignment of traces they are stacked assuming various values of α and β. When the maximum peak-to-trough value is obtained, then the correct values of apparent dips α and β will have been determined.

In practice, to compute δt to be applied to each trace in a gather, we commence with a chosen value of α and a fixed value of β in equation (6.3). Each individual trace in a swath CMP gather is time shifted by δt like a static correction, as an azimuthally dependent GMO correction. If the values of α and β are correct, the reflections will align as they would when applying the appropriate GMO correction in a conventional CMP gather. If they do not align, the values for α and β may be continually changed in a trial-and-error manner until the best reflection alignment is obtained. When a good alignment is obtained on all gathers along the CMP line, that is then the best estimate of α and β.

6.4 To determine the true dip

Having obtained the values for α and β, the true dip θ is given (see Appendix B) by:

$$\text{True dip value } \operatorname{Tan}\theta = (\operatorname{Tan}^2\alpha + \operatorname{Tan}^2\beta)^{1/2} . \qquad \text{(B-1)}$$

$$\text{The azimuth of true dip } \operatorname{Tan}\phi = \left(\frac{\operatorname{Tan}\beta}{\operatorname{Tan}\alpha} \right). \qquad \text{(B-2)}$$

However, for this research, the most important information for computing NMO corrections is a knowledge of the apparent dips α and β, their orientation with respect to the survey area, values for source and receiver locations, and the zero offset two-way time t_0 .

During this research, neither θ nor ϕ are used during the computation process since the GMO equation uses the separate apparent dip components of the true dip.

6.5 Orthogonal CMP test line

A parallel source/receiver line geometry only samples 90 degrees of the available 180 degree azimuths of the travel path directions, as shown in Figure 6.4. A better estimate of dip can result if the remaining azimuths are also sampled. If the source and receiver lines are rotated to be orthogonal to their previous orientation, raypaths would cover the remaining azimuths to provide a further estimate of dip. The new lines are source line 2 and receiver line 2 shown in Figure 6.4.

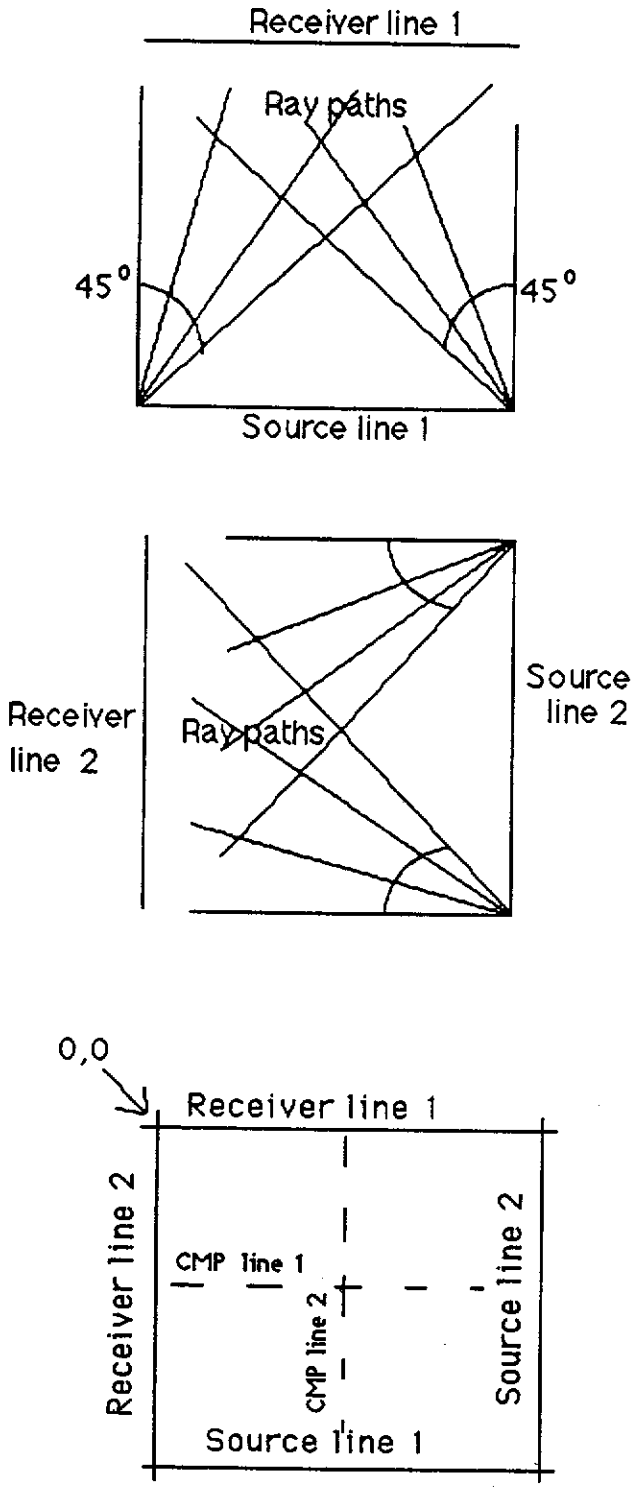

Figure 6.4. Azimuths for the square source/receiver configuration. Firing source line 1 into receiver line 1 produces raypaths over two ranges of 45 degrees. The configuration is then rotated by 90 degrees so that source line 2 is fired into receiver line 2, a further 90 degrees of raypaths are covered so that the maximum number of azimuths are sampled.

This produces a new set of apparent dip estimates using a line of CMPs at 90 degrees to the original set, completing a cross of CMP bin lines containing data from all azimuths.

α and β are now recomputed and averaged. A set of apparent dips has been determined from measurements over a wide range of azimuths, from which a more accurate true dip estimate will result.

6.6. Stacking bin lines without velocity analyses

The two orthogonal CMP lines that have been used for computing the apparent dip values may now have the GMO correction applied to traces in each gather and processed as stacked CMP lines. Each CMP gather is treated as a binned gather, in which reflection points are up-dip and scattered over a reflection area. The two CMP lines are perpendicular to each other and equivalent to conventional 2-D lines recorded without a knowledge of dip. In stacking such data, the objective is to show how a stack can be produced without the need for a velocity analysis. With LOFOLD3-D data, it is therefore useful to show that a bin line can be stacked using a small number of traces without velocity analysis which, as mentioned earlier, would be very difficult.

In order to determine the GMO correction δt for each binned trace along a CMP line, the centre of each bin now needs to have a value of 'h' determined. This is a simple computation since the true dip and its azimuth are known at the origin, as is the distance and azimuth to the bin's centre. Thereafter, all data along the CMP lines have their GMO corrections applied with respect to the midpoint of each gather. In the case of the two orthogonal lines, this will produce two stacked CMP bin lines, which can then be useful as a guide to data quality in two directions.

Such tests should be performed at the start of a survey. The major assumption throughout has been that the dips determined by this technique are consistent throughout the local survey area, and the GMO corrections of equation (6.4) may be applied to any individual swath CMP trace irrespective of apparent dip. This then allows the same velocity function for stacking binned data, without the need for a velocity analysis.

6.7 Testing the theory using a physical model

Following the foregoing theoretical development, the concept was tested by physical modelling experiments. The strategy was to collect data in two orthogonal directions, along dip and strike, and use the GMO expression containing values of α and β, to determine these values in the two directions. These would be compared with the known model values, to provide an indication of the method's accuracy for dip prediction.

The model would then be rotated to an arbitrary direction and the process repeated. The method would then have been shown to be working successfully by predicting values of dip for a physical model, in any chosen direction.

The technique used to obtain optimisation of the two variables in the general case requires fixing one variable and then varying the other in steps of one degree until a maximum peak and trough value is obtained. A best line-up will occur at some value of α. β may then be changed in one degree steps and the best event line-up obtained. This trial and error iteration method is continued thereafter in sub-degree values until the maximum peak and trough values have been obtained. Optimum values for α and β have then been established.

Following on from this, the data could be stacked along the two CMP lines, without the use of a velocity analysis. A three fold stack would be tested to observe if such a low fold stack would image physical model data adequately.

General procedure. The terminology used for raypaths from source to receiver was 'cross-dip', and 'down-dip', as explained in Chapter 3. The cross-dip shooting configuration recorded a line of mid-point data in the dip direction, as shown in Figure 6.5(a). The down-dip shooting configuration recorded a line of data in the strike direction, as shown in Figure 6.5(b). Finally, the model was rotated by 45 degrees as shown in Figure 6.5(c) and a '45 degree' data set recorded. It was decided that 24 sources and receivers would be used on each line (rather than 48, which reduced the amount of data to be handled). The source line therefore had 24 source locations, each 200 m apart (i.e., 5 mm on the model), and they fired into 24 receivers, each 200 m apart.

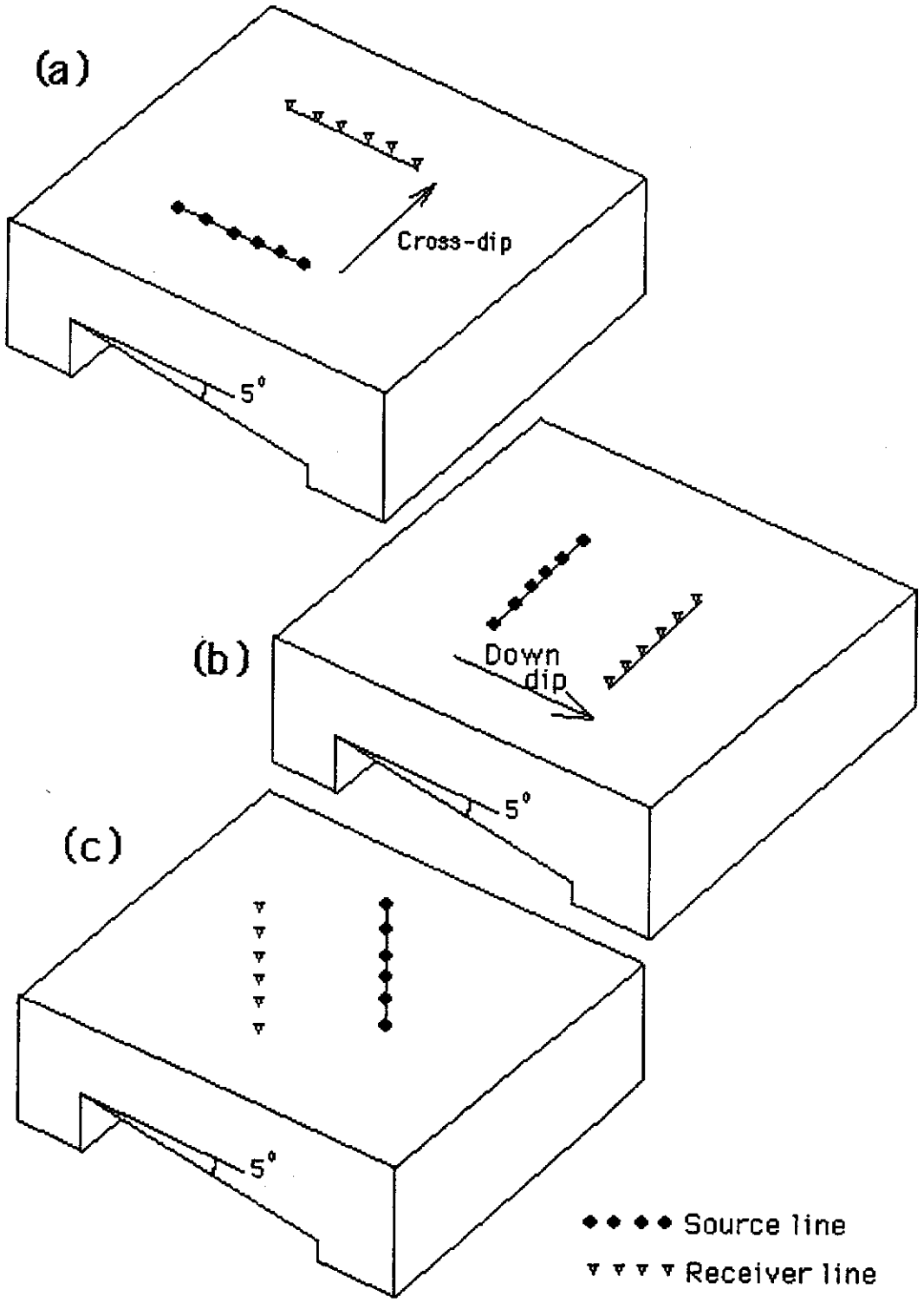

Figure 6.5. The physical model was used to record data in the (a) cross-dip and (b) down-dip directions, and (c) at an azimuth of 45 degrees to the dip direction.

The raw cross-dip records are shown in Figure 6.6, with down-dip records in Figure 6.7, and 45 degree records in Figure 6.8. The shot number and offsets are shown across the top of the figures.

Having collected the data, the geometry of each recording configuration was written into a DISCO file, so that all the offsets for each individual trace would be accessible by standard CMP sort routines from the DISCO data base.

The three input data sets were then resorted into CMP gathers and these are shown as Figures 6.9, 6.10 and 6.11 in which there are 48 CMP gathers for 24 shots and 24 receivers. The gathers have low fold at the line ends increasing to a maximum value at the centre of each line, because at the mid-point line ends, only a single trace is generated as a single shot is fired into each end receiver, whereas at the centre mid-point of each line, 24 shots have been fired into 24 receivers to generate 24 CMP traces.

The maximum fold, 24, is therefore found at the centre CMP. In Figure 6.9 (cross-dip), the reflections show increasing arrival times indicating the presence of dip in the section. In Figure 6.10 (down-dip), the arrival time of the reflector stays constant at around 670 ms, indicating no dip along the section. In Figure 6.11, the reflections show decreasing arrival time indicating the presence of dip in the section produced for the model rotated by 45 degrees.

For improved data analysis of the dip detection process, it was necessary to display the CMP with the most traces that would be used in any one gather, and this was CMP 24. The next step was to apply the process with CMP 24 as an example.

A program was written which allowed the specific recording geometry and variables to be input to compile a file in DISCO format, which then ran in interactive mode. The program was written in Fortran which requests all variables including the number of sources and receivers, their individual offsets and line offset; an estimate of the velocity and depth to the target horizon at the origin 0, and trial values of α and β.

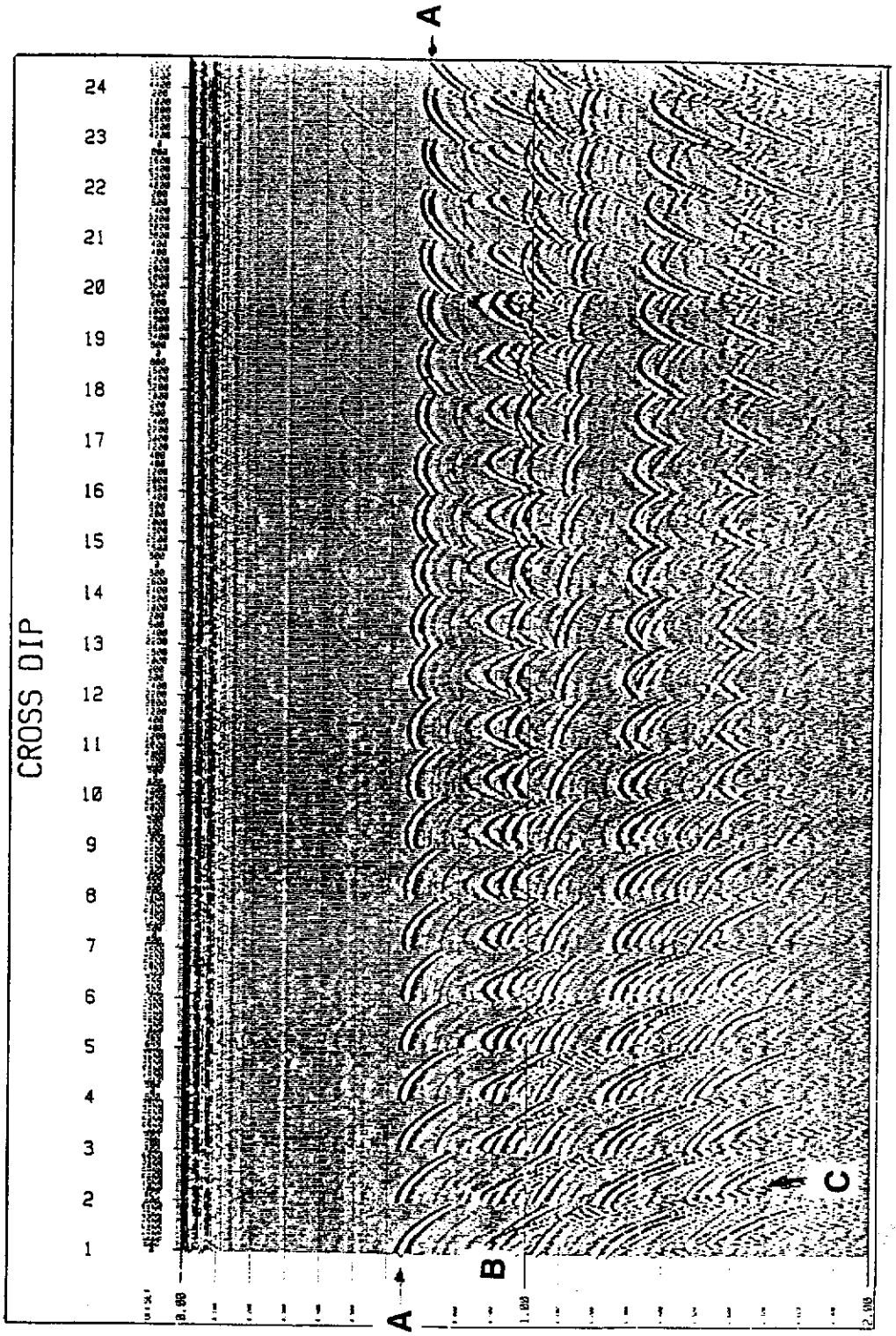

Figure 6.6. A suite of cross-dip shot records. The events commence on the left with move-out to the right, the events become symmetrical at the right of centre, and eventually move-out to the left by end of line. Event 'A' is the primary reflection and event 'B' is probably a converted wave reflection. Arrival times for 'A' are different at the ends of line, indicating the presence of dip. Event 'C' is the surface wave discussed earlier in Chapter 4.

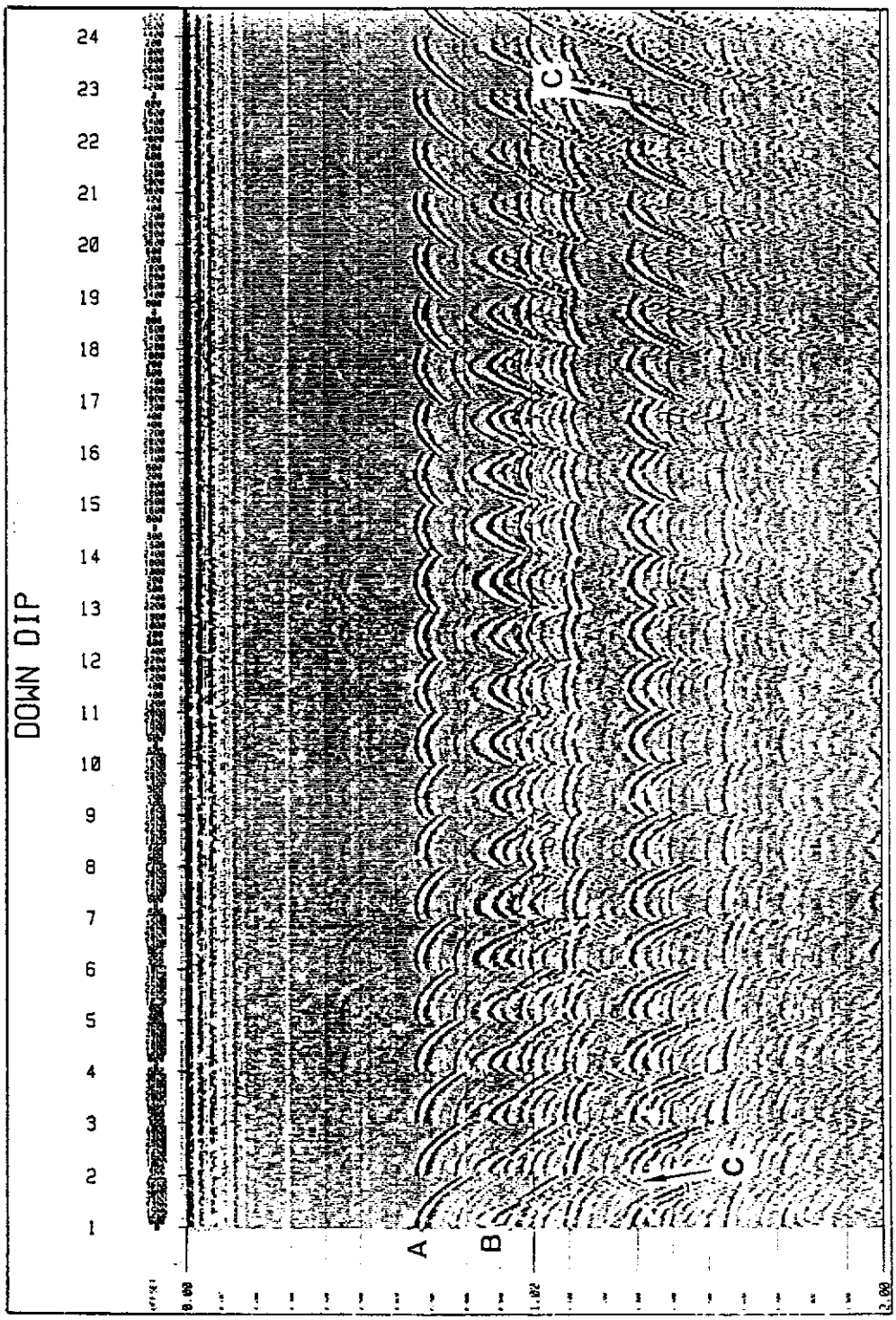

Figure 6.7. A suite of down-dip shot records. Events are similar to Figure 6.6, except that the arrival times of reflection event 'A' do not change along the line, indicating the absence of dip.

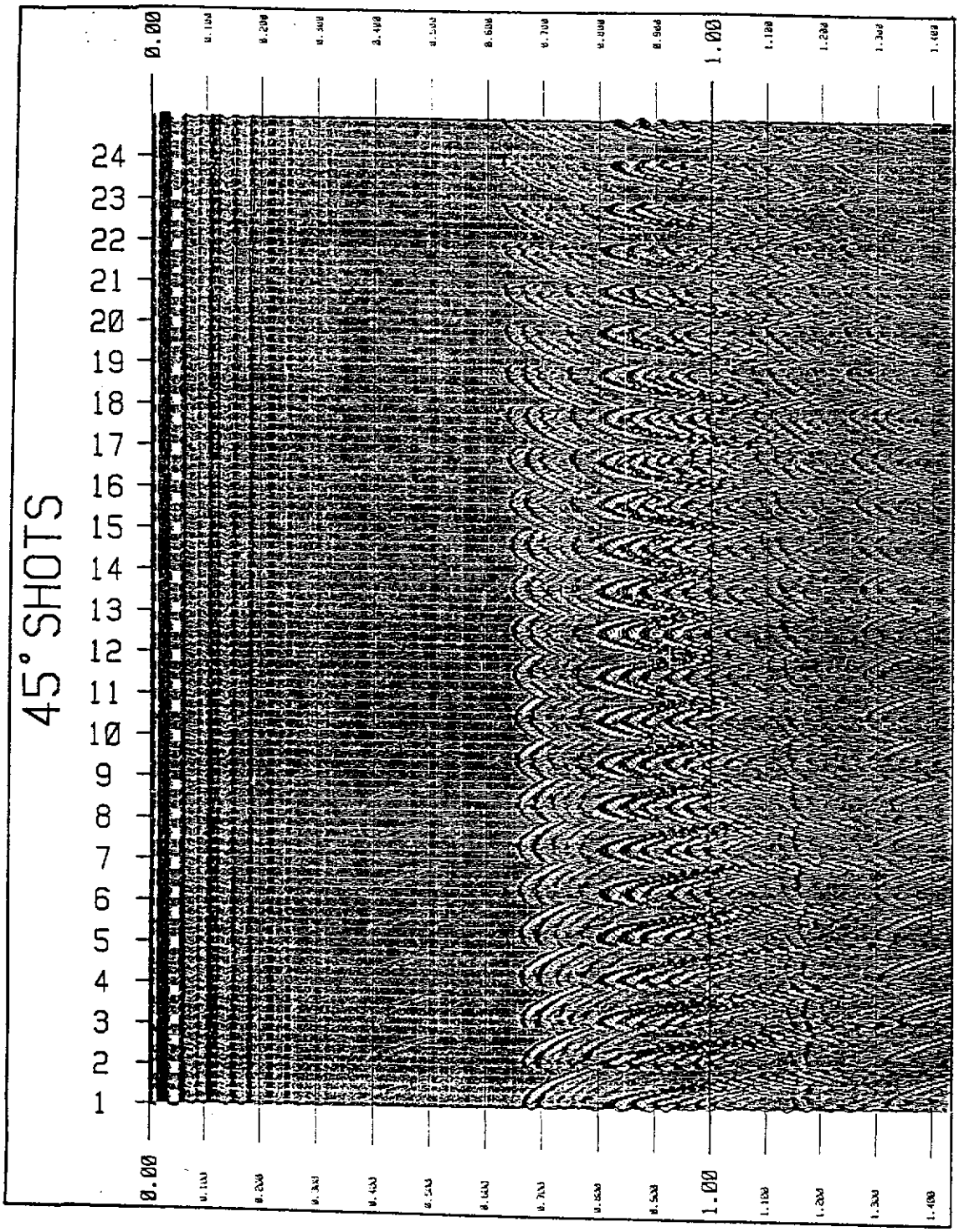

Figure 6.8. A suite of 45 degree shot records. Events appear similar to those in Figures 6.6 and 6.7, except that the arrival times decrease as the source moves along line. This is indicating that the source is moving up-dip from left to right of the figure.

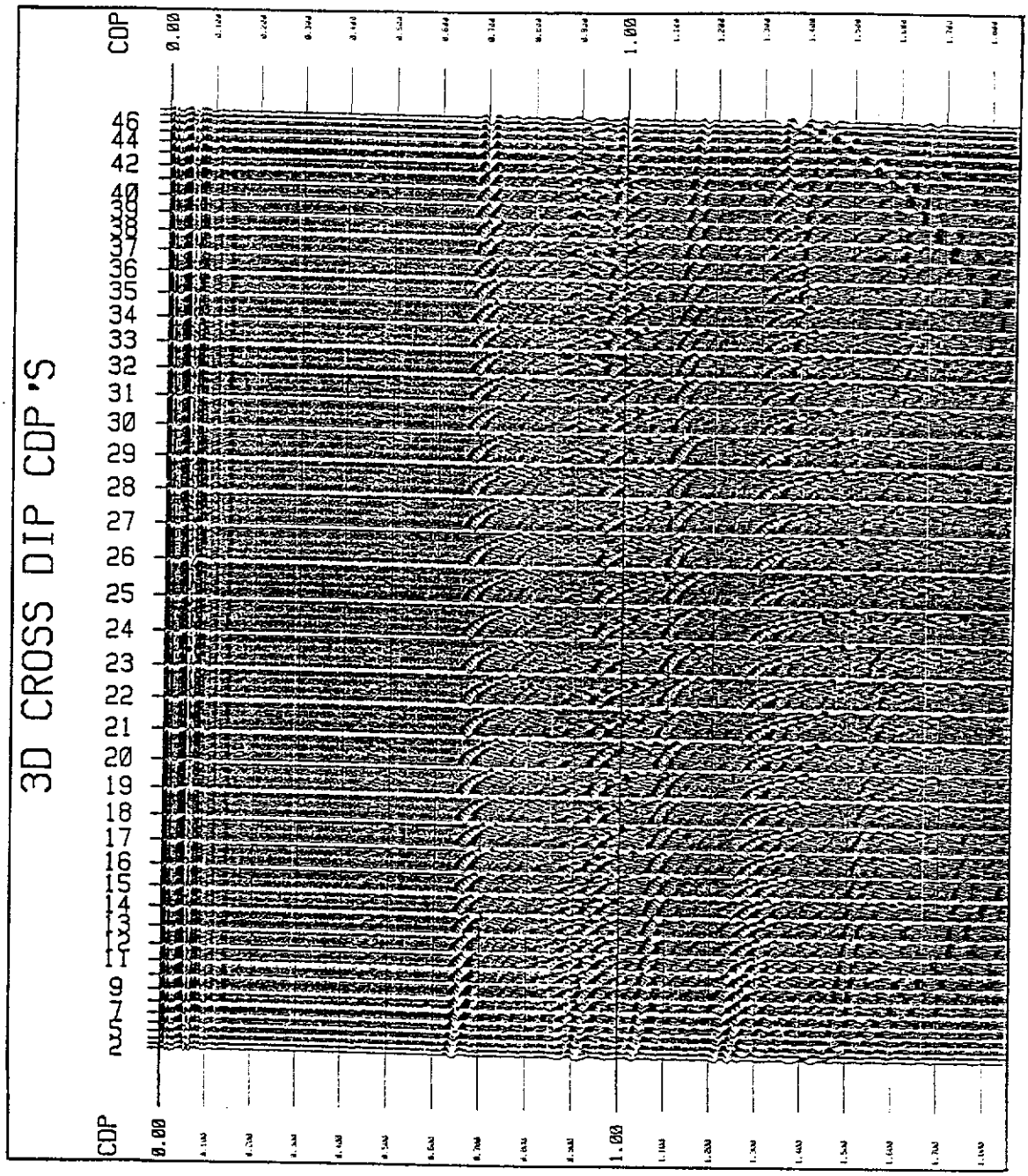

Figure 6.9. A suite of cross-dip CMP gathers. . The number of traces per CMP shows that the fold builds from the first shot point on the left (one trace) to the centre CMP 24 (24 fold) and reduces again to a single trace at last CMP. The reflections are moving down in time from left to right across the sections, indicating the presence of dip.

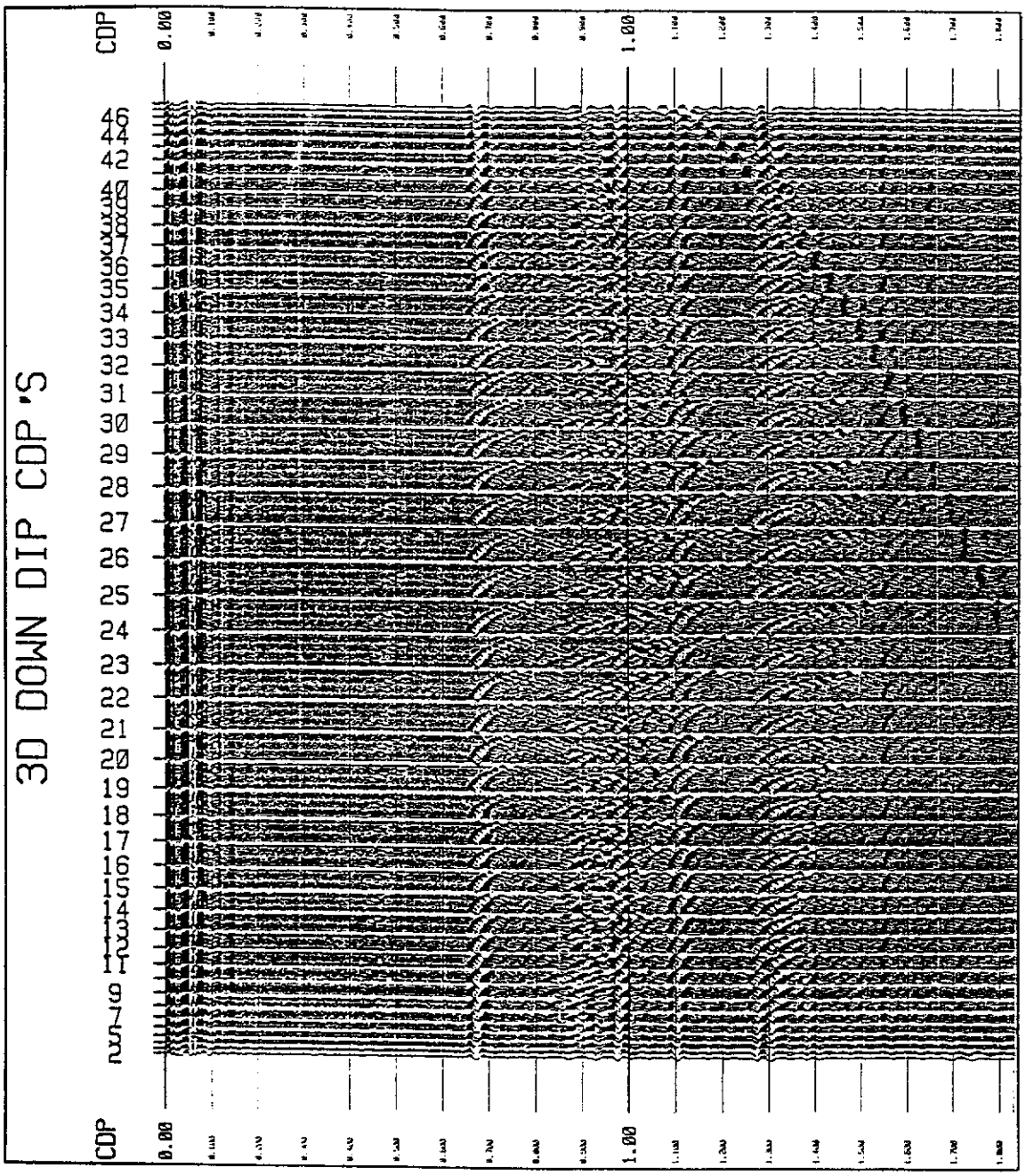

Figure 6.10. A suite of down-dip CMP gathers. . The CMP fold is similar to that for Figure 6.9. The timing of the reflector trough stays constant at around 670 ms indicating no dip along the section.

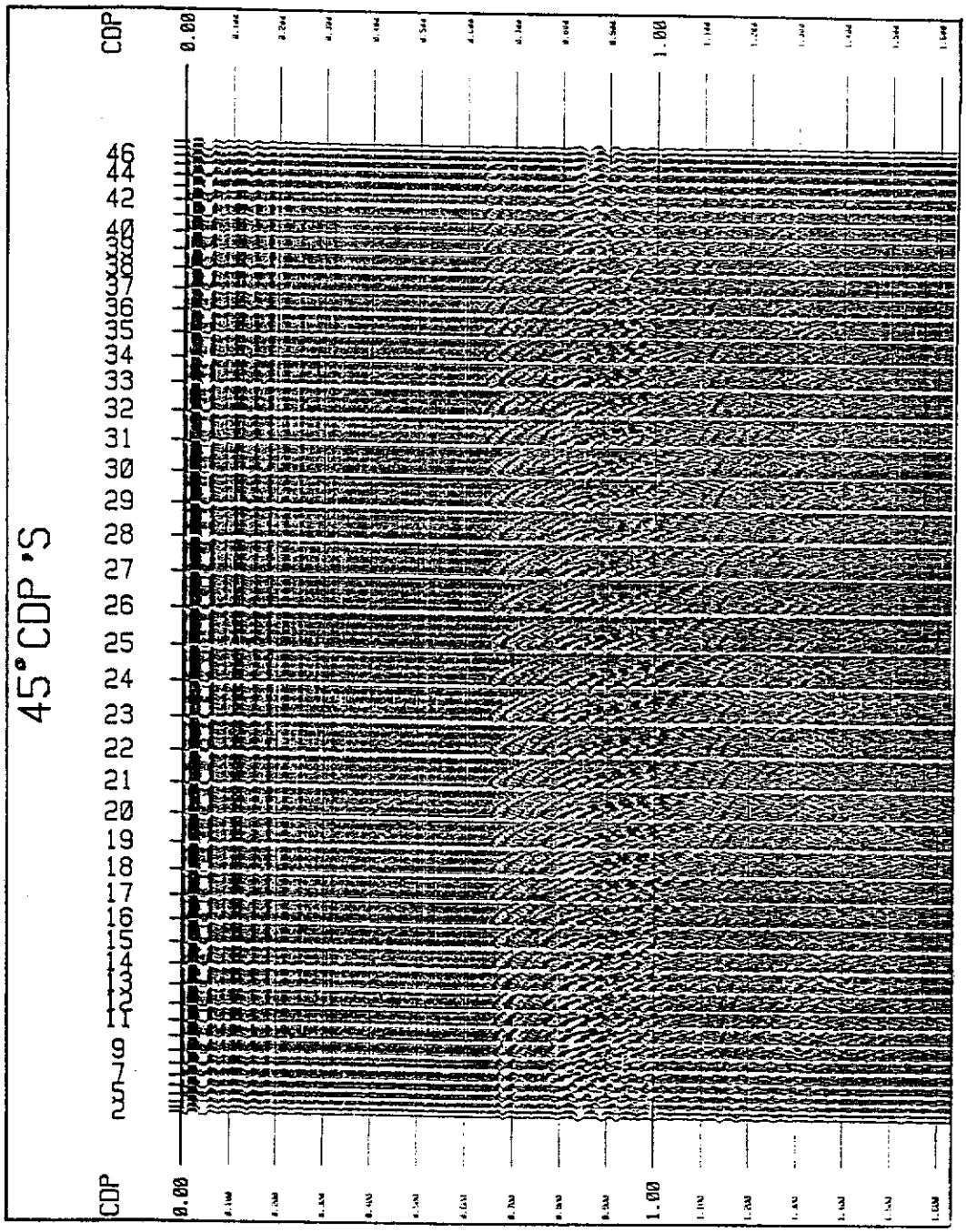

Figure 6.11. A suite of 45 degree CMP gathers. The CMP fold is similar to that for Figure 6.9 but in this case the reflections are moving upwards in time from left to right across the sections, indicating the presence of dip.

Having input these variables, the program sorted the data into CMP gathers, computed the shift required to align the traces in each CMP gather with the zero offset origin trace at 0, and then compiled a DISCO file with the values in appropriate trace headers. This file was run in batch mode, and plotted all the CMP gathers if required, or would just plot the centre CMP 24. A stack of all individual CMPs could be provided, with a display of them all stacked together into a single trace.

In cross-dip Figure 6.6, the initial event is the reflection 'A', while event 'B' is a converted wave reflection and event 'C' is the surface wave, as discussed in Chapter 4. The first records on the left have reflections with move-out to the right which is expected as the source is lateral to, but at one end of, the receiver line. The surface wave 'C' overlays the converted reflection 'B', and 'C' is shown on the left with an arrow indicating its path across the records. 'C' is also indicated on the right of the record where its direction has reversed.

As the source progresses along the shot line, the geometry becomes increasingly broadside, so that at shot 12, the shot point is midway along the receiver line and directly broadside. The reflection 'A' curves symmetrically on the channels to the right centre (shots 15 to 17) of the record, showing a change in reflection moveout (if the reflection symmetry had occurred at the centre shots, this would have indicated a non-dipping reflection). As the surface wave has a direct travel path from source to each receiver, its appearance is curved symmetrically. At the final shot 24 (at the end of line), both the reflection and surface wave have changed their moveout direction. Because the recording direction is cross-dip and therefore along the dip direction, the timing of the near-offset reflection changes with the reflection trough arriving at around 640 ms at shot 1 and moving gradually down to arrive at around 700 ms by shot 23, indicated by the arrows. This simply demonstrates the presence of dip.

Figure 6.7 shows the typical reflection and surface wave move-out when firing broadside in the down-dip direction (and therefore along strike). The timing for near-offset arrivals should be the same at the start of the line as it is at the end of line, and it is seen to be so by the near-offset reflection arriving at around 680 ms at both ends of the line, indicating the absence of reflector dip in that direction.

Figure 6.8 shows the recorded events as a result of turning the acrylic model through 45 degrees, with the move-out changing as the source moves along the receiver line, but this time the arrival times decrease as the source moves along the line. This is an indication that the reflection points are moving up-dip, since the model is homogenous and isotropic. The change in arrival time for this model can only be attributed to a change in the length of the travel path and therefore, dip.

Having produced the gathers in three directions, it was now necessary to test the dip prediction method. The best initial test of the method would be in the cross-dip data, where the reflector was known to have dip. Consequently the cross-dip data of Figure 6.12 is used as an example of the general approach to data analysis, which proceeded as follows:

(i) On the left, CMP 24 gather is shown. The amount of reflector flatness is an indication of the correctness of the chosen values for α and β.
(ii) In the centre, a CMP line shows the stacked CMP traces, which is a further indication of the accuracy of the chosen values for α and β. If these traces and those of CMP 24 gather are aligned, then the selected values of α and β are close to optimum.
(iii) On the right, a stack of all the traces along the stacked CMP line is shown, and is referred to as the 'stacked response'. (The trace shows only peak and trough departures from its zero value, due to a display problem in the Disco software, which was not resolved.) The peak and trough values were the most important data, since a maximum peak or trough value indicated an optimum line-up of wavelets in the stacked CMP profile of (ii). The log file provided a value of maximum peak (positive) and trough (negative) values of the final stacked trace, so that when this value is at its maximum, the optimum values of α and β are finally determined.

Prediction tests-*Cross-dip.* Having now determined the dip prediction approach, it becomes necessary to perform the prediction tests by applying specific values to the data.

Consequently, the cross-dip data were analysed in the manner described above. In this first test, values of α and β of - 4 degrees and 0, respectively were used in the GMO expression, and the stack plots produced as Figure 6.12.

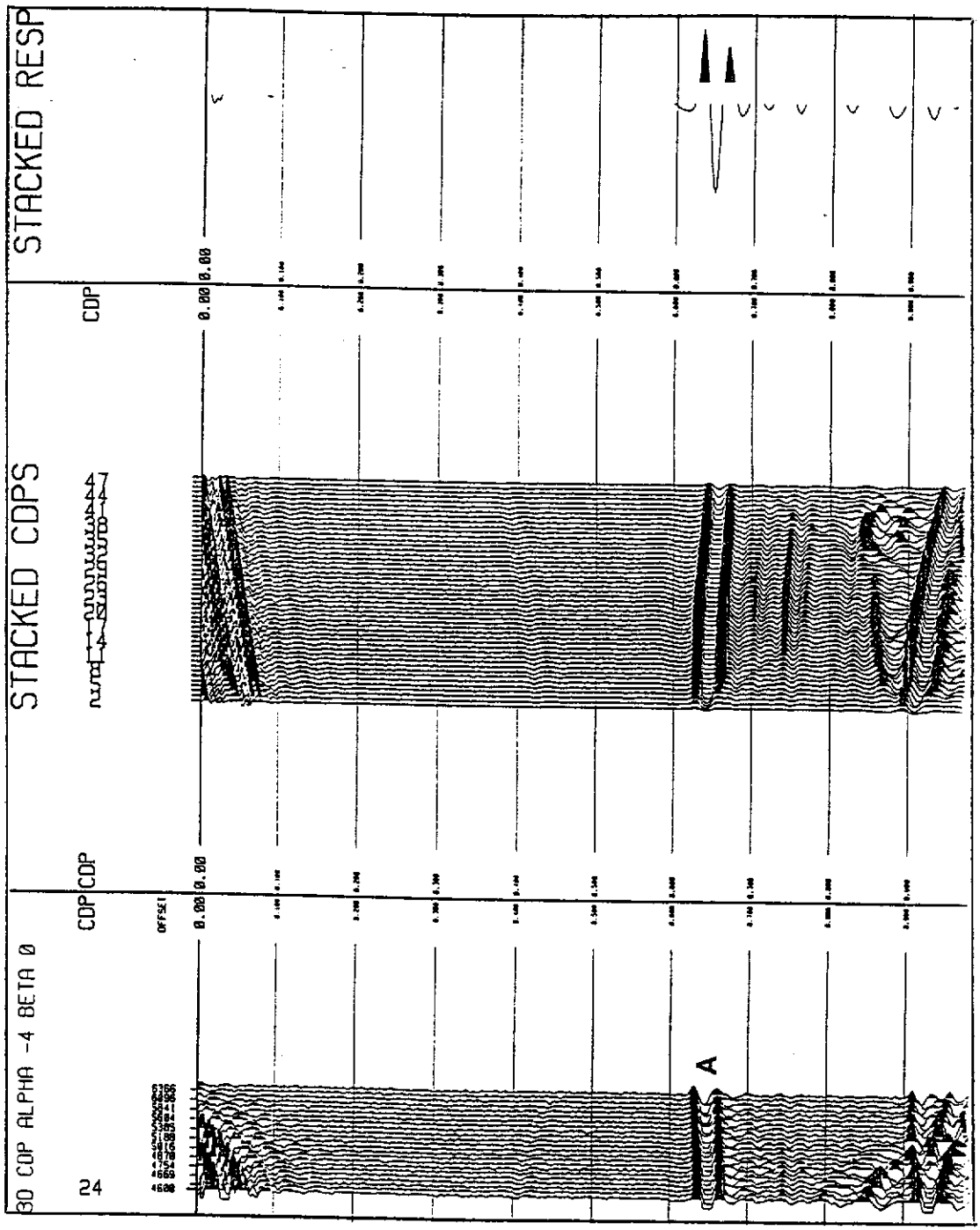

Figure 6.12. A cross-dip plot of CMP 24, CMPs along the line, and CMP traces stacked. With α of - 4 degrees and β of 0, the CMP traces do not align in a flat manner, the stacked line is not horizontal, and the maximum values are -32 and +24.

Working solely with CMP 24, the first reflection is shown as 'A' (the curved reflection at 850 ms is from the surface wave 'C' and the flatter event just after 900 ms is the converted reflection 'B' of Figure 6.6). The traces of reflection 'A' in CMP 24 do not line-up in a horizontal manner, and the display is similar to an over-corrected CMP gather. The corrected CMP line is not quite flat but dipping down to the right. Stacking all traces together produces the stacked response display (which from the log file has a maximum trough value of –32.0, a maximum peak value of +24.0, thereby giving a peak-to-peak value of 56.0). The reflection wavelets do not line-up because the values of apparent dip and strike are incorrect.

A second set of values were now tested to observe any improvement. A value of -5 degrees was used for α with zero for β in Figure 6.13, and the reflections line-up better, with a stacked response having values of –41/+38 and peak-to-peak of 79 (i.e., the improvement in maximum values indicates better alignment of the reflection).

It may be noted that throughout these tests, the stacked CMP profile reflections appear to have lower frequency content at the centre of the profile than at the ends. This reflection smearing is considered to be due to erroneous transducer positioning. Physical model tests have shown that transducer position repeatability is not always perfect. Transducer positioning is affected by drive screw gear positioning error. In addition, the simple placement of the transducer downwards onto the model surface (with a transmission lubricant between the two) can cause the transducer to slide an imperceptibly short distance, which is enough to provide a very small timing difference. Adding wavelets having such timing differences together in a high fold stack of say 24 fold data (such as at the centre of a CMP profile in these figures), then broadens the summed wavelet stack, giving a smeared appearance. Where there is a low fold level of stack (such as at the ends of the profiles), there is a reduced broadening of the wavelet stack producing a cleaner stacked wavelet and reduced smear appearance.

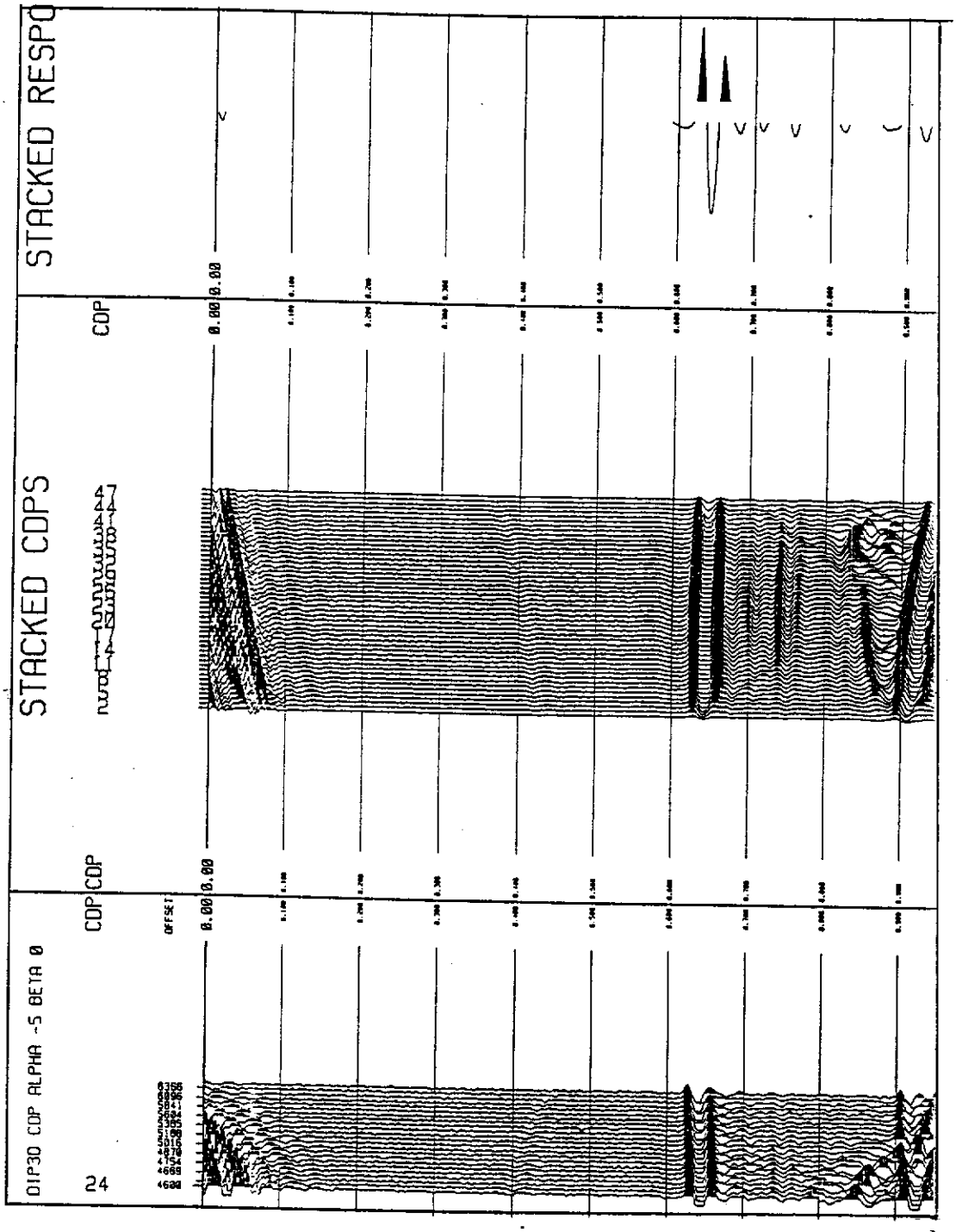

Figure 6.13. A cross-dip plot of CMP 24, CMPs along the line, and CMP traces stacked. With α of - 5 degrees and β of 0, the CMP traces align in a flat manner, the stacked line is horizontal, and the maximum values are -41 and +38.

Further tests were performed on the same midpoint data. Figure 6.14 is the plot using an α of - 5.5 degrees and β of zero, in which the reflection lines-up well, providing maximum values of -42 and +40. Figure 6.15 now uses an α of - 6 and β of zero, in which maximum values are –40 and +37.8. The optimum line-up for the cross-dip configuration was the gather with an α value of – 5.5 degrees and a β value of zero degrees. This is the correct value for the solid model that was machined with a true dip of 5.5 degrees. The dip detection process has therefore predicted a value of dip to within $\pm$ 0.5 degrees.

Prediction tests-*Down-dip.* Having determined the dip value in the true dip direction, the exercise was repeated in the orthogonal (i.e., 'down-dip') direction. The recording process was repeated with the source/receiver configuration rotated 90 degrees about the zero offset shot at the origin 0 and data was recorded in the down-dip direction (Figure 6.16). This is a simple convention which can be followed in the field, whereas here it is used to show that the dip computation works equally well irrespective of chosen source and receiver line orientation.

Figure 6.17 shows the plot using an α of -5 degrees and β of zero. There is a ripple in the reflection line-up in the CMP plot but the stacked data looks flat. Maximum trough/peak values are – 40.19 and + 38.9. Figure 6.18 shows the result for changing α to –5.5. The maximum values are – 41.7 and + 38.9. In Figure 6.19, α is now – 6 which provides maximum values of –42.0 and + 38.1. It is apparent that when determining the precise values of dip within one degree, the stacked wavelet shape can influence the optimum value, i.e., as the peak reduces in amplitude, the trough may increase to compensate and so sub-degree accuracy is limited. Consequently, it became necessary to determine a refinement to this optimisation process.

One approach which worked well was to take the square root of the sum of the squared peak values, which was called the RMS value of peak and trough. These values are provided in the following figures.

So for an α of – 5 degrees, the RMS value was 56.4; for α = – 5.5 degrees, the RMS = 57.03; for α = – 6 degrees, the RMS = 56.7. Thus, the largest RMS value indicated that the optimum dip value was – 5.5 degrees.

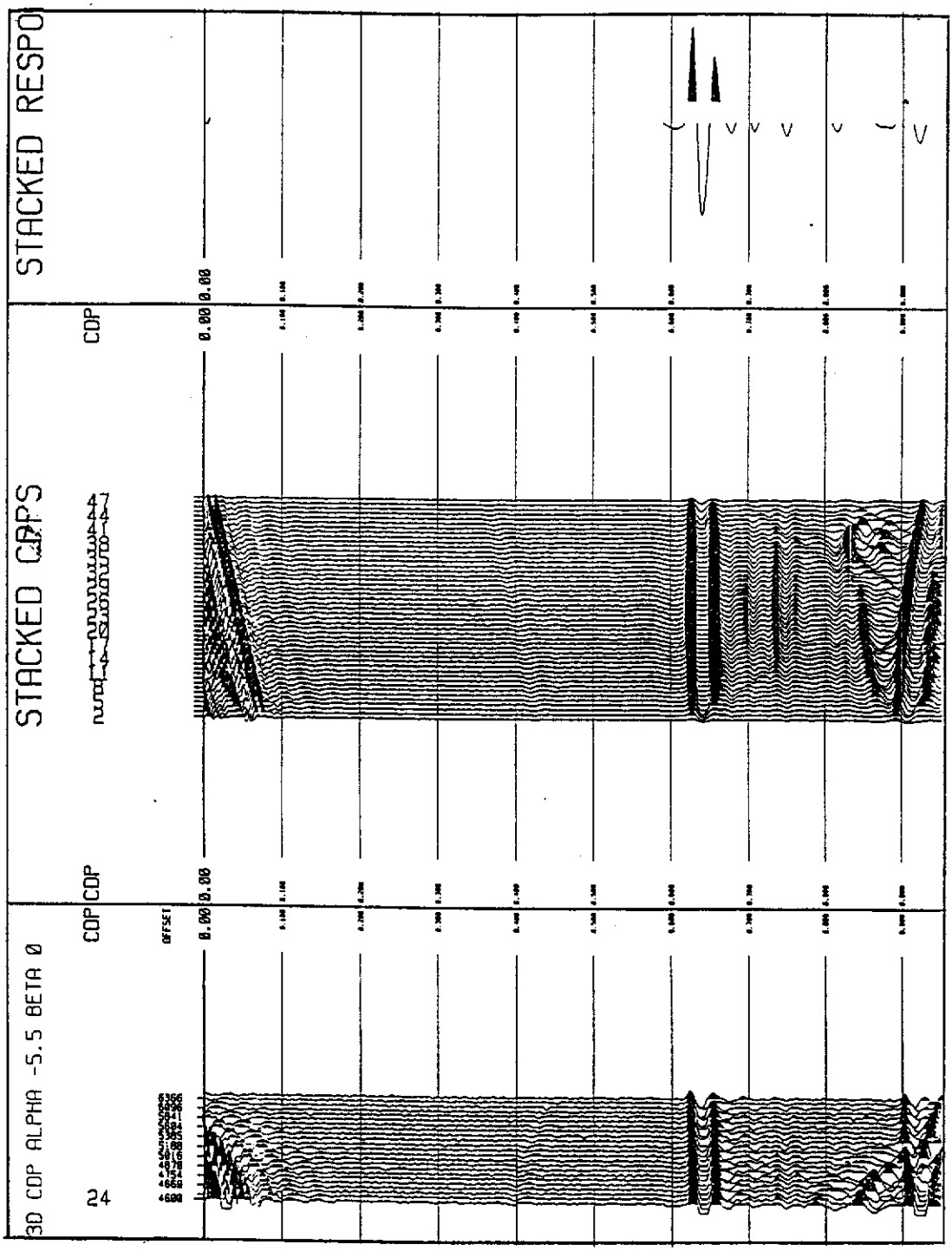

Figure 6.14. A cross-dip plot of CMP 24, CMPs along the line, and CMP traces stacked. With α of - 5.5 degrees and β of 0, the CMP traces align in a flat manner, the stacked line is horizontal, and the maximum values are -42 and +40.

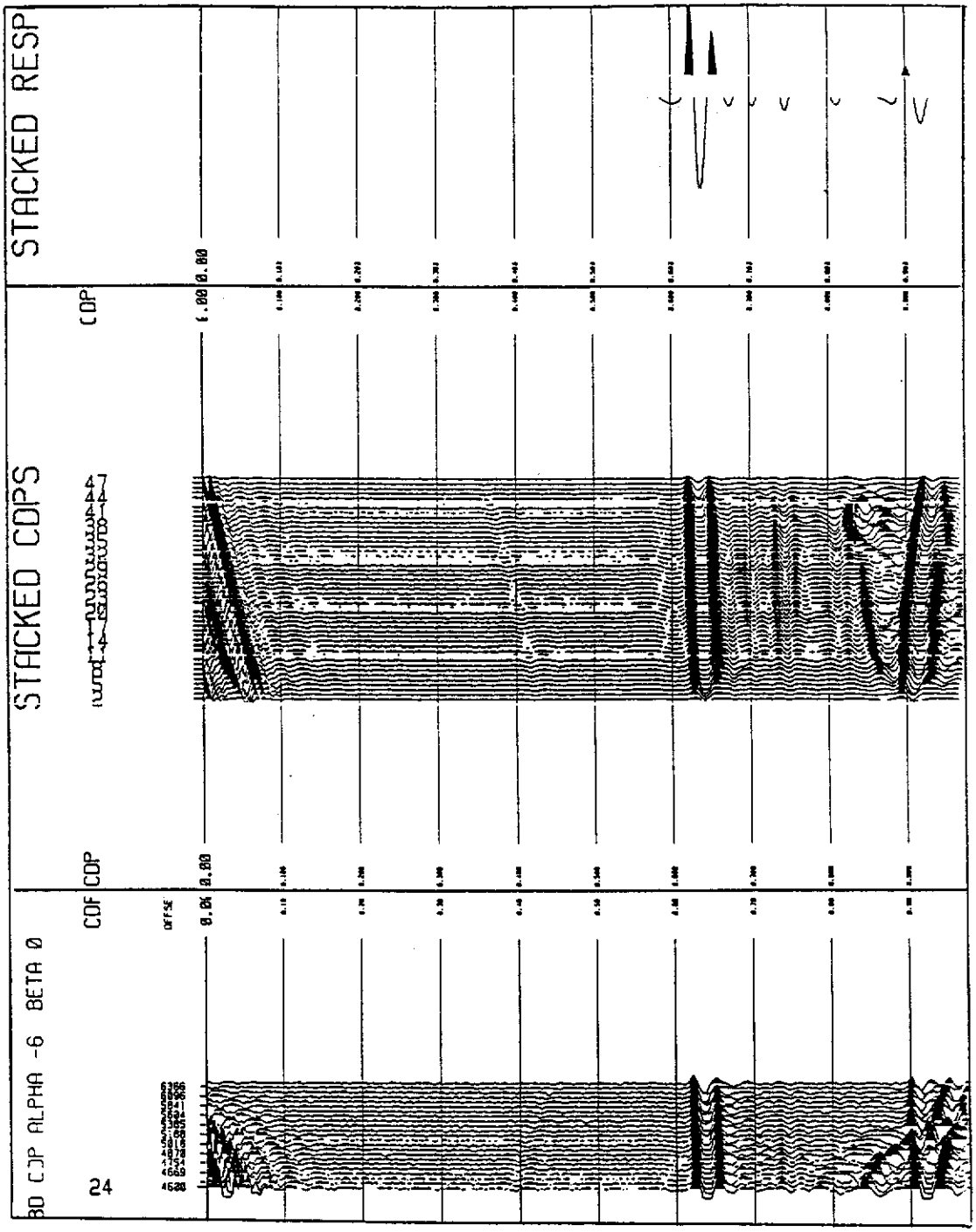

Figure 6.15. A cross-dip plot of CMP 24, CMPs along the line, and CMP traces stacked. With α of - 6 degrees and β of 0, the CMP traces align in a flat manner, the stacked line is horizontal, and the maximum values are - 40 and +37.8.

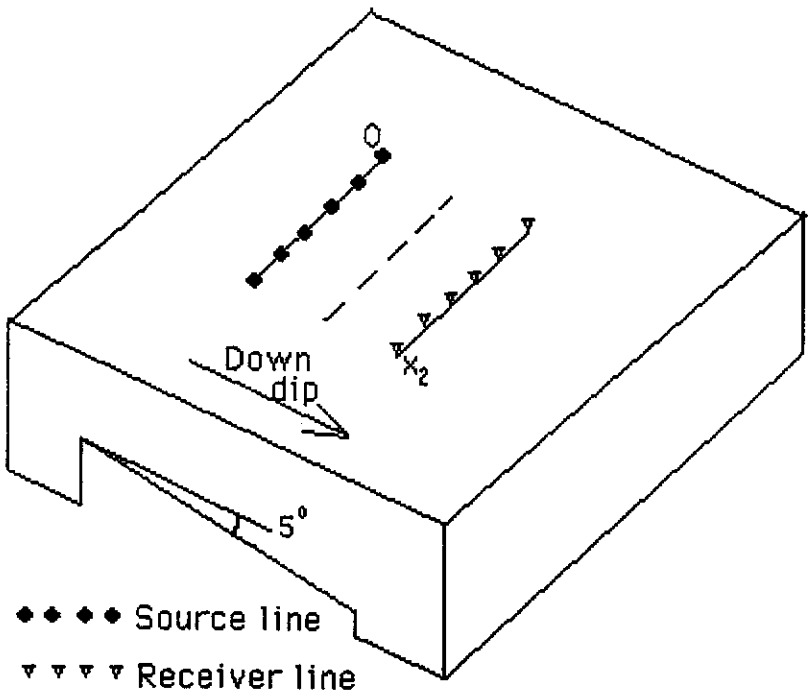

Figure 6.16. Down-dip recording configuration. The two parallel lines were now orthogonal to their cross-dip orientation, with the CMP line being in the strike direction. The dip estimation process was repeated until the values of α and β were determined again.

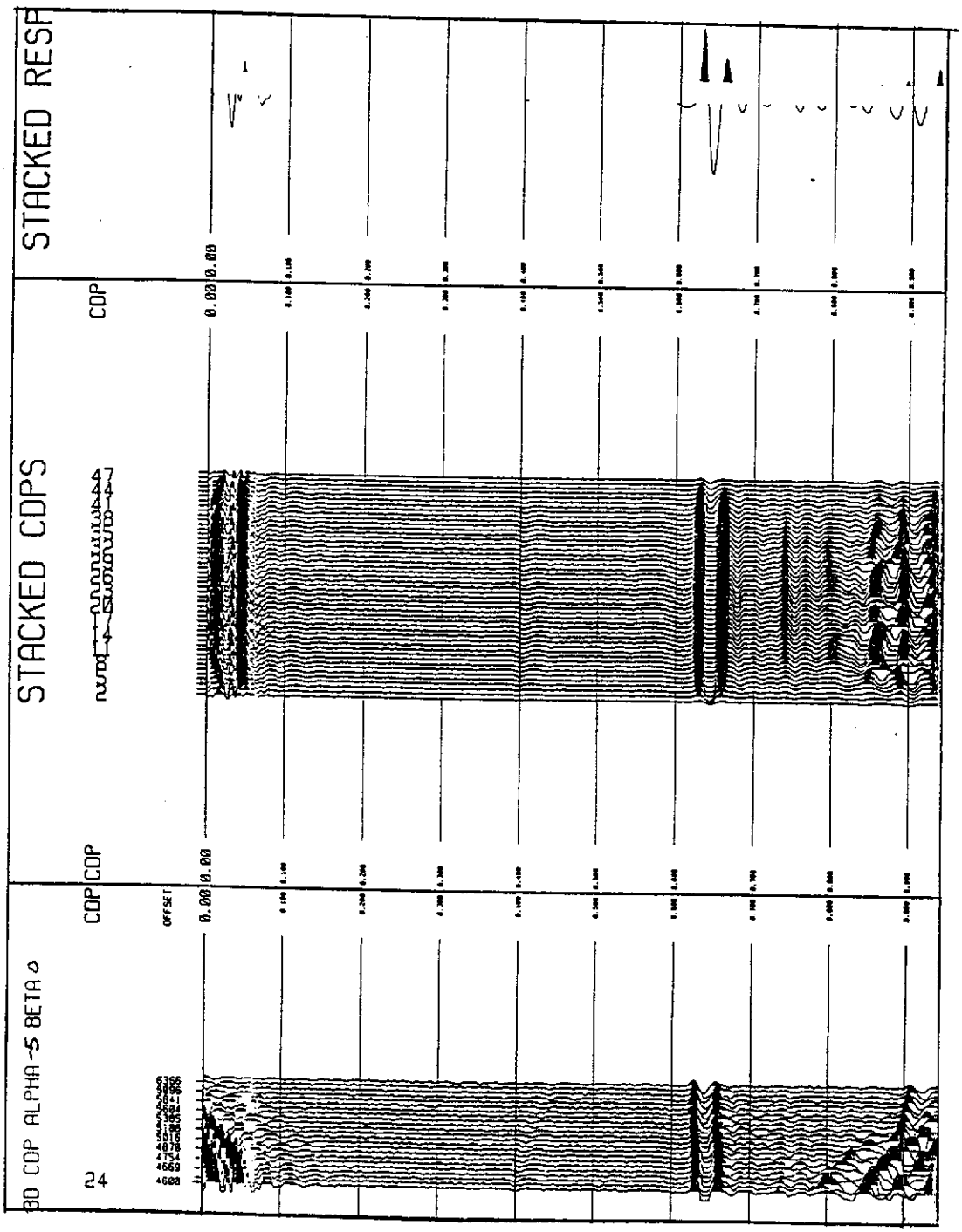

Figure 6.17. A down-dip plot of CMP 24, CMPs along the line, and CMP traces stacked. With α of - 5 degrees and β of 0, the CMP traces align in a flat manner, the stacked line is horizontal, and the maximum values become - 40.9 and +38.9, with the RMS value of 56.4.

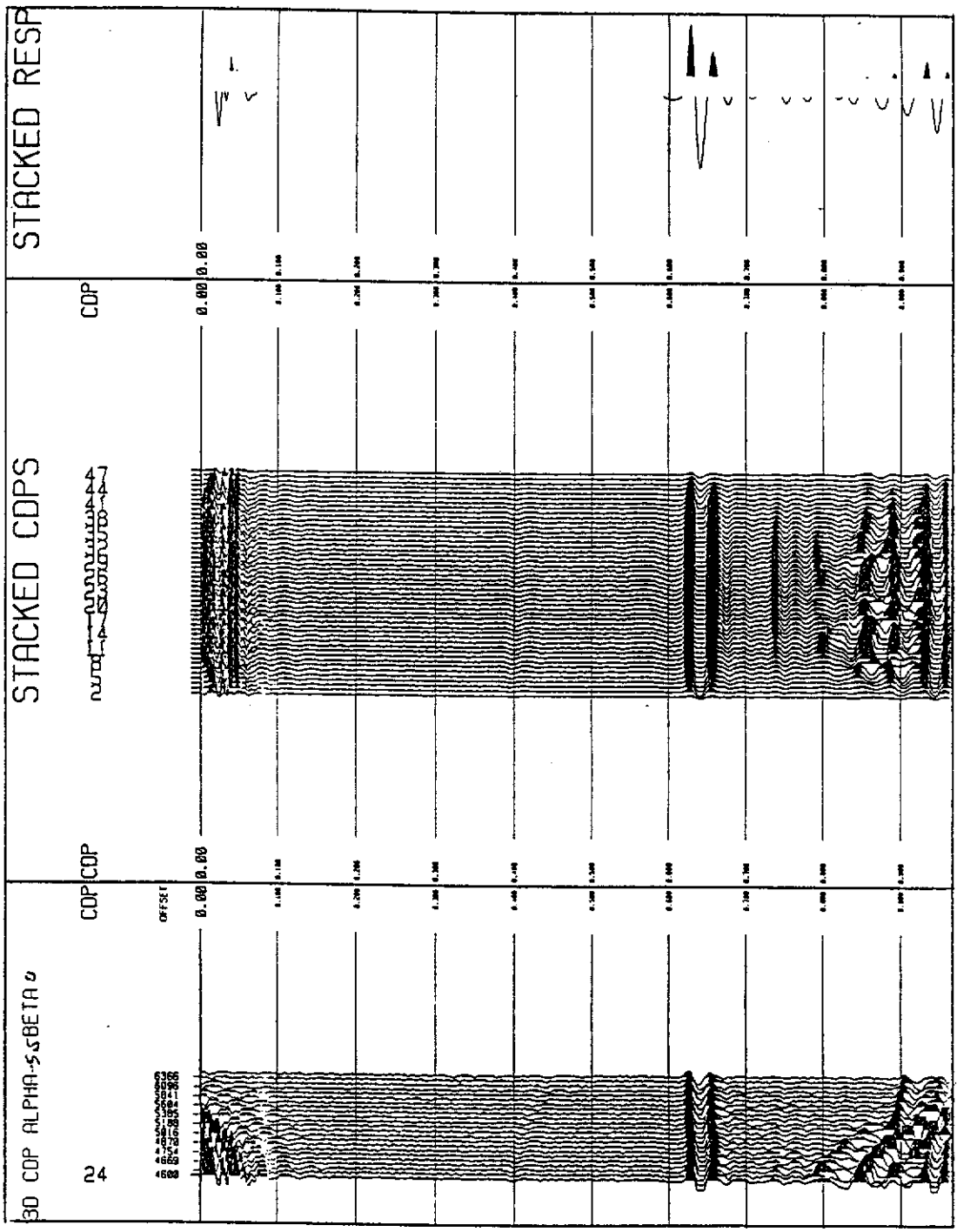

Figure 6.18. A down-dip plot of CMP 24, CMPs along the line, and CMP traces stacked. With α of - 5.5 degrees and β of 0, the CMP traces align, the stacked line is horizontal, the maximum values are - 41.7 and +38.9, and the RMS value is 57.03.

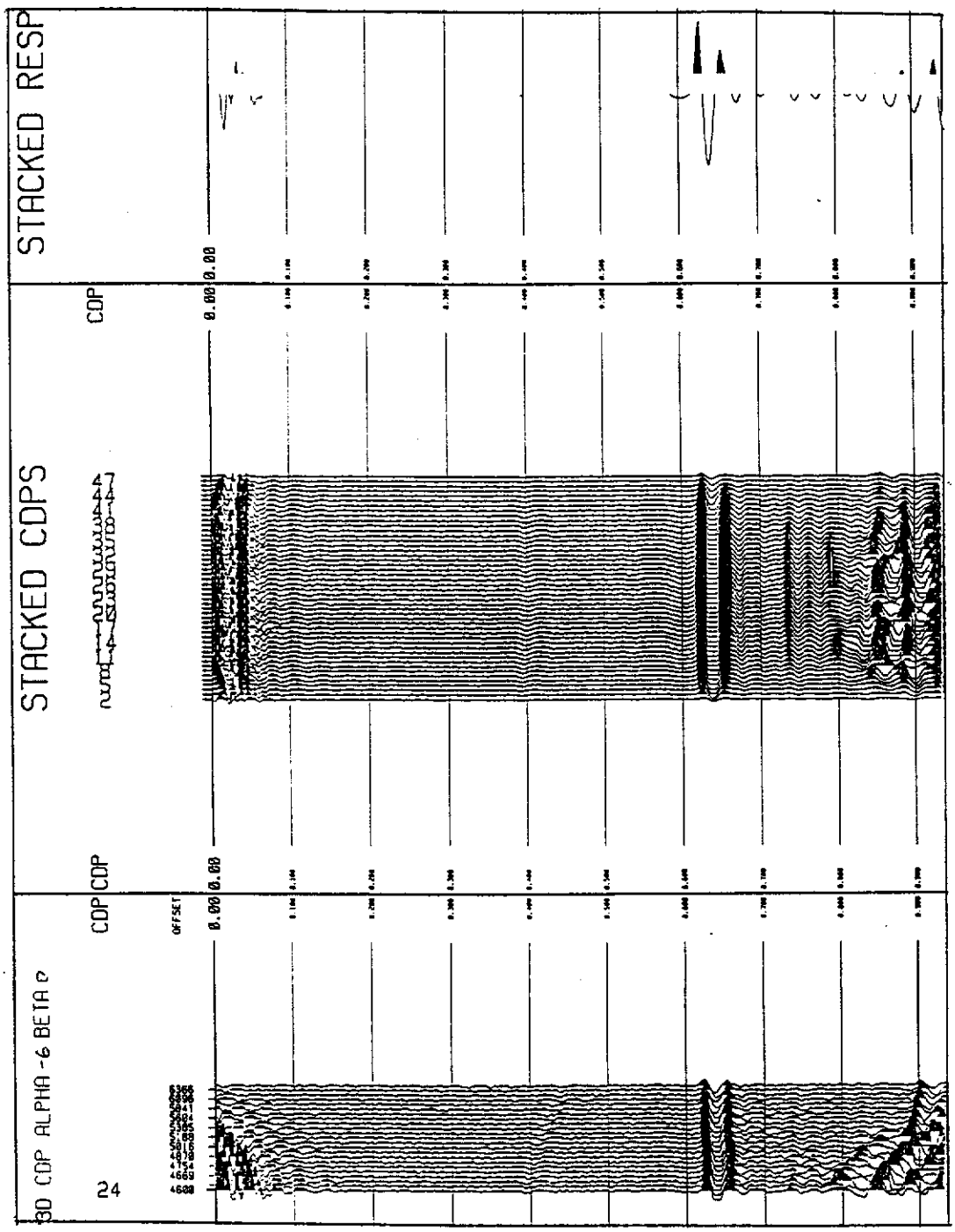

Figure 6.19. A down-dip plot of CMP 24, CMPs along the line, and CMP traces stacked. With α of - 6 degrees and β of 0, the CMP traces align, the stacked line is horizontal, the maximum values are - 42 and +38.1, and the RMS value is 56.7.

By recording data in one direction, followed by recording in an orthogonal direction, all azimuths of all possible raypaths have been used to provide an estimate of dip. Recording orthogonal directions in this manner also produces two orthogonal swath lines which could later be stacked for interpretation purposes.

Prediction tests-*45 degrees.* Having demonstrated how the dip detection technique works in two orthogonal directions, it was now necessary to test the method by using an arbitrary azimuth of recording with respect to the true dip direction.

Consequently, the physical model was rotated 45 degrees, with the configuration as shown in Figure 6.20(a). (With the model in this direction, the correct values for α and β were 3.9 degrees). Data were recorded and written to disk, using a range of values, but for brevity, the main values close to optimum will be discussed.

Figure 6.21 shows the result of using a value of α and β of 3.5 degrees. The wavelet of CMP 24 appears to weaken with offset in this direction, and this was considered to be due either to a change in transducer radiation pattern or a large variation in transducer coupling with position. With an α and β of 3.5 degrees, the stacked CMP profile is dipping upwards slightly to the right, while the trough and peak values were -21.45 and 18.83, respectively. This produced an RMS value of 28.54.

Figure 6.22 shows the result of using an α and β of 4.0 degrees. The stacked CMP profile was now quite flat, and the trough and peak values were -24.71 and 19.86, producing an RMS value of 31.70. These values for α and β were close to optimum.

Finally, Figure 6.23 shows the result of an α and β of 4.5 degrees. The stacked CMP profile was now dipping downwards to the right, and the trough and peak values were -24.33 and 18.0, producing an RMS value of 30.26. This confirmed that the optimum value was in the region of 4.0 degrees for α and β.

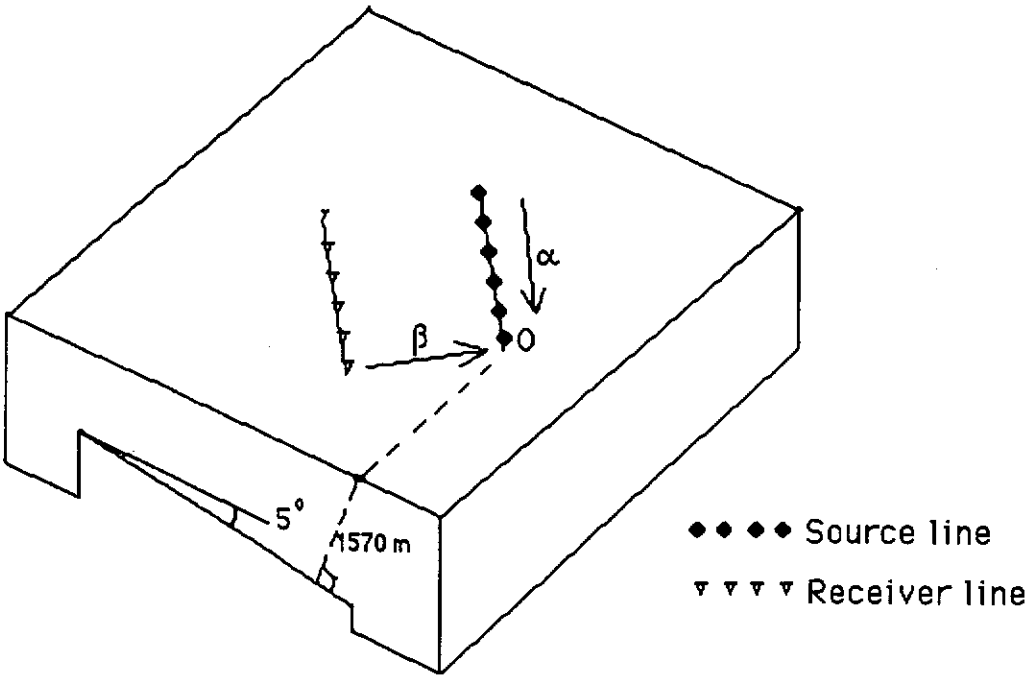

Figure 6.20(a). The model was rotated 45 degrees and data recording repeated. The correct values for α and β should be positive, because both α and β are dipping downwards towards the origin 0 (since only down dipping values of α and β are positive, by convention of Chapter 3.3).

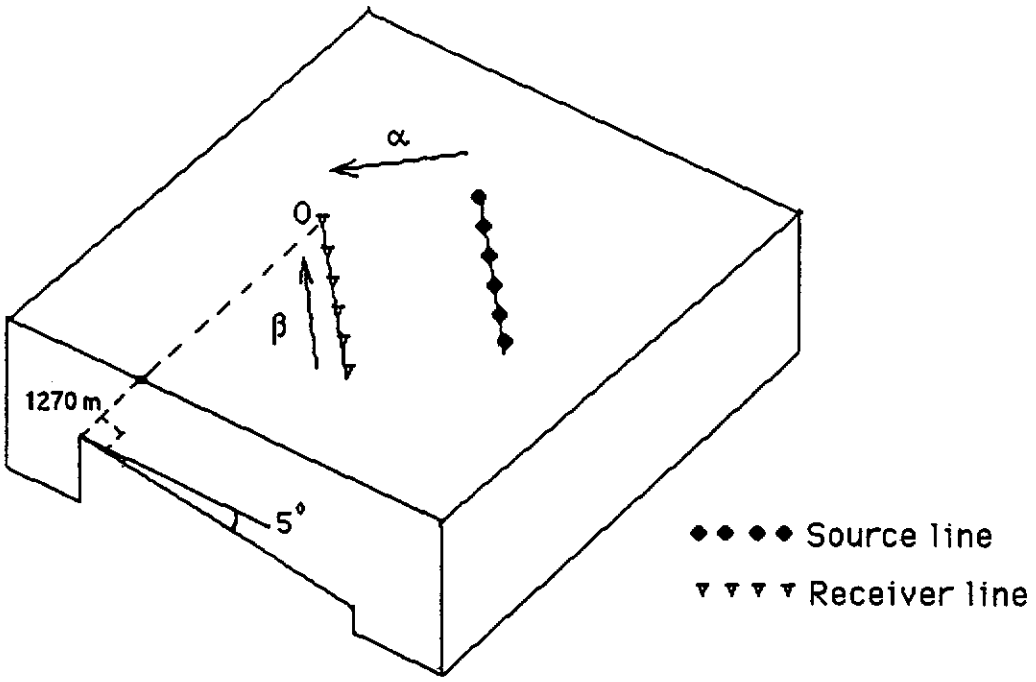

Figure 6.20(b). Using the same data set, with an alternative origin 0, the values for α and β are now negative.

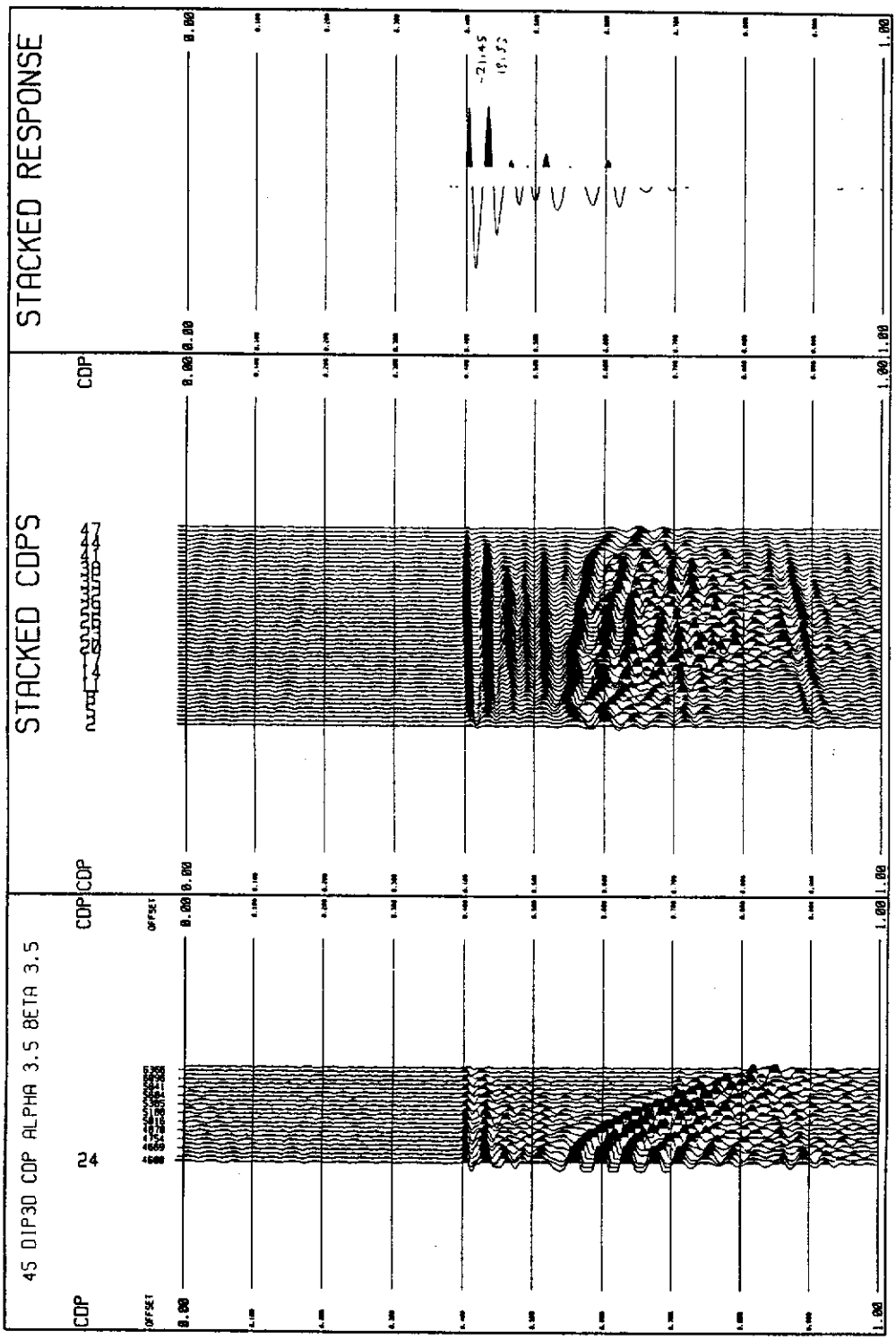

Figure 6.21. The 45 degree line plot of CMP 24, CMPs along the line, and CMP traces stacked. With α and β at 3.5 degrees, the stacked CMP profile is dipping upwards slightly to the right, while the trough and peak values were -21.45 and 18.83, which produced an RMS value of 28.54.

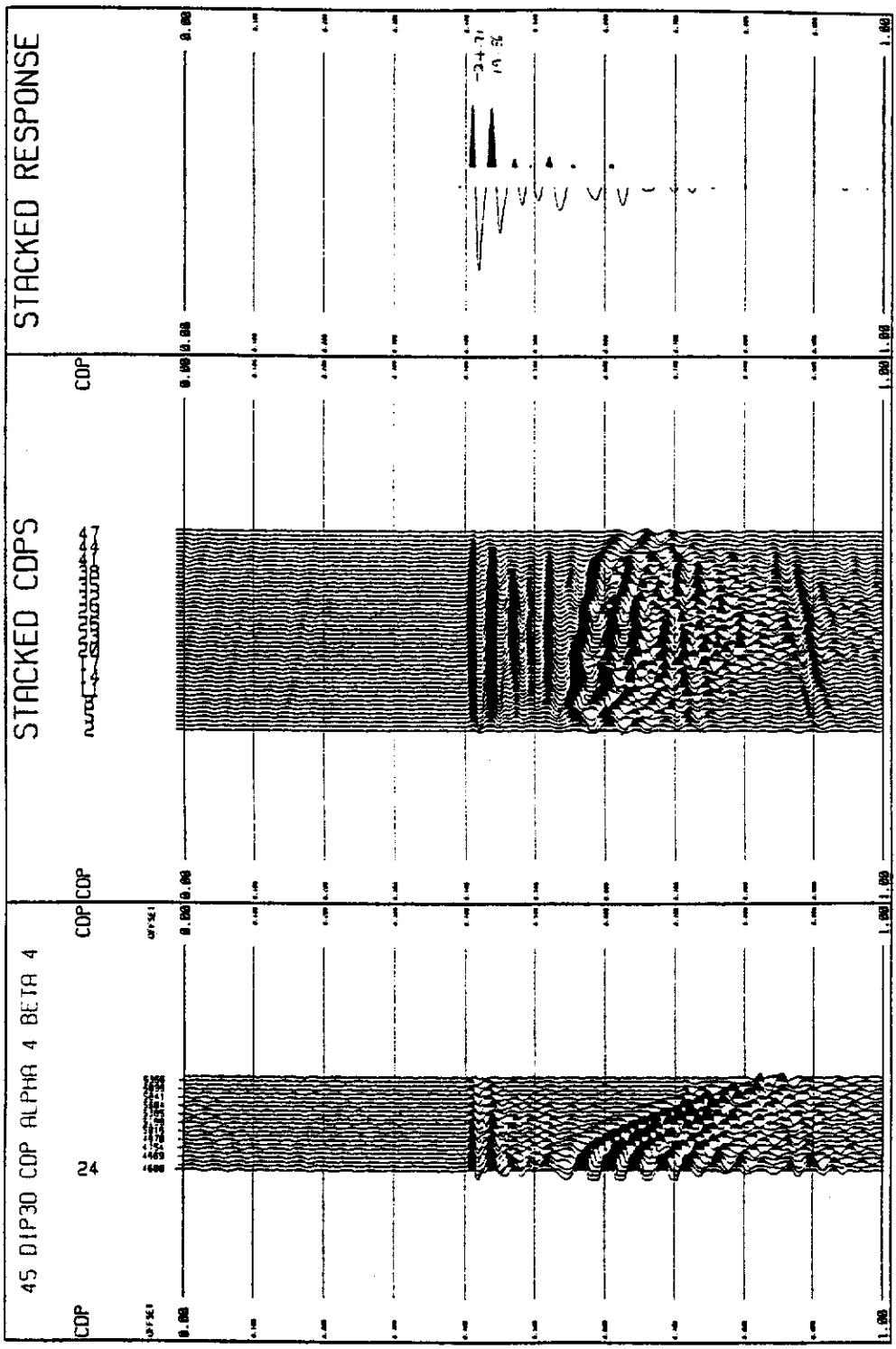

Figure 6.22. The 45 degree line plot of CMP 24, CMPs along the line, and CMP traces stacked. The stacked CMP profile was flat, and the trough and peak values were -24.71 and 19.86, producing an RMS value of 31.70. These values for α and β were close to optimum.

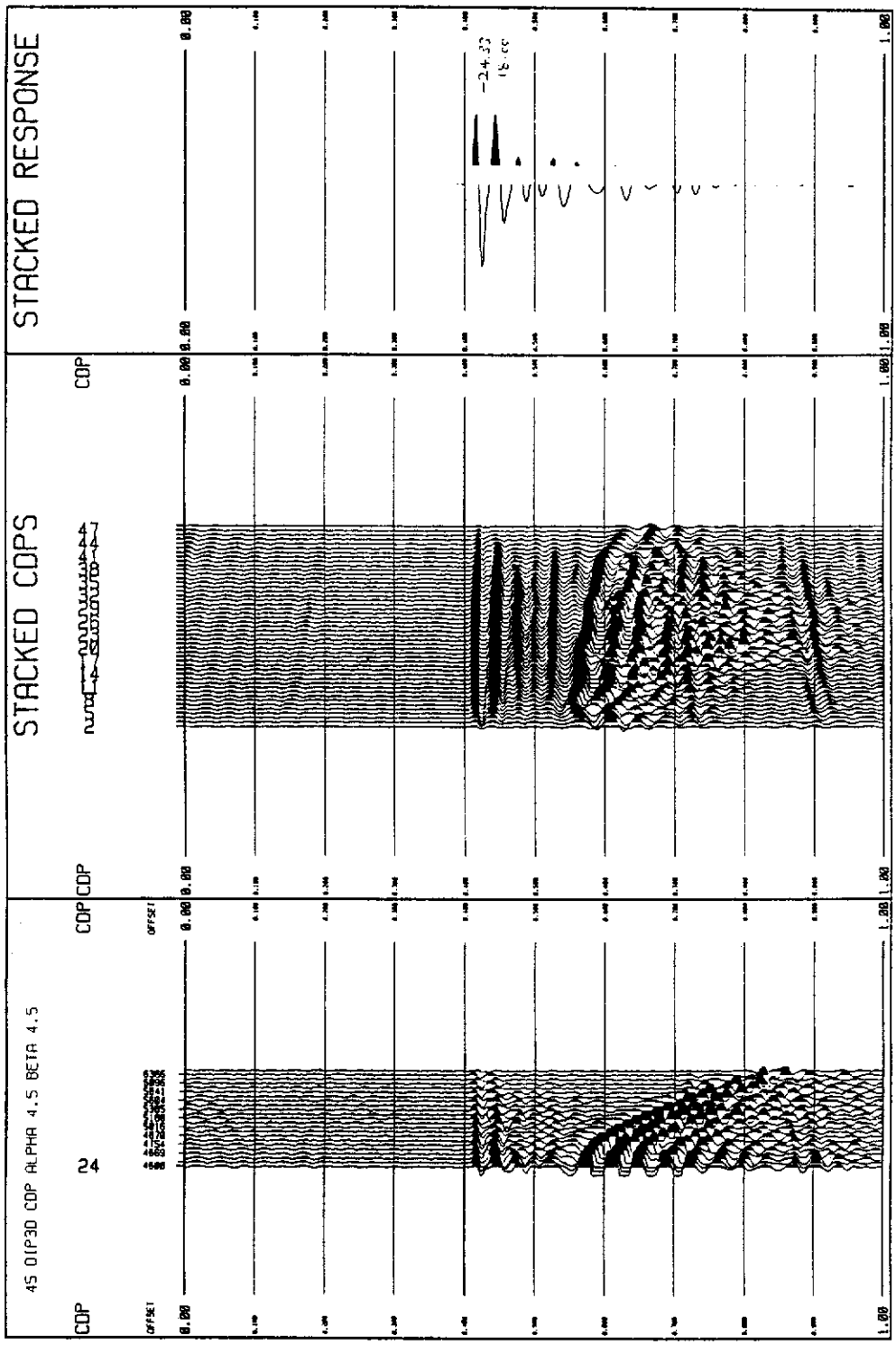

Figure 6.23. The 45 degree line plot of CMP 24, CMPs along the line, and CMP traces stacked. The stacked CMP profile dips downwards to the right, and the trough and peak values were -24.33 and 18.0, producing an RMS value of 30.26.

Origin location tests. Having shown that the dip detection method was successful with the model at some arbitrary azimuth, it was now of interest to observe whether changing the location of the origin made any difference to the process.

In Figure 6.20(b), the model was rotated 180 degrees from that of Figure 6.20(a), and should have negative values for α and β, because both α and β are dipping upwards towards the origin 0 (since only down dipping values of α and β are positive, by convention of Chapter 3.3). The zero offset distance ('h') from an origin 0, normal to the reflection was 1270 m.

Figure 6.24 shows a trial run with an α and β of + 4 degrees. While the CMP gather of Figure 6.24 appears reasonably flat, the stacked line is dipping instead of flat. There is a poor stacked response (or perhaps more precisely, no stacked response) of the dipping line, showing that the values for α and β are wrong.

Figure 6.25 shows the input values of α and β as - 4 degrees. This time, the CMP line-up is slightly dome shaped but the stacked line does show a continuous horizontal event. Therefore, the values of α and β are closer to some optimum value, but they are still not optimum. The stacked response now has a peak and trough. The conclusion is drawn that the event line-up provides an approximate determination of whether the chosen dip values are generally correct, whereas the stacked response values (using the reflector line-up within CMP 24) provides a far more accurate indication of the correct dip values.

With the same data set, the reference point was now changed to be at the other end of the model. A new reference point 0 was selected at the end of the receiver line where h = 1570 m, as shown in Figure 6.26(a). The method was tested using various values of α and β, and the optimum values were produced as being between + 3 degrees and + 5 degrees.

Figure 6.26 shows the plot for α and β of +3 degrees (with the reference 0 having a value for 'h' of 1570 m instead of 1270 m). Figure 6.27 shows the plot for α and β of + 5 degrees, and clearly the dip is some value between the two, at approximately 4 degrees (the dip was determined as 3.9 degrees, by measurement of the model). The method is sufficiently robust to allow a choice of a reference point anywhere.

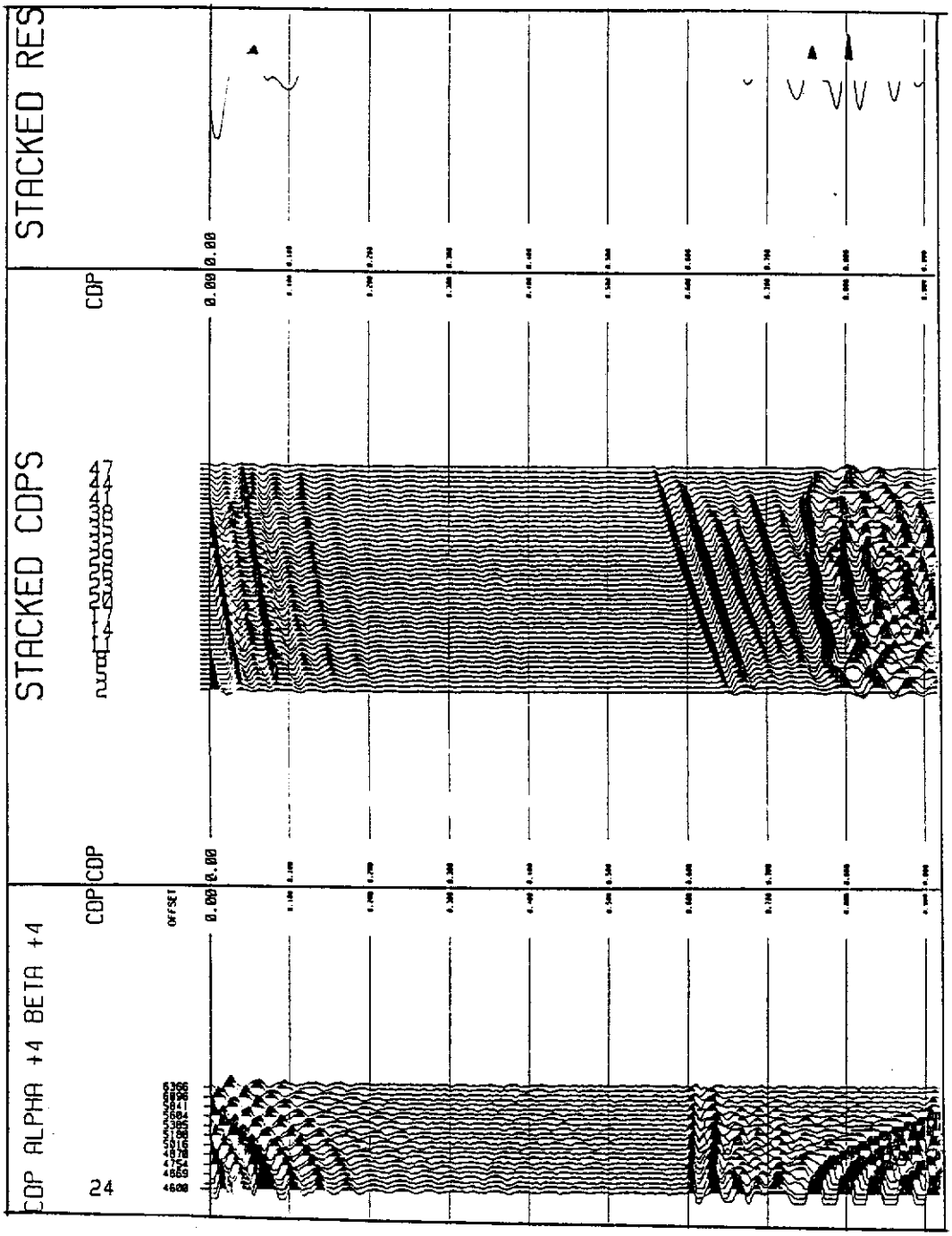

Figure 6.24. Trial values of α and β of + 4 degrees. While the CMP gather appears reasonably flat, the stacked line is dipping upwards. There is no stacked response, showing that the values for α and β are wrong.

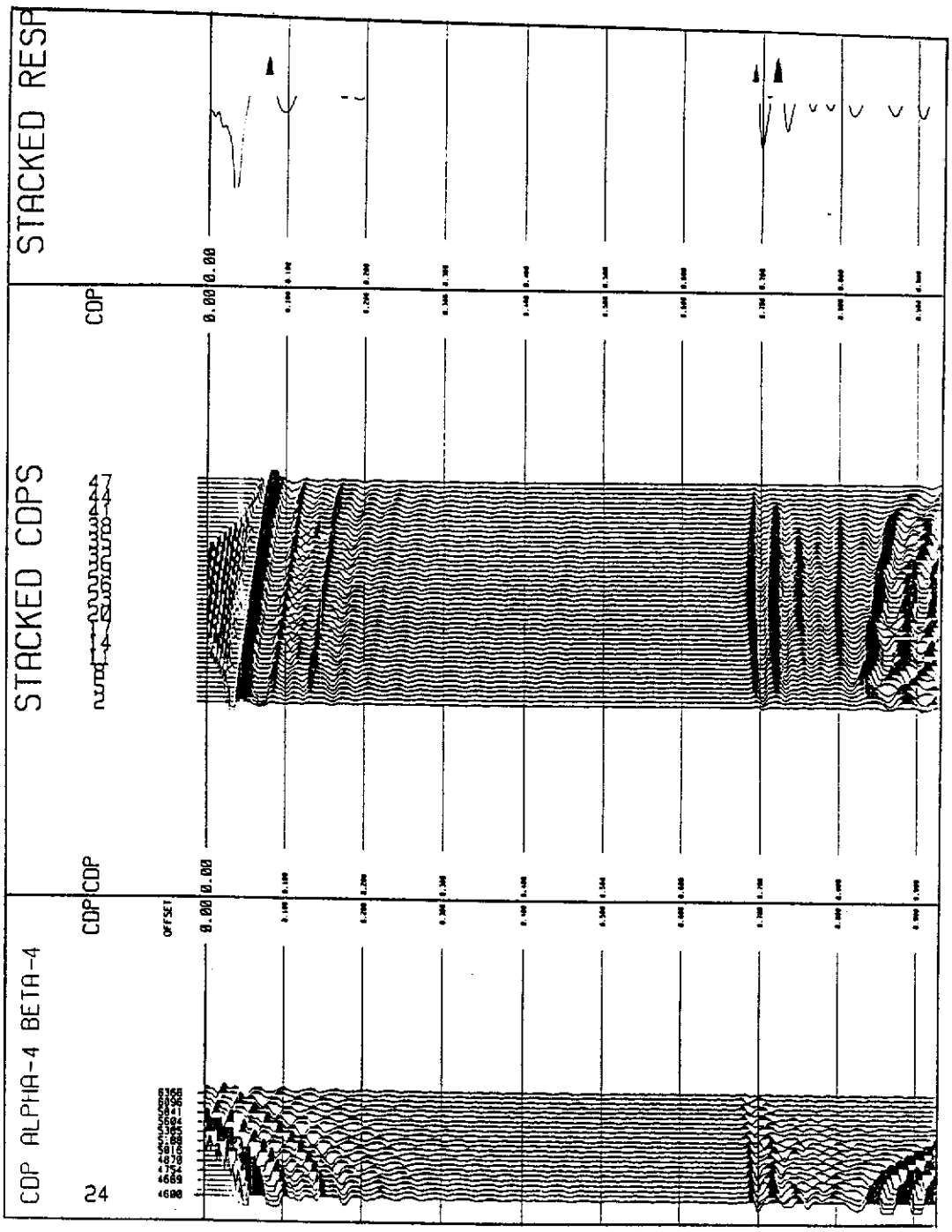

Figure 6.25. Trial values for α and β of – 4 degrees. The CMP gather appears to curve upwards, while the stacked line is flat. The stacked response of the line is low in value, indicating that the values for α and β are close to an optimum amount.

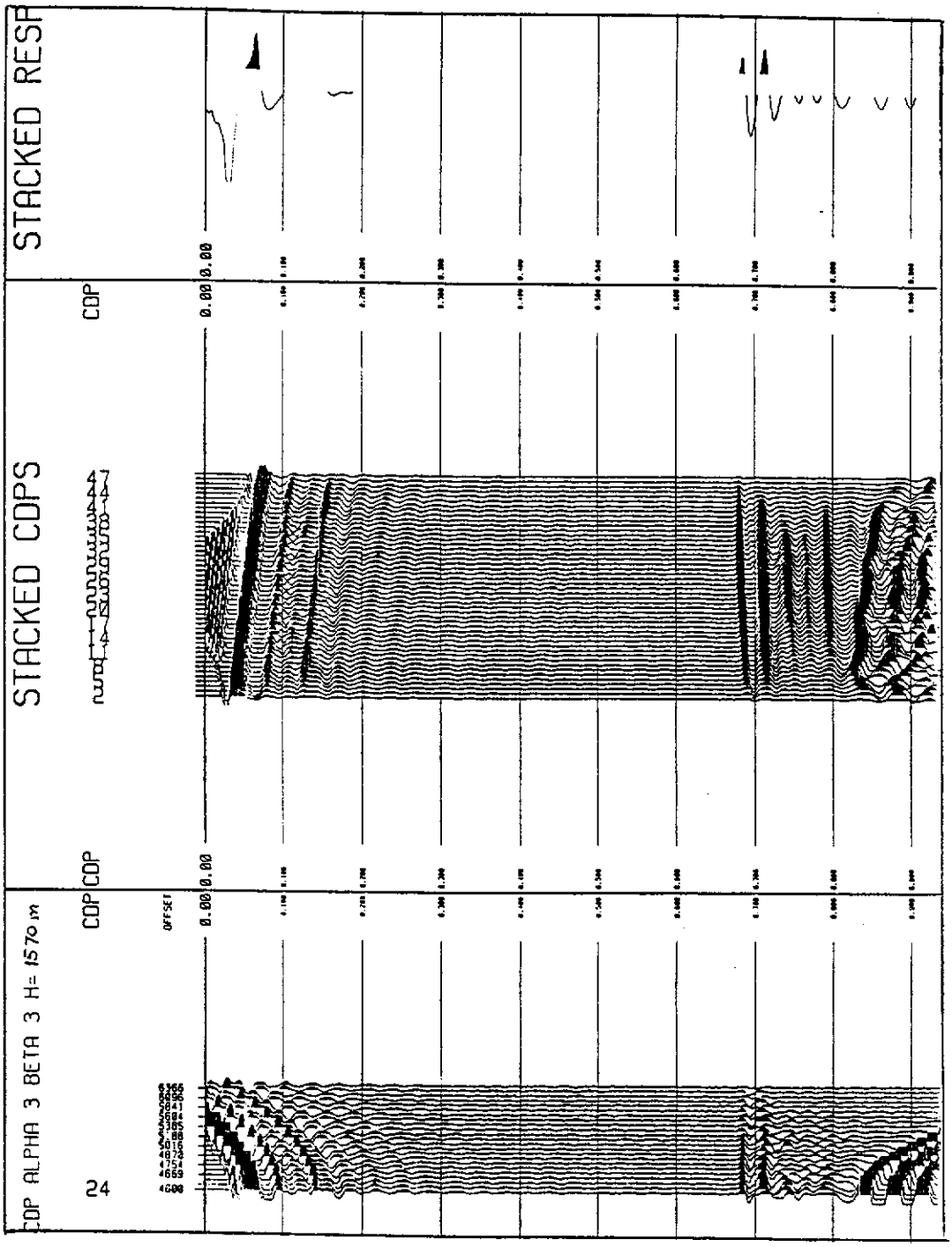

Figure 6.26. Trial values of α and β of + 3 degrees with an h = 1570 m. The CMP gather is flat, but the stacked line is dipping upwards. The stacked response of the line has a low value, showing that the values for α and β are close to an optimum amount.

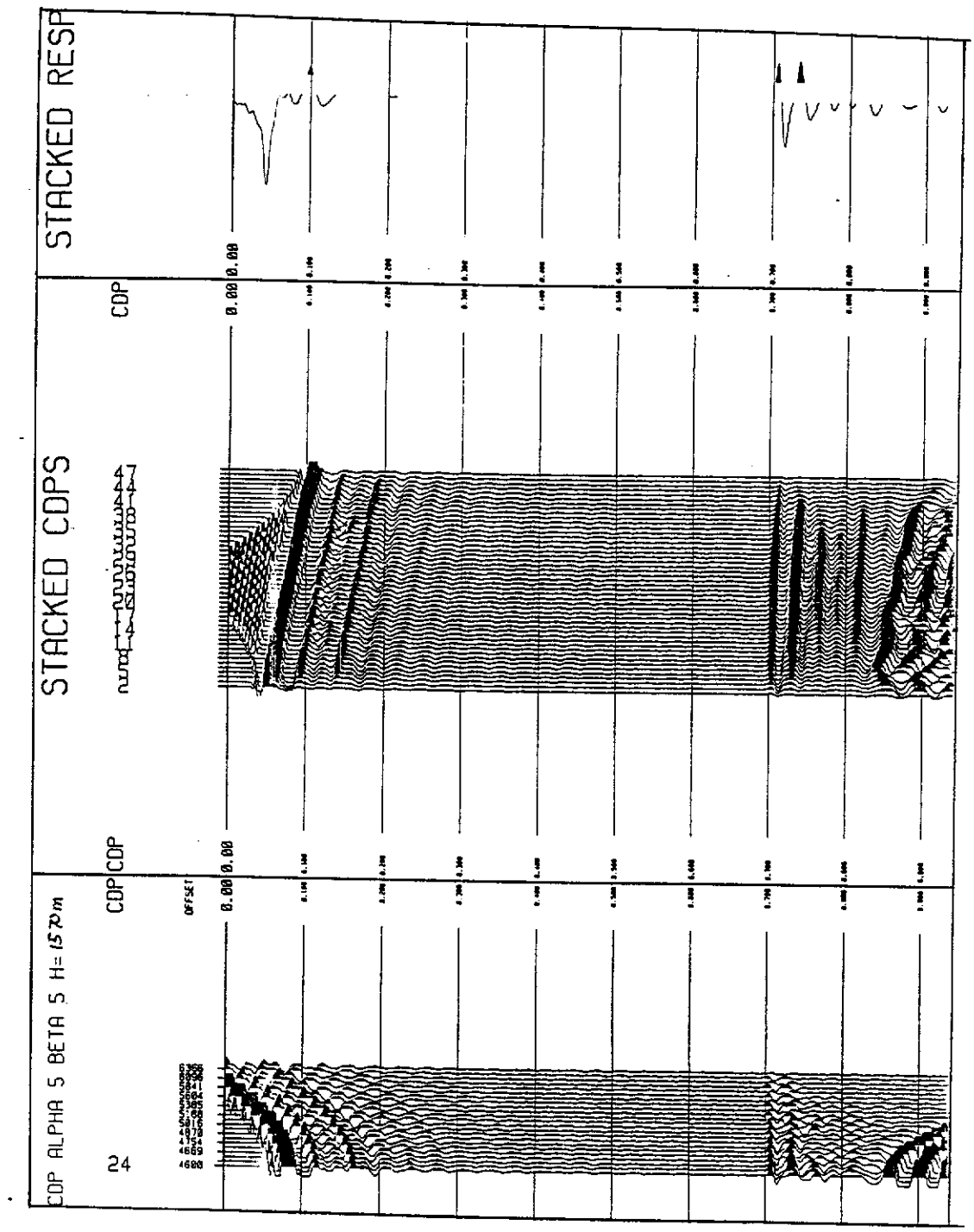

Figure 6.27. Trial values of α and β of + 5 degrees with an h = 1570 m. The CMP gather is flat, but the stacked line is dipping downwards. The stacked response of the line is low valued, showing that the values for α and β are of close to an optimum amount, somewhere between + 3 and + 5 degrees (i.e. 4 degrees).

While numerous tests were performed using the iterative process detailed earlier for obtaining dip values, only the trials using half degree steps in α and β between + 3.5 degrees and + 4.5 degrees are now discussed for brevity.

Figures 6.28(a), (b) and (c) show the results of using + 3.5 , + 4.0 and + 4.5 degrees. Figure 6.28(a) shows the stacked line dipping slightly to the left. Figure 6.28(b) shows the stacked line flat and Figure 6.28(c) shows the stacked line dipping downwards to the right. Peak and trough values had a maximum RMS value of 30.97 at α and β = + 4.0 degrees, and the flat stacked line showed that the values were close to an optimum. The values using an α and β of 3.8 to 4.0 degrees were tested, in which the optimum value for α and β was + 3.9 degrees with a maximum RMS value of 31.47. A value of + 3.9 degrees for α and β with a mid-point line at an azimuth of 45 degrees, gave a dip of 5.5 degrees, which after careful measurement, was the value within 0.1 degree of the dip machined into the model's base. The true dip was found to be 45 degrees with respect to the x-axis.

Conclusions. The dip value has been predicted within an experimental accuracy of at least a half degree or better, and to be along the true dip direction of the physical model.

After the rotation of the model by 45 degrees, the dip detection technique successfully measured the true dip and its azimuth when recording in an azimuth other than the true dip or strike directions.

Values of apparent dip along orthogonal directions can be determined by using the maximum value of peak-to-trough, or the computation of their RMS value, and displays no longer play the primary role. Thus, this dip detection method is available for automatic processing.

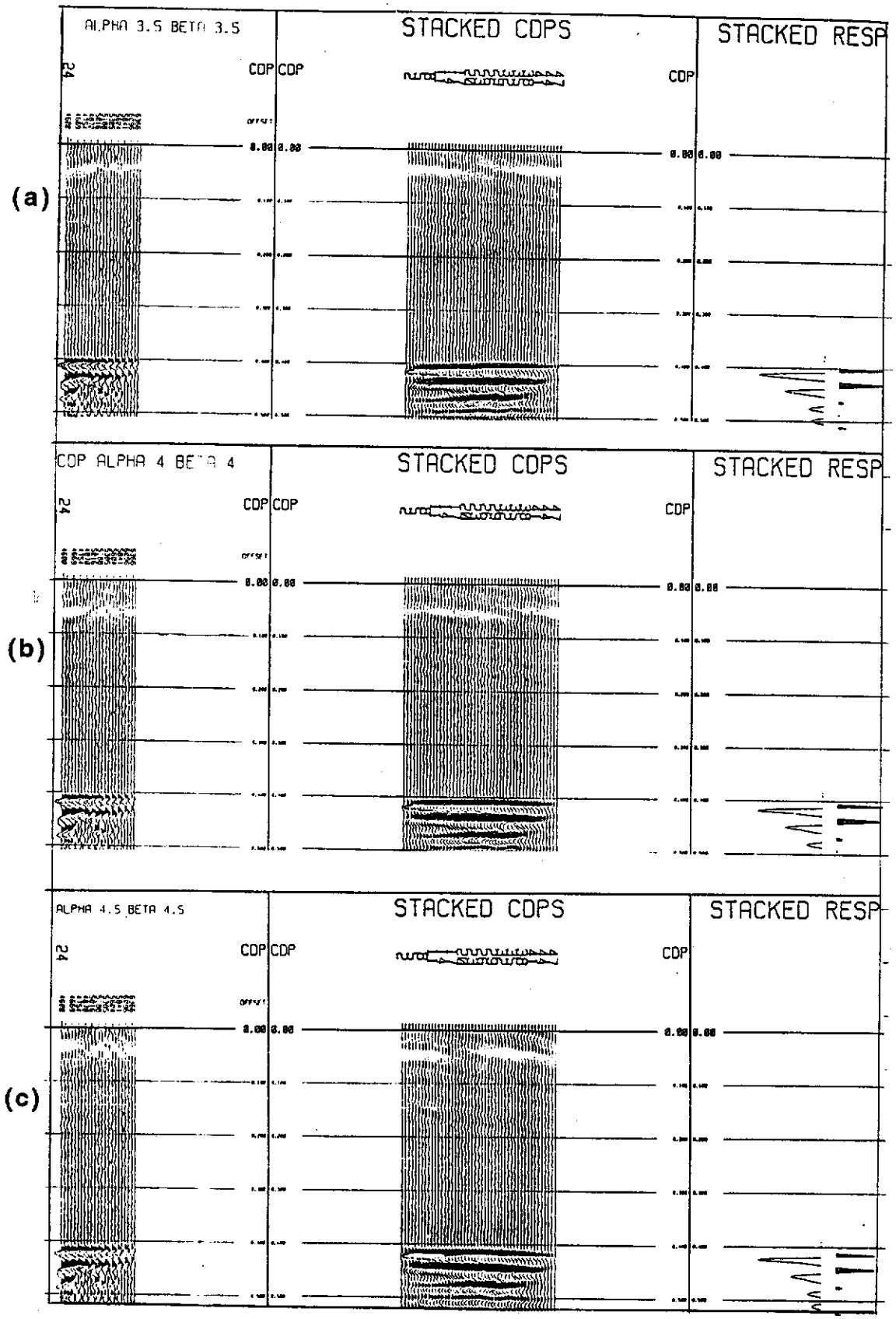

Figures 6.28(a), (b) and (c). (a) shows the stacked response using an α and β of +3.5 degrees, (b) has α and β of + 4.0 degrees and (c) has an α and β of +4.5 degrees. The optimum value for α and β was found to be +3.9 degrees with a maximum RMS value of 31.47.

6.8 Stacking of binned swath data.

So far, the CMP data collected during swath recording have been used to determine the apparent dip in two orthogonal directions (and subsequently the true dip value and its azimuth). If the gathers were treated as typical mid-point line data for stacking purposes, the conventional approach would be to stack the data using the most suitable stacking velocity. Such a feat is not trivial, because the stacking velocity changes with each trace's source/receiver azimuth.

Instead, the dip in two orthogonal directions can now be applied to obtain a GMO correction of each trace in every CMP bin gather to align the traces within each bin. To do this, a new value for the perpendicular length at the bin midpoint must be computed at the centre of each bin, which is termed h' in Appendix A, the simple expression of which is

$$|h'| = \left(t' \left(a^2 + b^2 + 1\right)\right)^{1/2} . \qquad \text{(A-8)}$$

A program computed the GMO correction for each trace in each bin, with reference perpendicular length **h** *replaced* by bin midpoint perpendicular length **h'** and the output results observed. Cross-dip input data were used to test the CMP profile with the greatest dip (along the line of true dip).

CDP 24 was then displayed using an α of –5.5 degrees, and a β of zero. The 24 fold (maximum) stack of Figure 6.29 showed acceptable quality, and was a swath CMP line located in the general direction of the true dip direction.

A computation of the expected change in two-way time from the first to the last trace along the line in the physical model gave a scaled time of 83 ms, whereas the scaled time difference observed on the figure was 80 ms. This value is therefore very close to the correct value (the data were sampled at a scaled time of 1 ms so were three samples different), and hence the section shows a dip similar to the true dip. We would not expect the apparent dip to be the same as the true dip, because the reflections along the general line direction are scattered and are up-dip as shown in Figure 2.12. The line would require pre-stack migration processing to move the reflections back to their correct locations, and then the dip would be expected to be closer to the true dip of 5.6 degrees.

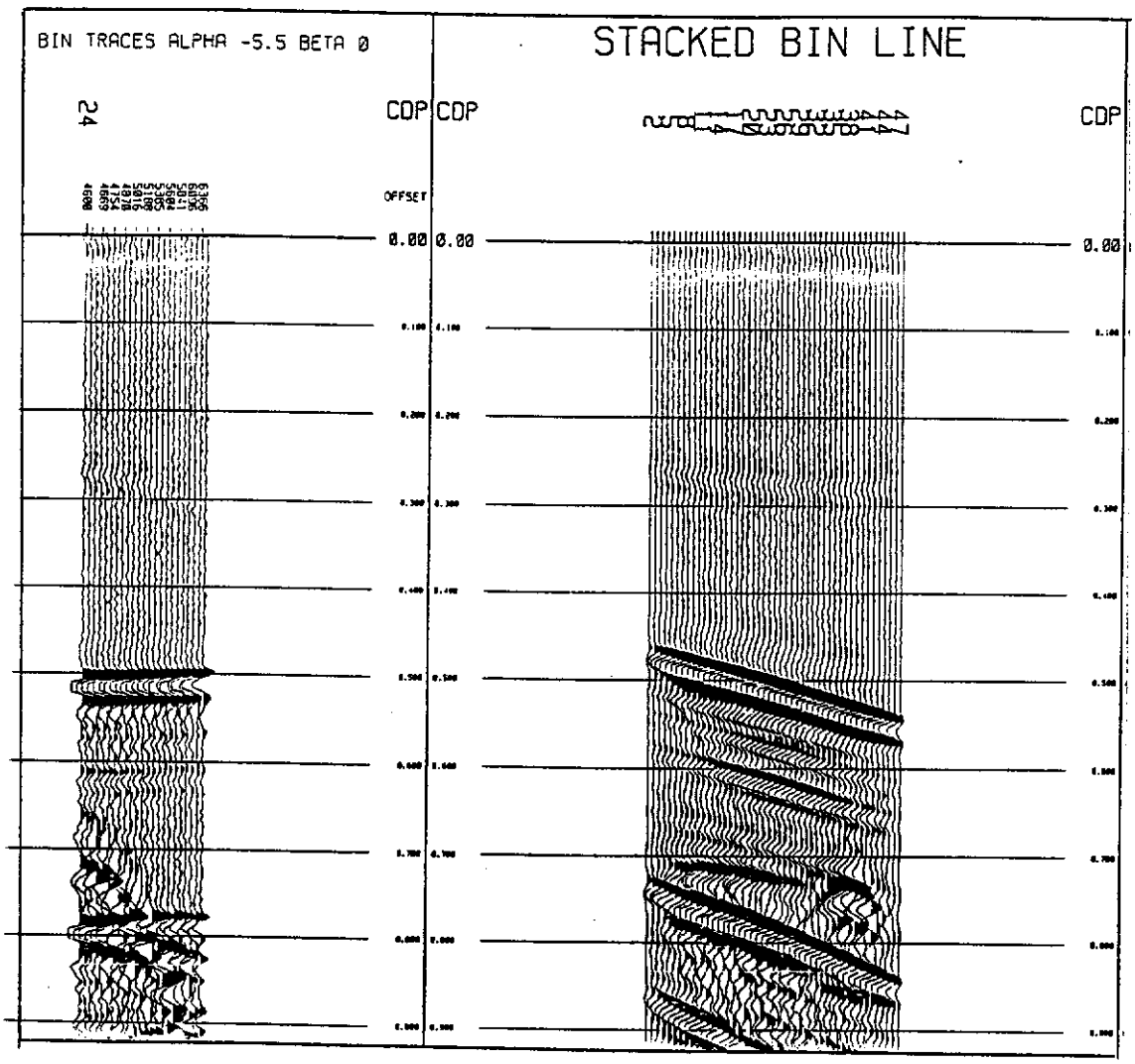

Figure 6.29. Cross-dip stacked mid-point line using an α of -5.5 degrees, and a β of zero. The section displays a dip of approximately 5.5 degrees, which compares with the measured dip of 5.6 degrees.

Figure 6.30 was now produced using an α and β of -3.9 degrees for the 45 degree line. CMP 24 gather shows a fairly flat event line-up, and therefore an acceptably stacked line. In the knowledge that this line was constructed from a stack of scattered reflection points along a line direction which was up-dip, the conclusion drawn is that if the correct dip values are used in the GMO equation together with the correct medium velocity, a best line-up of gathers will occur, and a best stack prior to further processing applications.

This stacked line is instructive since it indicates that the data collected is not only useful for dip determination, but also can indicate the stacking response and reflection strength of data in the chosen survey area. The next objective was to observe the low fold bin traces, to see if they appeared acceptably aligned, as would be required by LOFOLD3-D methods. The 45 degree line data four trace binned gather was checked, and is shown in Figure 6.31. An α and β of -3.9 was used again. The CMP gather shows an acceptable line-up of the reflection.

Using the same procedure, a three trace gather of the same line with the same parameters is shown as Figure 6.32. The traces are acceptably aligned and in this case stacks as trace 3 of the stacked bin line shown on the right. It would be quite impossible to perform a velocity analysis on such a low number of traces, and consequently this is a demonstration that an acceptable stack can be obtained using just three traces, without a velocity analysis. Furthermore in practice, the midpoint length h' could be replaced by a two-way traveltime, since the medium velocity is known.

Conclusions. A generalised moveout equation (GMO) was derived and successfully used to demonstrate a new dip detection method. The method worked successfully on a physical model, predicting the model's true dip (irrespective of dip azimuth) to an accuracy of within a half degree. The dip detection method operated on the assumption that the survey area had the same consistent dip throughout, and that the reflection medium's velocity was known (which is an acceptable condition for shallow coal mining exploration). Having obtained a value of dip in two orthogonal directions, the GMO equation was then used to bin a low number of traces without a velocity analysis. This then removed a major impediment to the method of LOFOLD3-D recording, i.e. that of binning low fold data without an adequate velocity analysis.

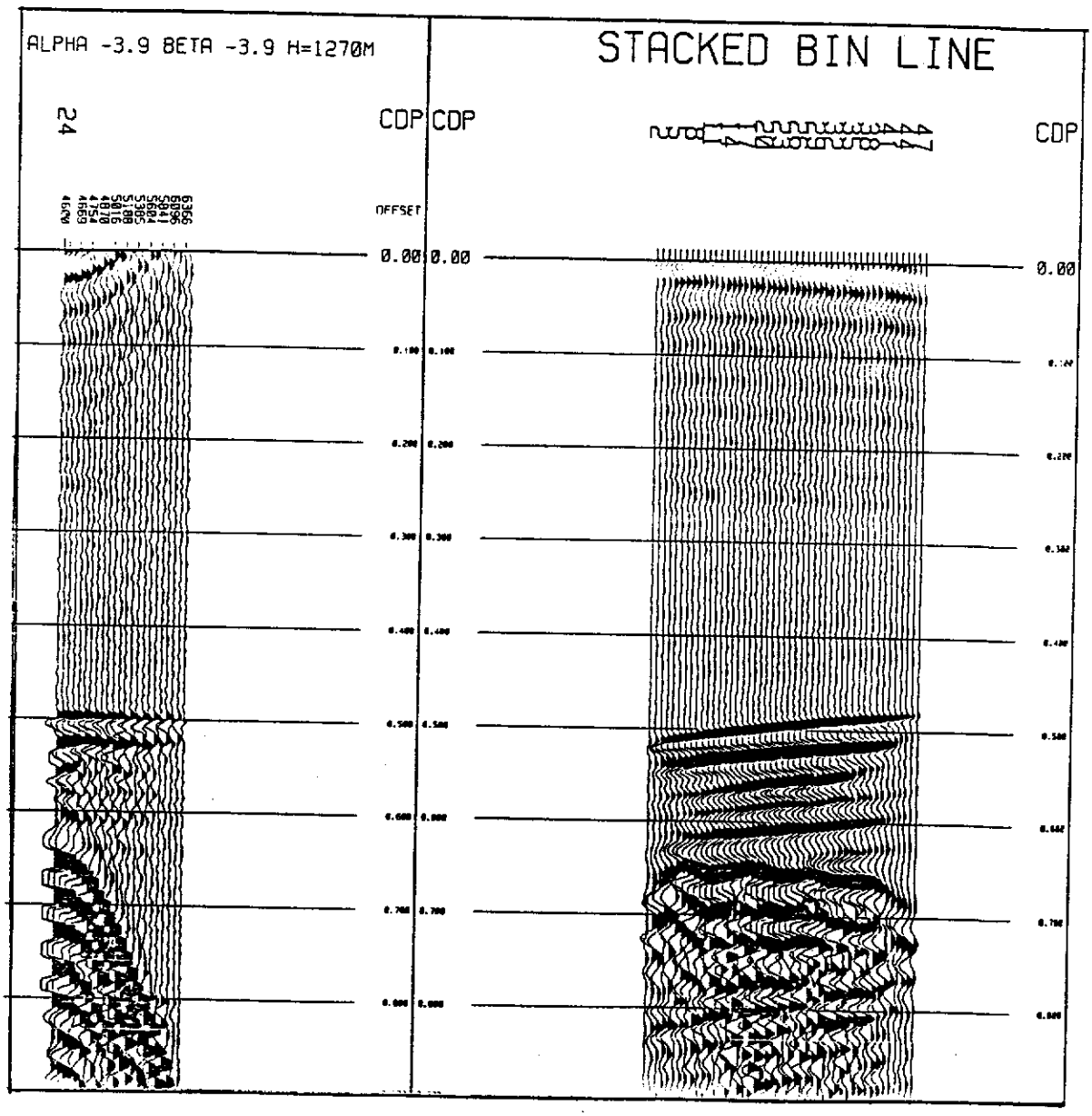

Figure 6.30. Using an α and β of -3.9 degrees for the 45 degree line, CMP 24 gather shows the line is aoceptably stacked.

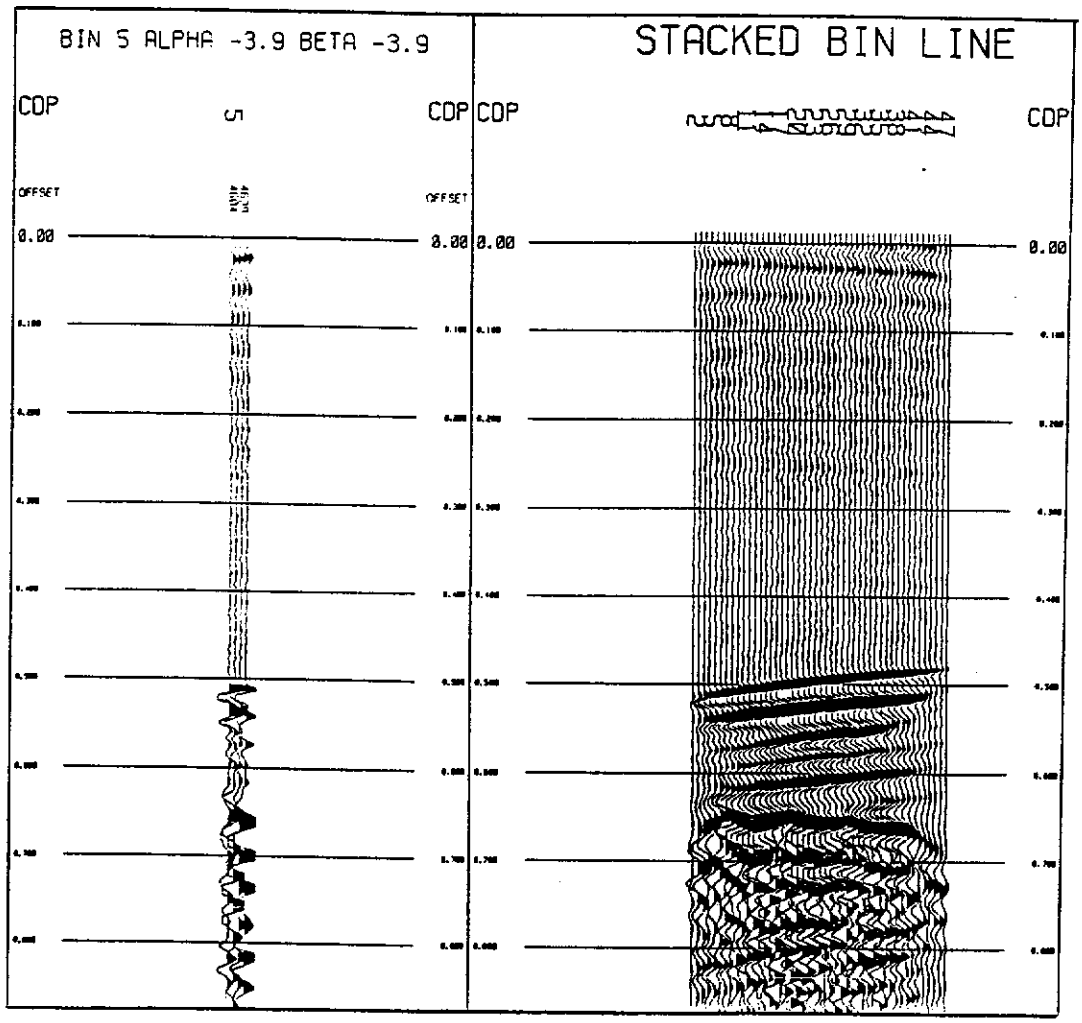

Figure 6.31. The four fold bin gather, using an α and β of - 3.9 for the 45 degree line. The gather shows a line-up of traces without velocity trials.

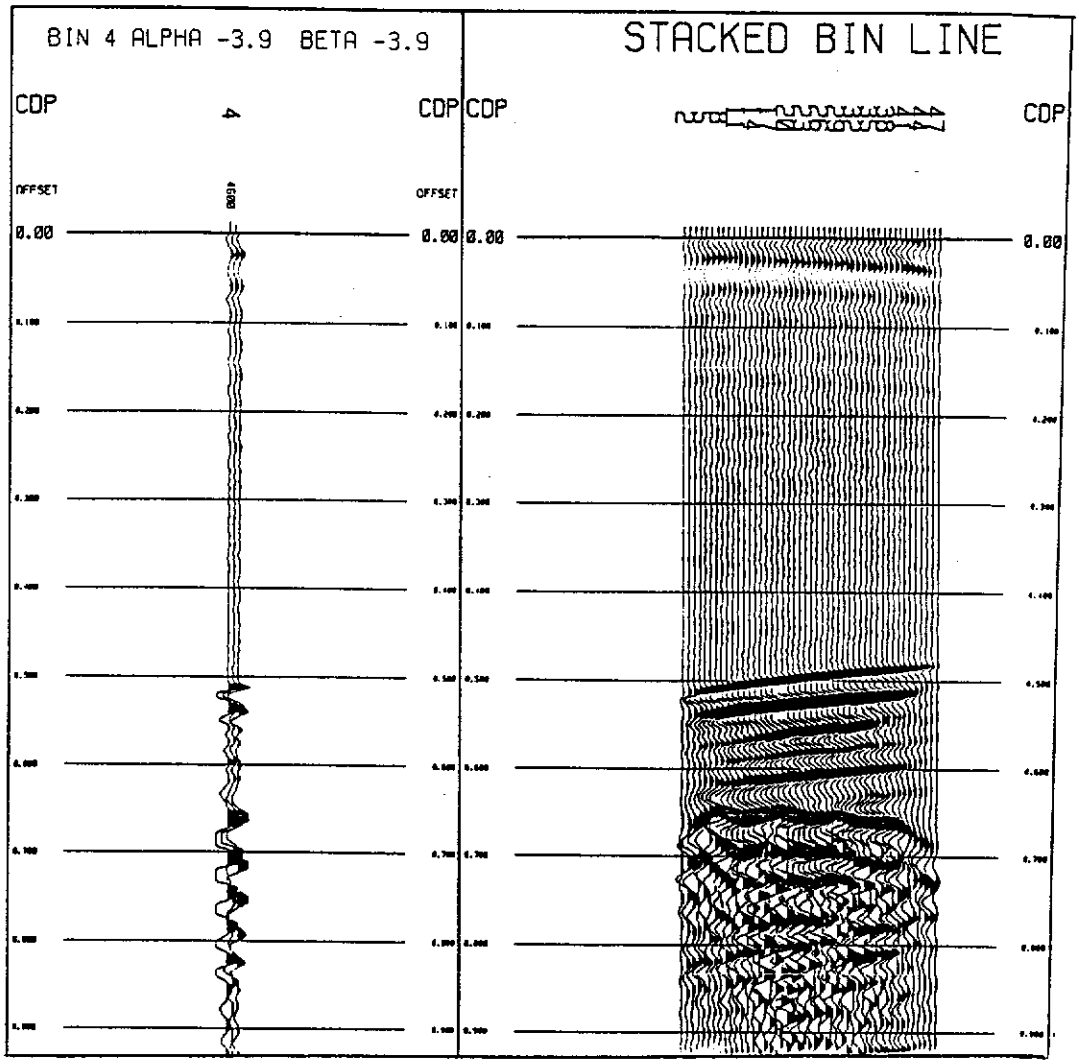

Figure 6.32. The three fold gather, using an α and β of - 3.9 for the 45 degree line. The gather shows an acceptable line-up of traces without any velocity trials.

CHAPTER 7
Conclusions and Recommendations

7.1 Conclusions

The simplest approach to reduce the cost of three-dimensional seismic surveying is to reduce the number of CMP bin traces which are recorded and processed into a low fold three-dimensional volume. The objective of this research has been to provide advancements, so that the application of low fold three-dimensional recording methods will maintain the quality of 3-D seismic data, while lowering the cost of data collection and processing, if possible.

The main failures of the low fold 3-D method are that:

(a) a low signal-to-noise ratio results from the use of a low number of CMP binned traces,
(b) the stack of a low number of traces provides poor imaging which is often due to the application of poor surface statics corrections on shot records, and
(c) the presence of dip in 3-D data, requires velocity analyses which are impossible when only a few CMP bin traces are used.

During the research, I developed solutions to these problems. In order to perform the research, I built a three-dimensional physical modelling system at the University of Houston and used it to demonstrate some of the results of this work.

Solutions were found as follows:

a) Surface Waves, the *Radial* and *Extended* transforms

In 3-D swath seismic surveying, surface waves arrive from different azimuths, and can have curved moveout which not only masks reflections, but they also have similar moveout to reflections. This makes it very difficult to enhance reflection signal amplitudes in data processing.

The *Radial* transform provides an alternative approach to attenuating curved surface waves and enhancing reflections. The transform replaces

the receiver offset distance by the radial offset distance from the source to each receiver, resulting in replacing the equal trace separation of the receiver coordinate domain by a variable trace separation in a *Radial* domain. Surface wave data is then linearized prior to applying other transformations. When τ-p transformation is applied in the *Radial* domain, it is equivalent to applying a curved trajectory τ-p transform in the linear receiver coordinate domain, thereby separating swath surface wave data from curved reflections, based on values of slowness.

An extension of the *Radial* transform, referred to as the *Extended* transform, offered the ability to apply pseudo radial offsets from source to receivers, which enabled the application of filtering in the *Extended* transform domain. Filtering in both domains could be applied by surgically muting data prior to inverse transformation.

The major benefit of the *Radial* transform is that it does not require a prior knowledge of the surface wave velocity since the transform is applied as a standard τ-p process. The major benefit of the *Extended* transform was the ability to simply apply a much larger pseudo offset than was used in the field, which then automatically summed data over a shorter range of slowness values than those required to be specified by the *Radial* transform. It therefore was much simpler to apply to swath data, and offered better signal-to-noise ratio results on a range of data, with the inherent artefacts which were minor.

Numerical, physical model and field data were used to test the viability of the transforms. The *Radial* transform was very successful in eliminating the surface waves from numerical model data, where the surface waves were ideally circular in arrival and had a 30 Hz Ricker centre frequency wavelet. The transform was less successfully applied to two LOFOLD3-D field data sets, but still provided relatively successful results since nature does not provide ideal data sets.

The *Moora* data set showed that the *Radial* transform could improve the general signal-to-noise ratio of the data, while the *Extended* transform showed even greater improvement in reflection coherency. The *German Creek* data set which displayed little moveout between reflections and surface wave noise, improved after transformation and muting, with the reflections substantially enhanced.

The *Radial* transform was less successful on the physical model data, where inner trace artefacts were generated due to the high amplitude near-offset noise. It did work well on the numerical and field data when surgical muting could be applied in the transform domain. Muting was not tested on the physical model data, since its application was considered to be demonstrated using the field data.

It has been shown that the *Radial* transform can be applied to swath 3-D data, and has been shown to operate in an acceptable manner, although it does produce artefacts. The *Radial* transform does not operate well where inner traces have strong noise amplitude values, but this criticism applies equally to the τ-p transform. A further limitation of the method is that it assumes that the surface wave will be circular, which if it is not, then the transform would be expected to fail.

However, the ability to use a variable lateral offset as an extended option in the *Extended* transform provides an extra filtering dimension to the transform which other transforms (such as the conventional τ-p transform) do not offer. This approach has been demonstrated as an effective filtering method of field data.

b) Refraction statics corrections

The refraction statics approach was developed during the term of this research. It became a necessary function of the basic processing of LOFOLD3-D data. It is a simple but effective approach to improving the continuity of reflections. It is based on the assumption that if an adequate velocity contrast exists between the weathering and subweathering layers, then the refraction raypath through the weathering layer will be very similar to the reflection raypath. Simple application of this methodology using linear moveout followed by surface-consistent statics has been shown to be effective in many 2-D and LOFOLD3-D surveys. The method is now commonly used to enhance the resolution of both 2-D and LOFOLD3-D surveys in coal exploration by improving reflector image continuity.

The statics correction method however, is difficult to apply when there are no refractions available for linear moveout application, or when there are

refractions but the velocity gradient is not large enough. Under such circumstances, the statics correction is no better than any other method.

c) Velocity Analysis and a generalised moveout expression

The problem of having a small number of CMP traces for velocity analysis has been addressed. A three-dimensional moveout GMO expression which uses a singular known medium velocity, has been developed. Instead of using velocity analysis to determine the best stacking velocity, the medium velocity is used as the velocity for all moveout corrections, thereby negating the requirement for a velocity analysis. The expression for the GMO however, requires a knowledge of the dip in two orthogonal directions.

The expression for the determination of three-dimensional dip dependent traveltime has been developed. With a knowledge of the dip in two orthogonal directions with respect to the survey line layout, it is now feasible to perform a moveout correction and stack data using medium velocities, which had not been previously possible. To determine the dip values, a new approach to recording and analysing field data was developed.

A new field test, which complements and can be performed during the conventional noise tests, is proposed. The field procedure is in three parts:
a) the recording of a zero offset trace providing two-way traveltime to a selected reflection, at an origin in terms of recording geometry (this may alternatively be determined using τ-p transform methods),
b) the recording of two short orthogonal swath seismic lines, which will allow the computation of dip in two orthogonal directions (or alternatively true dip and azimuth if needed), and
c) the application of the GMO corrections to stack 3-D bin data, as a useful check on data quality and as a later application for use in processing the data without velocity analyses.

A physical model was used to demonstrate the detection procedure's ability to correctly predict the value of the true dip and its azimuth, and this model indicated that the prediction would be accurate to within a half-degree of dip.

The method is initially applicable to coal field exploration, when the near surface velocity is fairly uniform. To execute the proposed procedure in the field, a single horizon may be initially chosen. An estimate of the average velocity to the horizon of known depth is made from existing data. The reference point may be at a drill hole or at an exploration well, or it may be derived from an estimated time/velocity pair from existing seismic data at a known location.

In the event that surface wave noise masks the reflected signal recorded during the dip detection test (thereby rendering the dip prediction method less accurate), either the *Radial or Extended* transforms could be applied to improve the reflected signal strength, to assist the dip prediction process and to improve the general record quality.

7.2 Recommendations

The Radial or Extended transforms could be applied to marine data where such marine data is recorded in 3-D swath manner in shallow water, where mud-roll contaminates the near traces. Such data were not available for test purposes during this research.

The statics method could be applied to records of deeper data than have been tested during the course of this research, and it is feasible that, while it has been developed for high resolution land surveying, it may have an application in marine surveying where the water is shallow, and the sea-bed has an acceptable velocity contrast with the water. Such conditions exist where the sea-bed has a velocity of around 2,200 m/s or greater.

The dip detection data processing procedure could be automated by using trial values of α and β to obtain the values of apparent dip. The optimum value is then that which produces the maximum RMS amplitude of the reflection wavelet after stack. If the program is made interactive, the data processor could either select values of dip from the gather displays, or the stacking process could produce the maximum amplitude stacked trace and thus determine true dip, strike, and azimuth. A plan view could be used to show the true dip direction of the chosen layer with respect to the source and receiver lines. Following the determination of dip, the process could be automated to compile a brute stack of the low fold data immediately.

In marine surveys, the ship's fathometer determines the water depth ahead of the towing equipment. When the fathometer is used to determine a zero offset two-way time to the sea-bed, the dip detection method and 3-D NMO equation could have an immediate application to real-time marine operations. A prior knowledge of the sea-bed's 3-D dip and its azimuth (before the arrival of the air-guns at that location) may be used as a front-end data base for other vessel-based computation exercises (such as multiple prediction and data binning).

References

Allen, J. and Howell, J.,1987, Using "Poor man's 3-D" to identify distributary channel sands in the Wilcox formation, Lavaca County, Texas: Leading Edge of Exploration, 6, 10.

Bessenova, E.N., Fishman, V.M., Ryaboyan, V.N., and Sitnoikova, G.A., 1974, The tau method for inversion of traveltimes - 1: Geophys. J.R. Astr. Soc., 46, 87-108.

Bisset, D.A. and Durrani, T.S., 1990, Radon transform migration below plane sloping layers: Geophysics, 55, 227-283.

Brysk, H. and McCowan, D.W., 1986, A slant-stack procedure for point-source data: Geophysics, 51, 1370-1386.

Brown, R.J.S., 1969, Normal moveout and velocity relations for flat and dipping beds and for long offsets: Geophysics, 34, 180-195.

Cressman, K.S., 1968, How velocity layering and steep dip affect CDP: Geophysics, 33, 399-411.

Daly, C, and Diggins, C, 1988, Use of refractor elevation models in the computation of refraction statics: 58th Annual SEG Symp. Expanded Abstracts, 574-577.

Diebold, J.B. and Stoffa, P.L.,1981, The traveltime equation, Tau-p mapping, and inversion of common mid-point data: Geophysics, 46, 238-254.

Deregowski, S.M., 1986, What is DMO?: First Break, 4, 7, 7-24.

Dietrich, M., 1988, Modelling of marine seismic profiles in the t-x and Tau-p domains: Geophysics, 53, 453-465.

Dobbs, S.L., Wilson, C.R. and Backus, M.M., 1990, Accounting for limited spatial aperture in the waveform inversion of p-T seismograms: Geophysics, 55, 452-457.

Ebrom, D.A. and McDonald, J.A., 1994, Seismic physical Modeling: Soc. of Expl. Geophys. reprint series, 15, Tulsa.

Evans, B.J., 1984, A handbook for seismic data acquisition in oil exploration: Curtin University publication.

Evans, B.J., Paterson, G.A.D. and Frey, S., 1987, Fault plane resolution using the low-fold 3D technique over the Woodada Gas Field, Perth Basin: Australian Petroleum Exploration Association Journal, 27, 289-302.

Evans B.J., 1988, Executive summary and project overview: Final WAMPRI Project 63 Sponsors Review, September.

Evans, B.J., 1991a, Slant-stacking of 3D data into the radial domain: Seismic Acoustics Laboratory Annual Progress Review, 24.

Evans, B.J., 1991b, ET - A three-dimensional slant stack transform: Exploration Geophysics, 22, 135-142.

Evans, B.J. and Urosevic, M., 1993, The physical modelling of Oliver gas field: Curtin University internal report SPS 600/1993/EG 27.

Evans, B.J. and Urosevic, M., 1995, The data acquisition, processing and interpretation of a 3-D seismic survey at Collie, W.A.: Report for Griffin Coal Mining Company.

French, W.S., 1974, Two-dimensional and three-dimensional migration of model-experiment reflection profiles: Geophysics, 39, 265-277.

Frey, S.E., 1986, Data acquisition, processing and structural interpretation of 2D and 3D seismic from the Woodada gas field, Western Australia: M.S. thesis, University of Houston.

Gerver, M. and Markushevich, V., 1966, Determination of seismic wave velocity from the travel-time curve: Geophys. J.R. Astr. Soc., 11, 165-173.

Goebel, V, and Evans, B.J., 1987, A new velocity filter for the attenuation of coherent seismic noise: Exploration Geophysics, 18, 73-75.

Hale D., 1991, Dip Moveout Processing: Society of Exploration Geophysicists Course Series, V. 4, Tulsa.

Harding, A.J., 1985, Slowness-time mapping of near-offset seismic reflection data: Geophys. J.R. Astr. Soc., 80, 463-492.

Hatherly, P.J., Urosevic, M., Lambourne A., and Evans, B.J., 1994, A simple approach to calculating refraction statics corrections: Geophysics, 59,156-160.

Hatherly, P.J. and Evans, B.J., 1991, Patent PK5823 refraction statics correction: Halford and Co., Sydney.

Howes, E.T., Tefada-Flores, L.H. and Lee, R., 1953, Seismic model study: Journal of the Acous. Soc. of America., 25, 915.

Ivakin, B.N., 1966, Methods of seismic modelling: Studia Geophysica et Geodetica, 10, 253-258.

Jervis, M.A., Uren, N.F. and Borisov, K., 1987, Some experiments in the suppression of coherent noise on land 3-D seismic shot records: Exploration Geophysics, 18, 110-114.

Kennett, B.L.N., 1977, The inversion of reflected wave traveltimes: Geophys. J.R. Astr. Soc., 49, 739-746.

Lambourne, A.N., Hatherly, P.J. and Evans, B.J., 1991, 3-D seismic reflection: examples of its application to mine planning and safety in Australian coal fields: Exploration Geophysics, 22, 227-230.

Lansley, R.M. and Gonzalez, A., 1992, 3-D Seismic Exploration: Society of Exploration Geophysics Short Course Notes, Tulsa.

Levin, F.K., 1971, Apparent velocity from dipping interface reflections: Geophysics, 36, 510-515.

Maginness, M.G., 1972, The reconstruction of elastic wave fields from measurements over a transducer array: J. of Sound and Vibration, 20, 219-240.

Mayne, W.H, 1962, Common reflection point horizontal data stacking techniques: Geophysics, 27, 927-938.

McDonald, J.A., Gardner, G.H.F. and Kotcher, J.S., 1981, Areal seismic methods for determining the extent of acoustic discontinuities: Geophysics, 46, 2-16.

McDonald, J.A. and Gardner, G.H.F., 1983, Physical modeling at the Seismic Acoustics Laboratory; *in* Seismic Studies in Physical Modeling: eds. J.A. McDonald, G.H.F. Gardner and F.J. Hiltermann, International Human Res. Dev. Corp., Boston, 1-19.

McMechan, G.A. and Ottolini, 1980, Direct observation of a p-tau curve in a slant stacked wavefield: S.S.A. Bull., 70, 775-789.

Meinardus, H.A., and McMahon, I.T., 1981, Velocity modeling for 3D NMO and stack: G.S.I. publication.

Menke, W. and Dubendorff, B., 1989, Seismology: Physical model studies: in D.E. James, Ed., Encyclopaedia of Geophysics, Van Nostrand and Reinhold, 1202-1211.

Miller, D., Oristaglio, M. and Beyklin, G., 1987, A new slant on seismic imaging: migration and integral velocity; Geophysics, 52, 943-964.

Mithal, R. and Vera, E.E., 1987, Comparison of plane wave decomposition and slant stacking of point-source seismic data: Geophysics, 52, 1631-1638.

Nestfold, E.O., 1992, 3-D seismic: Is the promise fulfilled?: The Leading Edge, 11, 12-21.

Northwood, T.D. and Anderson, D.V., 1953, Model Seismology: Bull. Seism. Soc. of America, 43, 239.

O'Brien, P.N. and Symes, M.P., 1971, Model Seismology: Am. Inst. of Physics, Progress in geophysics, 34, 697-718.

Ottolini, R. and Claerbout, J.F., 1984, The migration of common midpoint slant stacks: Geophysics, 49, 237-249.

Pant, D.R., Greenhalgh, S.A., and Watson, S., 1988, Seismic reflection scale model facility: Exploration Geophysics, 19, 499-512.

Radon, J., 1917, Uber die Bestimmung von Funktionen durch ihre Integralwerte langs gewisser Manningfaltigkeiten: Berichte der Sachischen Akendemie der Wissenschaften, 69, 262-277.

Riznichenko, Y.V., 1966, Seismic modelling, development and outlook: Studia Geophysica et Geodaetica, 10, 243-253.

Schultz, P.S., 1982, A method for the direct estimation of interval velocities: Geophysics, 47, 1657-1671.

Sheriff, R.E., 1991, Encyclopedic Dictionary of Exploration Geophysics: Society of Exploration Geophysics, Tulsa.

Sheriff, R.E. and Geldart, L.P., 1982, Exploration Seismology Vol.1: Cambridge University Press.

Slotnick, M. M., 1959, Lessons in seismic computing: Society of Exploration Geophysics, Tulsa.

Stewart, S.C. and Evans, B.J., 1989, A case history of a cost effective 3D seismic survey over the Perth Basin, Western Australia: Exploration Geophysics, 20, 229-236.

Tatham, R.H., Goolsbee, D.V., Massell, W.F. and Nelson, H.R., 1983, Seismic shear-wave observations in a physical model experiment: Geophysics, 48, 688-701.

Thomas, G.B. and Finney, R.L., 1992, Calculus and Analytic Geometry, 8 th Edition: Addison and Wesley, Chicago.

Treitel, S., Gutowski, P.R. and Wagner, D.E., 1982, Plane wave decomposition of seismograms: Geophysics, 47, 1375-1401.

Walton, G.G., 1972, Three-dimensional seismic method: Geophysics, 37, 417-430.

Young, R.A., 1987, Interval velocity analysis by tau-p methods: Exploration Geophysics, 18, Nos. 1/2, 242-244.

APPENDICES

Appendix A

Three-dimensional path length.

To compute the three-dimensional travel path length from a source to a reflection point and on to a receiver, the approach adopted is that of optics using the method of images. The distance from the source down to a reflection point and up to a receiver is the same as the distance from an image of the source to a receiver.

A three-dimensional box with coordinate axes X, Y and Z is shown in Figure A-1 . Consider the dipping reflection plane to have dip angles of α in the vertical X-Z plane, and β in the vertical Y-Z plane. α and β have a positive value when the reflection horizons dip down towards the origin, and a negative value when dipping upwards away from the origin; X and Y are positive in the directions as shown, while Z is positive downwards.

The equation of a plane passing through the origin is given by:

$$ax + by + z = 0 \ , \qquad \text{(A-1)}$$

where a, and b are variables of the dipping plane, shown in Figure A-1.

In Figure A-1, let the length of 0X be 1, so that the coordinates of C are (1,0,-a), and at X (1,0,0). In triangle 0CX, Tan $(-\alpha) = -\frac{a}{1}$, and hence,

$$a = \tan \alpha \, . \qquad \text{(A-2)}$$

$$\text{Similarly, } b = \tan \beta \, . \qquad \text{(A-3)}$$

Consider a plane parallel to the above plane, but intersecting the Z-axis at (0,0,d) as shown in Figure A-2. Let the length of a perpendicular from the origin to the plane be **h**.

The equation of the dipping plane is now given by:

$$ax + by + Z = d \, . \qquad \text{(A-4)}$$

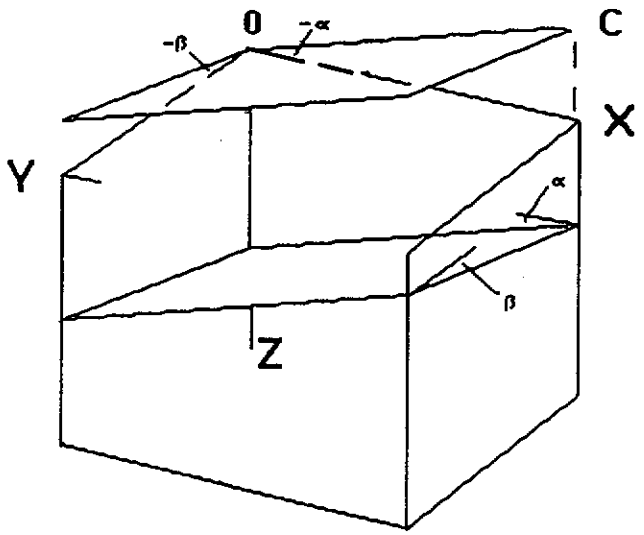

Figure A-1. A three-dimensional box showing a dipping plane making angles α and β with sides XZ and YZ, respectively.

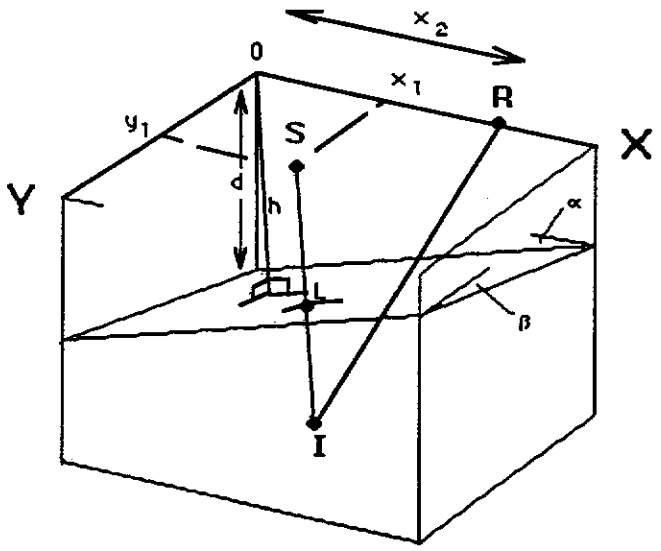

Figure A-2. Source S and receiver R with image point I form triangle SIR. A line drawn perpendicular to the reflecting surface from S to I passes through the plane at L.

The perpendicular distance from the origin to the plane is given by

$$h = \left| (0,0,d) \cdot \frac{(a,b,1)}{(a^2 + b^2 + 1)^{1/2}} \right| . \qquad \text{(Thomas and Finney, 1992)}$$

$$\text{i.e.} \quad h = \frac{d}{(a^2 + b^2 + 1)^{1/2}} ,$$

$$\text{so,} \quad \mathbf{d = h\ (a^2 + b^2 + 1)^{1/2}} \qquad \text{(A-5)}$$

A line from S perpendicular to the plane has the parametric equation:

$$(x, y, Z) = (x_1, y_1, 0) + t\,(a, b, 1) , \qquad \text{(Thomas and Finney, 1992)}$$

where t is a parameter determining the position of a point $(x_1, y_1, 0)$ on the line.

This perpendicular line intersects the plane at L when

$$a\,(x_1 + at) + b\,(y_1 + bt) + t = d.$$

$$\text{i.e.} \qquad a\,x_1 + by_1 + (a^2 + b^2 + 1)\,t = d.$$

$$\text{Therefore,} \qquad t = \frac{\mathbf{d - a\,x_1 - by_1}}{\mathbf{a^2 + b^2 + 1}} . \qquad \text{(A-6)}$$

The point of intersection L with the plane has coordinates:

$$(x_1 + at,\ y_1 + bt,\ t) .$$

Since SL = LI, then to obtain point I, use 2t instead of t. So I has coordinates $(x_1 , y_1 , 0) + 2t\,(a, b, 1) = (x_1 + 2at,\ y_1 + 2bt,\ 2t)$, and R has coordinates $(x_2 , 0, 0)$.

$$\mathbf{So} \quad |IR| = \left((x_1 - x_2 + 2at)^2 + (y_1 + 2bt)^2 + 4t^2 \right)^{1/2} . \qquad \text{(A-7)}$$

For the case where the midpoint perpendicular length to the reflection plane is to be calculated, where the mid-point is located at the surface mid-way between S and R, then

$$t' = \frac{d - a\left(\frac{(x_2 - x_1)}{2}\right) - \frac{by_1}{2}}{a^2 + b^2 + 1} \quad ,$$

where t' is the parameter determining a point on the perpendicular from the mid-point location to the reflecting plane.

The midpoint perpendicular has coordinates on the upper surface of

$$\left(\frac{x_2 - x_1}{2}, \frac{y_1}{2}, 0\right),$$

and coordinates at the reflection plane surface of

$$\left(\frac{x_2 - x_1}{2} + at', \frac{y_1}{2} + bt', t'\right).$$

If h' is the length of this midpoint perpendicular,

then $h' = \left(\left(\left(\frac{x_2 - x_1}{2}\right) + at' - \left(\frac{x_2 - x_1}{2}\right)\right)^2 + \left(\frac{y_1}{2} + bt' - \frac{y_1}{2}\right)^2 + (t' - 0)^2 \right)^{1/2}$,

or $|h'| = \left(t' (a^2 + b^2 + 1)\right)^{1/2}$. (A-8)

For the special case where the shot is at the origin (0), the receiver line is along the x-axis and the reflector dips at a value α along the x-axis,
i.e. $x_1 = y_1 = \beta = 0$,

$$(IR)^2 = (-x_2 + 2at)^2 + 4t^2,$$

$$= \left(-x_2 + 2 \operatorname{Tan}\alpha \cdot \frac{h(\operatorname{Tan}^2\alpha + 1)^{1/2}}{\operatorname{Tan}^2\alpha + 1}\right)^2 + 4\left(\frac{h(\operatorname{Tan}^2\alpha + 1)^{1/2}}{\operatorname{Tan}^2\alpha + 1}\right)^2$$

But $\sec^2\alpha = 1 + \tan^2\alpha$.

Therefore, $(IR)^2 = \left(-x_2 + 2h\dfrac{\operatorname{Tan}\alpha}{\operatorname{Sec}\alpha}\right)^2 + \dfrac{4h^2}{\operatorname{Sec}^2\alpha}$,

$$= x_2^2 + 4h^2 - 4hx_2\frac{\operatorname{Tan}\alpha}{\operatorname{Sec}\alpha},$$

$$(IR)^2 = x_2^2 + 4h^2 - 4hx_2 \operatorname{Sin}\alpha .$$

When there is no dip in the x direction either, $(IR)^2 = x_2^2 + 4h^2$.

Appendix B. True dip value θ and azimuth ϕ

To determine the true dip value, in the case where in Figure B-1 the X-axis dip is α and the Y-axis dip is β. Let ϕ be the angle in the horizontal plane between the X-axis and the true dip azimuth θ.

True dip value $\text{Tan}\,\theta = (\text{Tan}^2\,\alpha + \text{Tan}^2\,\beta)^{1/2}$. (B-1)

The azimuth of true dip $\text{Tan}\,\phi = \left(\dfrac{\text{Tan}\,\beta}{\text{Tan}\,\alpha} \right)$. (B-2)

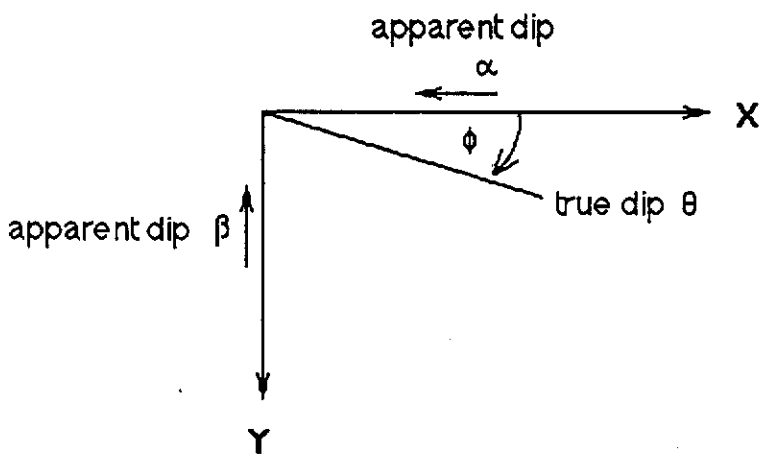

Figure B-1. Plan view of the apparent dip with respect to the true dip θ.

Appendix C. Some sample programs used in the research.
The Fortran programs produced an output file, which was then submitted as a batch DISCO processing job.

```
C-----------------------------------------------------------------------
C
C          TITLE:  SHOTINV.FOR, THE EXTENDED TRANSFORM
C                  AN INVERSE TAU-P TRANSFORM
C                  FOR 3-D SHOTS.
C
C          PROCESS: To compute the APPARENT swath wave
C                   shot to each in-line receiver and write it in each
C                   trace header, prior to INVERSE
C                   Tau-p transform. THERE IS A LIMIT OF 100 P
C                  traces OUTPUT.
C
C          INPUT:  Prompts for
C
C
C
C                   1) Number of p traces required
C                     LIMITED TO 100 RECORDS @ 48 TRACES INPUT.
C                   2) Lateral offset of shot to near receiver
C                   3) Number of receiver stations
C                   4) Station Interval
C                   5) Disk file to be used
C
C
C          OUTPUT: Output to a data file called SHOTET.DAT
C
C          AUTHOR: B.Evans, 14TH NOV 1993.
C-----------------------------------------------------------------------
      INTEGER*4 R,X,NSTAT,N
      CHARACTER*40 file2
      OPEN(UNIT=10,FILE='SHOTINV.DAT',STATUS='NEW',
     * CARRIAGECONTROL='LIST')
      WRITE(5,11)
11     FORMAT(1H1)
      CALL LIB$ERASE_PAGE(1,1)
      CALL LIB$SET_CURSOR(1,1)
      WRITE(5,1)
1     FORMAT(1X,'THIS PROGRAM BUILDS A FILE FOR INVERSE TAU-P
TRANSFORM'/)
      WRITE(5,2)
2     FORMAT(1X,'RESULTS ON DISC FILE SHOTINV.DAT'/)
      WRITE(5,25)
25     FORMAT(1X,'ENTER THE IN-LINE NEAR OFFSET')
      READ(5,*)N
26     FORMAT(I4)
      WRITE(*,30)
30     FORMAT(1X,'ENTER LATERAL OFFSET FROM SOURCE TO
NEAREST'/
     *      ' ORTHOGONAL RECEIVER')
```

```
      READ(*,*)R
35     FORMAT(I4)
      WRITE(5,40)
40     FORMAT(1X,'ENTER THE NUMBER OF RECEIVER STATIONS')
      READ(*,50)NSTAT
50     FORMAT(I4)
      WRITE(*,60)
60     FORMAT(1X,'ENTER THE FAR IN-LINE OFFSET')
      READ(*,61)X
61     FORMAT(I4)
      WRITE(*,63)
63     FORMAT(1X,'ENTER DATA FILENAME  DCI----')
      READ(*,64)FILE2
64     FORMAT(A40)
      WRITE(10,65)FILE2,NSTAT,N,X,R
C WRITE JOB IN DISCO
65     FORMAT(1X,T1,'*JOB',T9,'EVANS',T17,'WDG',/,
     * T1,'*ALT',T9,'ILTP',T17,'USR$DISK:[SPLBJE.ILTP]',/,
     * T1,'*CALL',T9,'DSKRD',T17,A40,/,
     * T1,'*CALL',T9,'TABLE',T17,'CHAN',/,
     * T1,'*CALL',T9,'SECPLOT',T33,'10.0',T41,'4.0',/,
     * 1X,T1,'PLOTOPT',T9,'/NAME=1',/,
     * 1X,T1,'TIMING',T9,'3',T17,'1',/,
     * 1X,T1,'LABEL',T9,'OFFSET',T17,'1',/,
     * 1X,T1,'TITLE',T9,'INPUT RADIAL TRANSFORM',/,
     * 1X,T1,'TRANGE',T9,'0.',T17,'2000',/,
     * 1X,T1,'*CALL',T9,'ILTP',T17,I4,T25,I4,T33,I4,T41,I4,T49,'2',/,
     * 1X,T1,'*CALL',T9,'SECPLOT',T33,'10.0',T41,'4.0',/,
     * 1X,T1,'PLOTOPT',T9,'/NAME=2/POS=(AFTER,1,0.,0.)',/,
     * 1X,T1,'TIMING',T9,'3',T17,'1',/,
     * 1X,T1,'LABEL',T9,'OFFSET',T17,'1',/,
     * 1X,T1,'TITLE',T9,'INVERSE ET',/,
     * 1X,T1,'*END')
      STOP
      END
```

```
C-----------------------------------------------------------------------
C
C          TITLE:  NMO.FOR, TRUE 3-D DIP NMO USING 3-D SHOTS.
C
C          PROCESS: To compute the NMO of a bin trace due to 3-D dip
C                between source and receiver, and display bin traces.
C
C          INPUT:  Prompts for
C
C                1) Estimated velocity of medium.
C                2) Depth to reflector at ref point.
C                3) No. of CMP traces.
C                5) Offset of shot line to receiver line
C                6) First and last station numbers.
C                7) Estimated alpha and beta angles.
C                8) Disk file to be input (raw data)
C                9) If individual bin gathers are needed.
C
C          OUTPUT: Outputs a data file NMO.DAT.
C
C          AUTHOR: B.Evans, 30 Nov., 1993.
C-----------------------------------------------------------------------
      INTEGER*4 SHOTS
      CHARACTER*40 file2
      INTEGER ANS,BIN
      LOGICAL A1,A2,A3,A4,A5,A6,A7
      OPEN(UNIT=10,FILE='NMO.DAT',STATUS='NEW',
     * CARRIAGECONTROL='LIST')
      WRITE(5,11)
11     FORMAT(1H1)
      CALL LIB$ERASE_PAGE(1,1)
      CALL LIB$SET_CURSOR(1,1)
      WRITE(5,1)
1     FORMAT(1X,'THIS PROGRAM COMPUTES THE NMO'/
     *     ' TO FLATTEN CMP TRACES RESULTING FROM 3-D DIP'/)
      WRITE(5,2)
2     FORMAT(1X,'RESULTS ARE ON DISC FILE NMO.DAT'/)
      WRITE(5,10)
10     FORMAT(1X,'ENTER ESTIMATE OF VELOCITY (m/s)')
      READ(5,*)VEL
      WRITE(5,20)
20     FORMAT(1X,'ENTER DEPTH TO REFLECTOR at REF POINT IN m.')
      READ(5,*)H
      WRITE(5,21)
21     FORMAT(1X,'ENTER FIRST SHOT POINT NUMBER')
      READ(5,*)K
      WRITE(5,22)
22     FORMAT(1X,'ENTER MAX NUMBER OF SHOTS')
      READ(5,*)SHOTS
      WRITE(5,23)
23     FORMAT(1X,'ENTER FIRST RECEIVER NUMBER')
      READ(5,*)J
      WRITE(5,25)
```

```
25    FORMAT(1X,'ENTER MAX NUMBER OF RECEIVER TRACES')
      READ(5,*)N
26    FORMAT(I4)
      WRITE(*,30)
30    FORMAT(1X,'ENTER OFFSET FROM SOURCE LINE TO'/
     *     ' RECEIVER LINE')
      READ(*,*)Y
31    FORMAT(I4)
      WRITE(*,32)
32    FORMAT(1X,'ENTER SHOT INCREMENT')
      READ(*,*)SHOTINC
33    FORMAT(I4)
      WRITE(*,34)
34    FORMAT(1X,'ENTER RECEIVER INCREMENT')
      READ(*,*)RXINC
35    FORMAT(5F)
      WRITE(5,40)
40    FORMAT(1X,'ENTER ALPHA, 0 TO +90 OR 0 TO -90')
      READ(*,*)ALPHA
50    FORMAT(4I)

54    CONTINUE
      WRITE(*,60)
60    FORMAT(1X,'ENTER BETA, 0 TO +90 OR 0 TO -90')
      READ(*,*)BETA
      WRITE(*,63)
63    FORMAT(1X,'ENTER DATA FILENAME  DCI----')
      READ(*,64)FILE2
64    FORMAT(A40)
69    CONTINUE


      WRITE(10,73)FILE2
C WRITE JOB IN DISCO
73    FORMAT(1X,T1,'*JOB',T9,'EVANS',T17,'WDG',/,
     *  T1,'*CALL',T9,'DSKRD',T17,A40,/,
     *  T1,'*CALL',T9,'HDRMATH',/,
     *  T1,'HHMUL',T9,'SEQNO',T17,'RCVRSPRDSHOT',/,
     *  T1,'HHMUL',T9,'CHAN',T17,'TRACE',T25,'CHAN',/,
     *  T1,'*CALL',T9,'PROFILE',/,
     *  T1,'*CALL',T9,'HEADPUT',T17,'LINSTAT',
     *  T25,'STORE',T33,'FLOAT',/,
     *  T1,'INPUT',T9,'SHOT',T17,'ALL',T25,'CHAN')


80    X1 = (SHOTINC * (K-1))
84    X2 = (RXINC * (J-1))
      IF (X1.LT.X2) THEN
      X3=X1
      ELSE
      X3=X2
      ENDIF

C CALCULATE SHIFT
```

```
86      X=ABS(X2 - X1)
       IF (ALPHA.EQ.0..AND.BETA.EQ.0.) THEN
       F1=0
       ELSE
        IF (ALPHA.EQ.0.) THEN
        F1=90
        ELSE

87       F1=ATAND(BETA/ALPHA)
C  THIS IS THE AZIMUTH W.R.T. THE X-AXIS
        ENDIF
       ENDIF


88      IF (X1.EQ.0..AND.X2.EQ.0.) THEN
        F2=90
        ELSE
        F2=ATAND(Y/(X1+X2))
       ENDIF

95      IF (F1.GT.0.) THEN
        F=ABS(ABS(F1)-F2)
        ELSE
        F=ABS(ABS(F1)+F2)
       ENDIF
       A1 = (ALPHA.EQ.0).AND.(BETA.EQ.O)
       A2 = (ALPHA.GT.0.0).AND.(BETA.GT.0.0)
       A3 = (ALPHA.GT.0.0).AND.(BETA.LT.0.0)
       A4 = ABS(ALPHA).GT.ABS(BETA)
       A5 = (BETA.GT.0.0).AND.(ALPHA.LT.0.0)
       A6 = ABS(BETA).GT.ABS(ALPHA)
97      IF (A1.OR.A2.OR.A3.AND.A4.OR.A5.AND.A6) THEN
         G=SQRT((ALPHA**2)+(BETA**2))
       ELSE
           A1 = (ALPHA.LT.0.).AND.(BETA.LT.0.)
           A2 = (ALPHA.LT.0.).AND.(BETA.EQ.0.)
           A3 = (ALPHA.EQ.0.).AND.(BETA.LT.0.)
           A4 = (ALPHA.GT.0.).AND.(BETA.LT.0.)
           A5 = ABS(BETA).GT.ABS(ALPHA)
           A6 = (BETA.GT.0.).AND.(ALPHA.LT.0.)
           A7 = ABS(ALPHA).GT.ABS(BETA)

        IF (A1.OR.A2.OR.A3.OR.A4.AND.A5.OR.A6.AND.A7) THEN
         G=- SQRT((ALPHA**2)+(BETA**2))
       ELSE
         G= 0
       ENDIF
       ENDIF

       W=ATAND((TAND(G))*COSD(F))
       H1=H-((SQRT(((X3+(X/2))**2)+((Y**2)/4)))*SIND(W))
```

```
        A=TAND(ALPHA)
        B=TAND(BETA)
        D=H*SQRT( (A**2) + (B**2) +1 )
        T=(D-(A*X1)-(B*Y))/( (A**2) + (B**2) +1 )

        IR=SQRT((((X1-X2) + 2*A*T))**2 )+((Y + (2*B*T)**2) + (4*(T**2)))

      SIR=-H+SQRT((Y**2)+(4*(H**2)))
C   H IS ADDED TO SHIFT DATA UP TO REMOVE SUMMING EXCESSIVE
SURFACE WAVE IF NEEDED

      DT=-1000*(IR-(2*H1))/VEL

104     WRITE(10,105)K,J,DT
105     FORMAT(1X,T1,'TRACE',T9,I4,T17,I3,T25,F8.2)

106     CONTINUE

107      J=J+1

108     IF (J.GT.N) THEN
109      J=1
       GOTO 110
       ELSE
       GOTO 80
      ENDIF

110     IF (K.EQ.SHOTS) THEN
       GOTO 112
       ELSE
       K=K+1
       GOTO 80
      ENDIF

112     CONTINUE

      WRITE(10,114)
114     FORMAT(1X,T1,'*CALL',T9,'STATIC',T17,'LINSTAT',T25,'APPLY',/,
     *  1X,T1,'*CALL',T9,'SORT',T17,'100',T25,'400',/,
     *  1X,T1,'MAJOR',T9,'CDP',/,
     *  1X,T1,'MINOR',T9,'OFFSET',/,
     *  1X,T1,'*CALL',T9,'TABLE',T17,'SHOT',T25,'CHAN',T33,'OFFSET')

c    *  1X,T1,'*CALL',T9,'DSKWRT',T17,'DCI_DATDIR:DIP3D.DSK',/,

      WRITE(*,120)
120     FORMAT(1X,'DO YOU WANT EACH CDP DISPLAY (1=YES) ?')
      READ(*,*)ANS

121     IF (ANS.EQ.1) THEN
       GOTO 175
       ELSE
       GOTO 122
      ENDIF
```

```
122    CONTINUE
      WRITE(*,123)
123    FORMAT(1X,'WHAT CDP BIN TRACES DO YOU WANT?')
      READ(*,*)BIN
124    FORMAT(I4)

      WRITE(10,125)BIN,BIN
125    FORMAT(1X,T1,'*IF',/,
     * 1X,T1,'LIST',T9,'CDP',/,
     * 1X,T1,I4,/,
     * 1X,T1,'*CALL',T9,'SECPLOT',T33,'20.0',T41,'8.0',/,
     * 1X,T1,'PLOTOPT',T9,'/NAME=1',/,
     * 1X,T1,'TIMING',T9,'3',T17,'1',/,
     * 1X,T1,'LABEL',T9,'CDP',T17,'1',T25,'1',T33,'OFFSET',T41,'1',/,
     * 1X,T1,'TITLE',T9,'BIN TRACES ALPHA  BETA',/,
     * 1X,T1,'TRANGE',T9,'0.',T17,'1000.',/,
     * 1X,T1,'*RESET',/,
     * 1X,T1,'*CALL',T9,'STACK',T17,'600',/,
     * 1X,T1,'*CALL',T9,'SECPLOT',T33,'20.0',T41,'8.0',/,
     * 1X,T1,'PLOTOPT',T9,'/NAME=2/POS=(AFTER,1,0.,0.)',/,
     * 1X,T1,'TIMING',T9,'3',T17,'1',/,
     * 1X,T1,'LABEL',T9,'CDP',T17,'1',/,
     * 1X,T1,'TITLE',T9,' STACKED BIN LINE ',/,
     * 1X,T1,'TRANGE',T9,'0.',T17,'1000.',/,
     * 1X,T1,'*IF',/,
     * 1X,T1,'LIST',T9,'CDP',/,
     * 1X,T1,I4,/,
     * 1X,T1,'*CALL',T9,'SECPLOT',T33,'10.0',T41,'8.0',T49,'10.0',/,
     * 1X,T1,'PLOTOPT',T9,'/NAME=3/POS=(AFTER,2,0.,0.)',/,
     * 1X,T1,'TIMING',T9,'3',T17,'1',/,
     * 1X,T1,'LABEL',T9,'CDP',T17,'1',/,
     * 1X,T1,'TITLE',T9,'BIN TRACES STACKED',/,
     * 1X,T1,'TRANGE',T9,'0.',T17,'1000.',/,
     * 1X,T1,'*CALL',T9,'RANGE',/,
     * 1X,T1,'*RESET',/,
     * 1X,T1,'*END')
      STOP


175    CONTINUE

      WRITE(10,180)
180     FORMAT(1X,T1,'*CALL',T9,'SECPLOT',T33,'20.0',T41,'8.0',/,
     * 1X,T1,'TIMING',T9,'3',T17,'1',/,
     * 1X,T1,'LABEL',T9,'CDP',T17,'1',T25,'1',T33,'OFFSET',T41,'1',/,
     * 1X,T1,'BREAK',T9,'CDP',T17,'1',/,
     * 1X,T1,'TITLE',T9,' DIP3D CDP PRESTACK LINE',/,
     * 1X,T1,'*END')

c    * 1X,T1,'*CALL',T9,'STACK',T17,I4,T25,'1',/,
      STOP
190    END
```

Appendix D. Sample papers on the methods used in this research, presented during the period of this research.

1. Fault plane resolution using the low-fold 3D seismic technique over Woodada gas field, Perth Basin, Western Australia. APEA Journal, 1987.
2. A case history of a cost effective 3D seismic survey over the Perth Basin, Western Australia. Exploration Geophysics, 1989.
3. ET - A slant-stack transform of three dimensional data. Exploration Geophysics, 1991.
4. The application of the 3D seismic surveying technique to coal seam imaging - case histories from the Arckaringa and Sydney Basins. Exploration Geophysics, 1990.
5. 3D seismic reflection: Examples of its application to mine planning and safety in Australian coalfields. Exploration Geophysics,1991.
6. Areal coal seam mapping by 3-D seismic reflection surveying: A case history from the Sydney Basin, Australia. Soc. of Expl. Geophys. Conf., 1991.
7. Applications of 3-D seismic methods to detection of subtle faults in coal seams. Soc. of Expl. Geophys. Conf., 1992.
8. Improved static corrections plus pre-stack interpretation improves the resolution of 2-D seismic data. Exploration Geophysics, 1993.
9. A simple approach to calculating refraction statics corrections. Geophysics, 59, 1994.
10. A method for determining in 3-D, the true dip and azimuth of a reflecting horizon. Soc. of Expl. Geophys. Conf., 1994.
11. New developments in coal exploration in Australia. Soc. of Expl. Geophys. Conf., 1994.

Note: For copyright reasons Appendix D has not been reproduced.

(Co-ordinator, ADT Project (Retrospective), Curtin University of Technology, 8.1.03)